1st GeoMandu
NGS international conference series
(Since 2023)

Geohazards and Geo-Infra Disasters

International Conference Series of NGS

16-17 March 2023
Kathmandu, Nepal

Extended Abstract Volume of Proceedings

Organizer
Nepal Geotechnical Society

Proud Member of
SIMSG ISSMGE

1st GeoMandu
NGS International conference series (Since 2023)

Geohazards and Geo-Infra Disasters

International Conference Series of NGS

16-17 March 2023
Kathmandu, Nepal

Extended Abstract Volume of Proceedings

Organizer
Nepal Geotechnical Society

Proud Member of
SIMSG ISSMGE

6th Executive Committee of Nepal Geotechnical Society

President

Prof. Dr. Netra Prakash Bhandary

Vice President

A/Prof. Dr. Indra Prasad Acharya
Er. Shiva Prasad Nepal
Dr. Mandip Subedi

General Secretary

Er. Udaya Raj Neupane

Joint Secretary

Dr. Narayan Gurung
Er. Kalpana Adhikari

Treasurer

Er. Arjun Poudel

Executive Members

Er. Bharat Bahadur Dhakal
Dr. Bhim Kumar Dahal
Er. Tulasi Ram Bhattarai
Er. Sanjay Kumar Jain
Er. Mandakini Karki
Er. Darshan Babu Adhikari
Er. Harish Paneru

Youth Coordinator

Er. Rajan K.C.

1st GeoMandu - 2023, Organizing Committee

Honorary Chair : Dr. Marc Ballouz, ISSMGE President
Chair : Prof. Dr. Netra Prakash Bhandary
Convener : Dr. Mandip Subedi

Members:

A/Prof. Dr. Indra Pd. Acharya
Er. Shiva Prasad Nepal
Er. Uday Raj Neupane
Dr. Narayan Gurung
Er. Kalpana Adhikari
Er. Arjun Poudel
Er. Darshan Babu Adhikari
Er. Sanjay Kumar Jain
Er. Tulsi Ram Bhattarai
Er. Bharat Bahadur Dhakal
Dr. Bhim Kumar Dahal
Er. Mandakini Karki
Er. Harish Paneru
Er. Jibendra Mishra
Er. Rajan K.C.
Er. Indu Sharma Dhakal
Er. Tuk Lal Adhikari
Dr. Bishwa Ranjan Shahi
Dr. Basanta Raj Adhikari
Dr. Mohan Prasad Acharya
Dr. Dhundi Raj Pathak
Dr. Suman Panthee
Er. Buddhi Raj Joshi
Er. Prabhat Kumar Jha
Er. Naresh Man Shakya
Er. Subarna Singh Raut
Er. Manab Rijal
Er. Sandeep Sherestha
Er. Pawan Babu Bastola
Er. Ujjwal Niraula
Er. Kushalta Neupane
Er. Saroj Adhikari

Advisory Committee

Dr. Ram Krishna Poudel, IoE, TU, Nepal
Dr. Akal Bahadur Singh, IoE, TU, Nepal
Dr. Chhatra Bahadur Basnet, Geotechnical Engineer, Nepal
Dr. Surendra Tamrakar, Kantipur Engineering College, Nepal
Dr. Dibangar Koteja, Nepal Engineering College, Nepal
Dr. Indra Narayan Yadav, Thapathali Campus, IoE, Nepal
Er. Akhilesh Kumar Karn, Geotechnical Engineer, Nepal
Er. Dipendra Gautam, Cosmos College of Engineering and Management, Nepal
Er. Prem Nath Bastola, Western Regional Campus, IoE, Nepal
Er. Shreedhar Khakurel, Western Regional Campus, IoE, Nepal
Er. Harendra Kalauni, Farwestern University, Nepal
Er. Jay Ram Panthee, Midwestern University, Nepal
Er. Pawan Kumar Shrestha, Geotechnical Engineer, Nepal
Subhash Sunuwar, Engineering Geologist, Nepal
Er. Gyanendra Lal Shrestha, Nepal Tunnelling Association
Er. Uttam Lal Pradhan, Department of Roads, Nepal
Dr. Amod Mani Dixit, NSET, UESC, Nepal
Dr. Santosh Kumar Yadav, IoE, TU, Nepal
Dr. Bhesh Raj Thapa, UESC, Nepal
Dr. Rajan Suwal, Structural Engineers' Association- Nepal
Mr. Ahyutananda Bhandary, Nepal Landslide Society
Dr. Gangalal Tuladhar, Himalaya Conservation Group
Ar. Rajesh Thapa, Society of Nepalese Architecture, Nepal
Dr. Ananta Prasad Gajurel, Nepal Geological Society
Dr. Ranjan Kumar Dahal, Nepalese Society of Engineering Geologists
Dr. Hari Krishna Shrestha, Himalayan Landslide Society
Prof. Dr. Krishna Kant Panthi, NTNU, Norway
Dr. Keshab Sharma, Geotechnical Engineer, Canada
Dr. Arvind Kumar Jha, IIT Patna, India
Prof. Dr. Binod Tiwari, California State University Fullerton, USA
Dr. Gyaneshwor Pokharel, Geotechnical Engineer, USA
Dr. Tara Nidhi Lohani, Kobe University, Japan
Prof. Hemanta Hazarika, Kyushu University, Japan
Er. Naresh Koirala, Geotechnical Engineer, Canada

Scientific Committee

Prof. Dr. Netra Prakash Bhandary
A/Prof. Dr. Indra Prasad Acharya
Dr. Mohan Prasad Acharya
Dr. Bhim Kumar Dahal
Dr. Basanta Raj Adhikari
Dr. Saroj Karki
Dr. Mandip Subedi
Er. Harish Paneru

Government of Nepal
Ministry of Physical Infrastructure and Transport

URL : www.mopit.gov.np
email:info@mopit.gov.np
Tel 4211880, 4211931, 4211655
Fax No.: 4211720
Singhdurbar, Kathmandu, Nepal

Ref.No.

Date: March 13, 2023

Message from the Cheif Guest of Inaugural Program

I am pleased to extend my heartfelt congratulations to all members of Nepal Geotechnical Society (NGS) for organizing the First GeoMandu. I believe this international conference will be a wider platform for geotechnical engineers, geo-researchers, and academics from different parts of the world to share their latest findings, research, and best practices, and holds a great importance to the field of geotechnical engineering, geohazards, and geo-infra disasters.

As the Deputy Prime Minister of this country, I acknowledge and appreciate the contributions NGS has made to the field of geotechnical engineering in Nepal over the years. I am confident that NGS has played a crucial role in sustainable development of national infrastructures and economy. As one of the important platforms to share and exchange geotechnical knowledge, this conference as I suppose will be an opportunity to all national and international professionals towards networking for a better and safer world leading to new collaborations, partnerships, and professional development, which I also believe will contribute to an accelerated development of our nation.

The theme of this international conference, Geohazards and Geo-Infra Disasters, is highly relevant to our context in Nepal because of the unprecedented challenges we face in these fields. The need for innovation and sustainable geotechnical solutions has become increasingly important, and we must work together to come out with newer technologies, new methods, and better strategies to help build safer habitats and sustainable infrastructures.

We have come through profound impacts of the COVID-19 pandemic on all aspects of our lives and expect to be affected further by hard-hit world economy. Building infrastructures of all kind especially in a country like ours where we still strive for faster national roads, multipurpose high dams, congestion-free urban roads, mass rapid transit, and so on, I think will help us grow faster even in the post-pandemic period of difficulties. Geotechnical engineering surely remains on the base of all these infrastructures, and I am sure the NGS members will play a key role in our efforts to build national infrastructures and overcome the challenges of the 21st century.

Finally, I would like to thank the organizing committee of GeoMandu for inviting me to the inaugural program. I hope the conference will be a great success.

Thank you.

Narayan Kaji Shrestha
Deputy Prime Minister

ISSMGE SIMSG

INTERNATIONAL SOCIETY FOR SOIL MECHANICS AND GEOTECHNICAL ENGINEERING

Message from the ISSMGE President

March 13, 2023

First and foremost, I congratulate the Nepal Geotechnical Engineering Society and all its members for taking initiatives to hold **GeoMandu.** Holding this international conference series, every three years would be an event that the ISSMGE would fully support. I am confident that this first GeoMandu scheduled for 16-17 March 2023 will be a great success, and promise that the next one will not occur without my presence in person. Who wouldn't visit the highest country on the planet !

As a member of the International Society for Soil Mechanics and Geotechnical Engineering (ISSMGE), Nepal Geotechnical Engineering Society has played an important role in strengthening and expanding the geotechnical network in Asia. ISSMGE currently has a world network of 90 national member societies, in which the biggest representation is from Europe with 38 and Asia stands second with 26. Of the total 48 nations in Asia, nearly half do not have geotechnical societies and ISSMGE will not spare any effort in making all of the Asian countries be part of the international geotechnical engineering family, in fact all countries in the world. Despite their remote location and as a young society, the Nepal geotechnical Engineering Society represents an inspiration to other countries and now a leader with this international conference.

I took the office as the ISSMGE President last May and since then I visited 13 countries with 18 travel trips in less than a year supporting geotechnical activities and events. I like to apologize for not being able to join in person this time because of my schedule conflict, but assure all my friends and colleagues in Nepal that I will visit you soon. I am so happy and honoured to be with you online at the inauguration of GeoMandu, with a congratulatory message and presentation of our ISSMGE family.

As far as I know, Nepal is essentially a mountainous country with active tectonics and comparatively heavy amount of annual precipitation. These three natural conditions combined with high level of vulnerability are the main causes of natural disasters, subjects of some main Technical Committees of ISSMGE such as TC 203, 208, 213, 303, & 304. So, in this sense, the theme of this first GeoMandu, "*Geohazards and Geo-Infra Disasters*" seems quite relevant and pertinent in context of Nepal and I encourage the participants to take part and serve on those ISSMGE Technical Committees. The soil mechanics and geotechnics of the geohazards and geo-infra disasters are the fundamental topics to be discussed while we plan for the mitigation of natural disasters. I am certain that this milestone conference of Nepal Geotechnical Engineering Society will help draw a course of better plan for the mitigation of geodisasters.

With these words, I would once again like to congratulate Nepal Geotechnical Engineering Society for holding this international conference on such an important theme worldwide.

Thank you.

Dr. Marc Ballouz
President of ISSMGE
President.ISSMGE@gmail.com
+15127891335

March 13, 2023

Message from the ISSMGE Vice President (Asia)

It is an honor for me to send this congratulatory message to Nepal Geotechnical Society colleagues for the successful efforts they have made in organizing the first GeoMandu, an international conference series of the society. As the Vice President of International Society for Soils Mechanics and Geotechnical Engineering (ISSMGE) for the Asian Region, I would represent all geotechnical engineering fraternity of Asia as well as the whole ISSMGE network to express our good wishes to all the members of Nepal Geotechnical Society for their prosperity and development.

As an Asian member society of ISSMGE, Nepal Geotechnical Society has been playing an important role in strengthening the geotechnical engineering network. I have come to know that it has already completed 28 years since its establishment and has been in the ISSMGE network for more than 25 years by now. These long years are evident that Nepal Geotechnical Society is an important member society on the ISSMGE.

I have been in the office of ISSMGE Vice President for Asia since 2022. Many countries in Asia are still out of the geotechnical engineering network. I hope that Nepal society provide a good example for the existing and future affiliated societies in Asia region.

Finally, I wish the GeoMandu be a successful event and hope the attendees enjoy the time in Kathmandu.

Keh-Jian Shou

.....

Keh-Jian Shou, Distinguished Prof., Ph.D.
Vice President (Asia)
International Society for Soil Mechanics and Geotechnical Engineering
13 March 2023

Message from the Organizing Committee Chair

First of all, I thank all the supporting hands in our mission to make this international conference of Nepal Geotechnical Society a success.

As a testimony to this international conference, we have come up with this volume of conference proceedings, which only consists of extended abstracts of the submitted papers while we also plan to publish the final volume of proceedings in a book form later within this year. We will collect the full papers after the conference and review them for final acceptance. Springer Nature will take all responsibilities to edit and publish the book in international standard and quality. We look forward to receiving the full papers from all extended abstract submitters.

Our initial plan to have this conference was for November 2021, but the situation of COVID-19 spread and control measures taken thereafter led us to postpone it twice, once to May 2022 and the next to March 2023. From the conception to final conference dates, we have had enough time to prepare; yet there have been so many unforeseen hurdles in between that have led us to work in rush in the last 3-4 months, just ahead of the conference dates. Through this message, I as the Chair of the organizing committee would like to apologize to all participants, presenters, and invited speakers for irregular and delayed communications we made during the last few months. Finally, we are ready to have this international conference held as scheduled, and I do appreciate the help we have received from all our well wishers, program sponsors, local stakeholders, and our members.

We have planned this international conference to be a brand event of Nepal Geotechnical Society, and we have named it "GeoMandu," an NGS international conference series. This is the first GeoMandu and the conference theme for this first event has been chosen to be "Geohazards and Geo-Infra Disasters." Needless to mention but Nepal is blessed with dynamic crustal landforms, high mountains, and heavy precipitation. All these natural conditions and phenomena, at the same time, are often unwanted elements since they promote disasters. When we talk of geotechnical engineering in Nepal, we mostly come across geohazard issues of natural disasters. More recently, as we move forward with building transportation and energy infrastructures, we confront with the geo and infrastructure-related disasters, which are more of anthropogenic nature or human intervention-related events. So, Nepal Geotechnical Society should be committed to put all its efforts in ensuring zero disasters in geotechnical engineering projects.

Holding an international conference in this part of the world is always difficult, mainly in terms of attracting international participants and doing it on an international standard. Resources are surely a constraint but culture is more importantly an issue that needs to be changed. The whole human society here moves with its own culture but international presenters and participants need more time to plan and prepare. This time, we have not been able to attract as many international participants as we initially planned for, and the reason is lack of preparation at our side. For this, I as the Chair of the organizing committee as well as the President of the society do apologize to all our members and well wishers.

In this conference, we have invited our South Asian national member society colleagues too. Currently, we have India, Bangladesh, Nepal, Pakistan, and Sri Lanka in the ISSMGE network, but because of schedule conflict of Bangladesh and Pakistan, we will have representation from India and Sri Lanka only although we have requested Bangladesh to be a part of this conference by joining us online. Exploiting this opportunity, we have proposed a plan to build a loose South Asian Association of Geotechnical Societies (SAAGS), and we also plan to hold a meeting of attending South Asian member nation delegates in this direction. I thank our South Asian member nation colleagues for accepting our invitation.

To witness the status of geotechnical engineering in Nepal, we have also invited the ISSMGE President Dr. Marc Ballouz and the Vice President for Asia Prof. Dr. Keh-Jian Shou. President Dr. Ballouz is set to show up online with a message during the opening program, but Vice President Prof. Dr. Shou is with us here in the conference venue for his message during the opening program as well as for a keynote lecture. On behalf of the whole Nepal Geotechnical Society family, I thank these two top gentlemen of our geotechnical fraternity in the world.

Last but not the least, this international event of ours is going to be successfully held because of our individual and institutional participants, paper presenters, invited and keynote lecturers, and more than anyone because of our sponsors. Through this message, I thank all the above individuals, institutions, and organizations. Thank you!

.....

Netra Prakash Bhandary (Prof. Dr.)
Chair, Organizing Committee, the First GeoMandu
President, Nepal Geotechnical Society
16 March 2023

Message from the Conference Convener

Dear esteemed colleagues and attendees,

It gives me great pleasure to welcome you to the first and the largest international conference of the Nepal Geotechnical Society, GeoMandu 2023, held on 16-17 March 2023 held at Radisson Hotel, Lazimpat. We are honored to host a diverse group of experts and scholars from around the world who have gathered here to share their knowledge and insights with us. This conference presents a unique opportunity for us to engage in meaningful discussions and exchange ideas on a wide range of topics related to our field. Our goal is to foster collaboration and promote innovation that will help us tackle the challenges of our time. In the line with the theme of this year's conference, I want to emphasize the importance of this event in advancing the field of "Geohazards and Geo-Infra Disaster". Our discipline plays a crucial role in ensuring the safety and stability of infrastructure projects, as well as protecting the environment. Through our discussions, I am confident that we will be able to come up with radical approaches and strategies to address these challenges.

As we gather for this international conference, let us be mindful of the importance of our work and the impact it can have on society. Our research, ideas, and collaborations have the power to shape the future of our respective fields and make a difference in the world.

Because of still ongoing restrictions on international travels, the conference programs have been designed to take place in hybrid mode so that some international participants and speakers may also join the conference online. The conference is going to be participated by about 40 international, 10 SAARC and 200+ national participants from the entire civil engineering and geotechnical fraternity along with government policy makers as well as entrepreneurs from various sectors. The conference will also have international geotechnical engineers/researchers and experts as participants along with the international delegates from ISSMGE (International Society for Soil Mechanics and Geotechnical Engineering) in addition to many eminent national speakers. I strongly encourage all , of you to actively engage in the conference sessions, ask questions, and participate in the various workshops and presentations. This is a chance for us to learn from each other and to explore new perspectives and approaches to geotechnical challenges.

I would also like to extend my gratitude to all the sponsors, organizers, and volunteers who have worked tirelessly to make this event possible. Your dedication and commitment are truly commendable.

Finally, I encourage all participants to take full advantage of this opportunity to network, learn from one another, and build lasting professional relationships. I wish you all a fruitful and enjoyable conference.

.....

Mandip Subedi (Dr.)
Convener, the First GeoMandu Conference
Vice President, Nepal Geotechnical Society
16 March 2023

Table of Contents

#key-1:

On the Landslide Hazard with the Impact of Climate Change in Taiwan

K.J. Shou[1], W.J. Lin[1], W.C. Lai[1]
[1]Department of Civil Engineering
National Chung-Hsing University, Taiwan

1. INTRODUCTION

Following the Hyogo Framework for Action, initiated on the 2005 World Conference on Disaster Reduction (WCDR), Sendai Framework for Disaster Risk Reduction (SFDRR) was presented in 2015, in which the disaster resilience was more clearly defined to improve the capabililty of recovering from a disaster, by the countermeasures in the aspects of social, economy, policy, etc. The most popular definition of resilience could be "the capability of an ecosystem enduring external disturbance and returning to the state before the disturbance". But it is still scarce for the research on the quantitative disaster resilience, including the geohazard-related reslilience. In view of the rainfall induced landslide hazards in Taiwan, quantifying and enhancing the resilience are critical to protect the life, property, and infrastructure in the landslide area. This study comprises two major part, i.e., calculating the landslide susceptibility as a hazard factor, and collecting data of the control factors, then establishing the landslide resilience model of the research area.

2. METHODOLOGY

The study area is located in the upstream of Wu River watershed in Central Taiwan, with focuses on the mountain highway and the six villages (see Figure 1). Data of the landslide causative factors and the resilience control factors before and after rainfall events in study area were collected, then the landslide susceptibility values were calculated and the landslide disaster resilience models were established.

2.1 Rainfall predictions

This study employs rainfall frequency analysis together with the atmospheric general circulation model (AGCM) downscaling estimation to understand the temporal rainfall trends (see Fig. 4), distributions, and intensities in the adopted study area in Central Taiwan.

To assess the spatial hazard of the landslides along the mountain highways, landslide susceptibility analysis was applied. Landslide susceptibility model established by logistic regression method was applied and discussed.

2.2 Landslide Susceptibility Analysis

This study adopted the Logistic Regression method of Lin (2016), with the nine causative factors, i.e., elevation, slope, slope, dip slope index, distance to fault, distance to road, distance to river, greenness index, and 72 hour cumulative rainfall. Among them, the hourly rainfall data

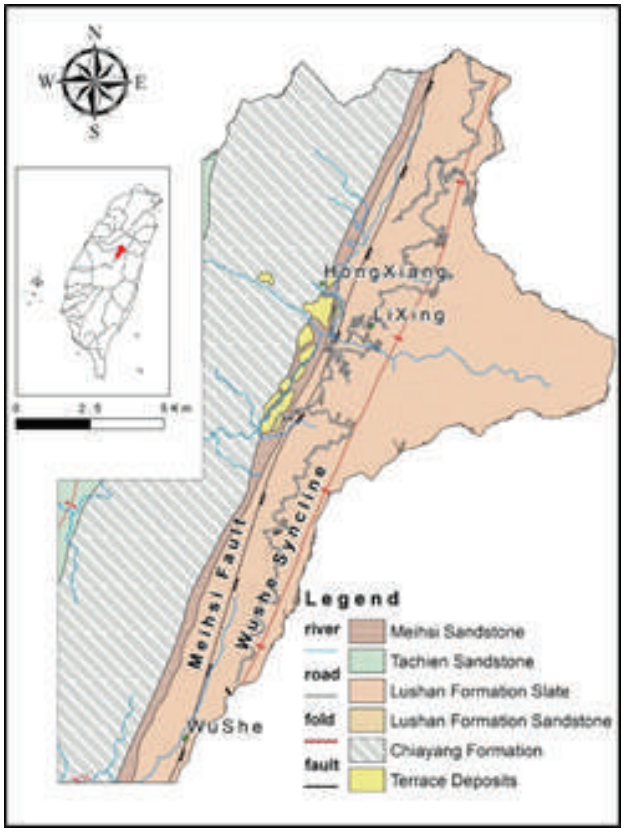

Figure 1. The location and geology of the study area study are in the upstream of Wu River watershed in Central Taiwan.

during 2012~2017 was further analyzed to find the largest 72-hour cumulative in a quarterly basis for each rainfall station, such that we can explore the spatial changing trend of rainfall in the study area.

Considering the villages as the analysis units, the Thiessen's Polygon method was used to obtain the rainfall distribution. By introducing the seasonal rainfall data to the following Logistic Regression model of Lin (2016), as described in Eq. (1), we can obtain the seasonal landslide susceptibility values of each village.

$$ln\ [P\ /(1-P)]=-0.577*F1+1.545*\ F2+0.077*F3-0.038*F4-0.242*F5-0.102*F6-0.458*F7-3.564*F8+0.560*F9-0.406 \quad (1)$$

3. RESULTS AND DISCUSSION

By using Eq. (1), we can estimate the landslide susceptibility of 2009 Morakot and 2012 Saola based on their specific rainfalls. The ROC curves for these estimations shows the AUC values are 0.806 for 2009 Morakot and 0.717 for 2012 Saola, which also reveal an acceptable performance of the 2004 Mindulle model. For the predictive analysis, the rainfall in the future was estimated by the climate change model introduced as below. The Taiwan Climate Change Projection and Information Platform Project (TCCIP), analyzes the results from the assessment reports of the United Nations

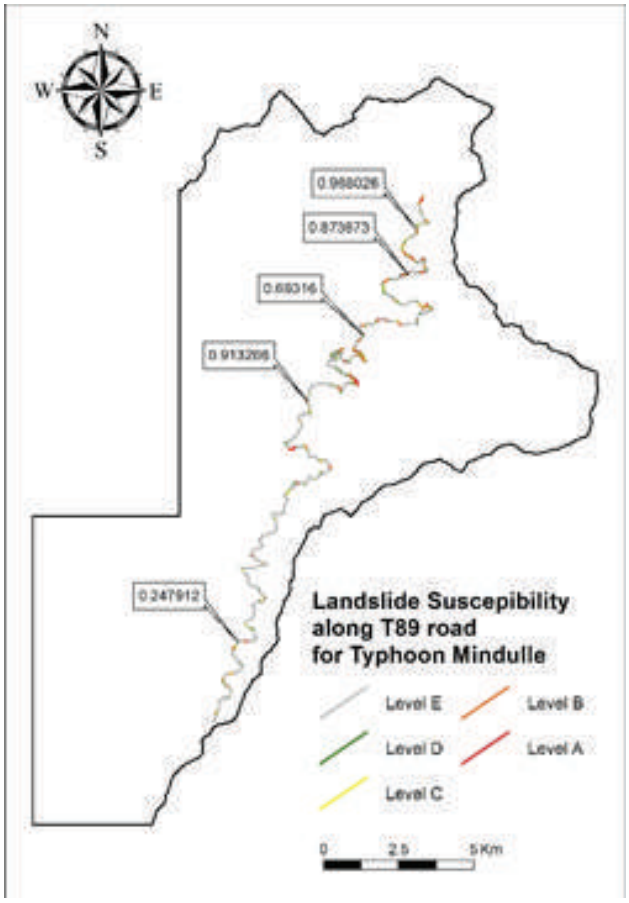

Figure 2. The landslide susceptibility along Nantou County Road #89 estimated by 2004 Mindulle model

Table 1: Comparison of the Landslide Susceptibility and Risk Ranking of the Large Scale Landslides ge distribution of Nepal Geotechnical

Site	Mindulle Landslide Susceptibility		Predict Top1 Typhoon(2075-2099) Landslide Susceptibility	
	Value	Ranking	Value	Ranking
12k+300	0.9680	1	0.9665	1
15k+850	0.8737	3	0.8683	3
22k+530	0.6932	4	0.6880	4
32k+500	0.9133	2	0.9147	2
49k+000	0.2479	5	0.2713	5

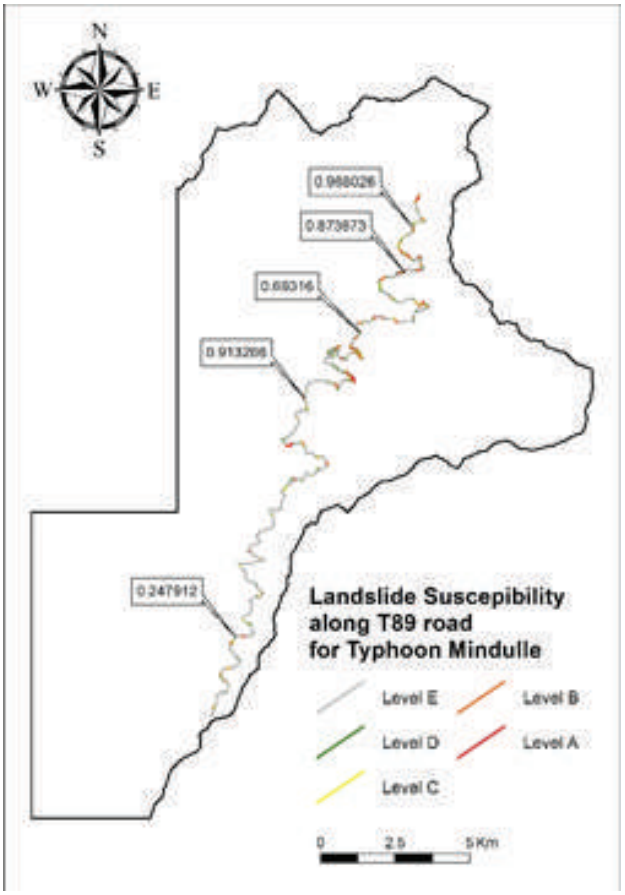

Figure 3. The landslide susceptibility along Nantou County Road #89 estimated by the TCCIP Top1 Typhoon

Intergovernmental Panel on Climate Change (IPCC), results of 2004Mindulle and Top1 Typhoon show as figs. 2~3, and compare of cells number as Table 1.

4. CONCLUSION

In this study, rainfall frequency analysis and the atmospheric general circulation model (AGCM) downscaling estimation were applied to understand the temporal rainfall trends and distributions in the study area. The susceptibility analysis in catchment scale and local scale were performed for the hazard assessment of the mountain highway, i.e., Nantou County Road # 89 in Central Taiwan. The hazard of the major landslides can be ranked to prioritize the hazard mitigation. It is worth noting that the results of local scale analysis also suggest a similar hazard ranking of these landslides, i.e. the sites 15k+850 and 12k+300 are the most dangerous.

ACKNOWLEDGEMENT

This research was made possible by the financial support of the Ministry of Science and Technology (Project No. 107-2625-M-005-005-005) of Taiwan. We also deeply appreciate the databases and support from the research groups conducting the Central Geological Survey project (Project No. 97-5826901000-05).

REFERENCES

Central Weather Bureau, Taiwan. 2016. Records of historical typhoons. http://www.cwb.gov.tw in Chinese.

Chu, H.J., Pan, T.Y., Liou, J.J. 2011. Extreme precipitation estimation with Typhoon Morakot using frequency and spatial analysis. Terr. Atmos. Ocean. Sci., 22 (6), 549–558.

Shou, K.J. and Yang, C.M. 2015. Predictive analysis of landslide susceptibility under climate change conditions – a Study on the Chingshui River Watershed of Taiwan. Engineering Geology, 192. 46-62

Swets, J.A. 1988. Measuring the accuracy of diagnostic systems. Science, 240, 1285-1293

#Key-2:

Geohazards in Mountain Environments in Response to a Rapidly Changing Cryosphere and the Role of Geotechnical Engineering

Lukas U Arenson[1]
[1]*BGC Engineering Inc.*
Vancouver, BC, Canada

1. INTRODUCTION

Not only in terrains north of 60° latitude, geotechnical designs and geohazard are affected by cold climate, glaciers and permafrost but also many areas around the world are subject to impacts from freezing conditions or are affected by permafrost, in particular within high mountain regions. As climate is changing, historic records may no longer be representative for future behaviour, making designs and geohazard assessments that rely on the past unreliable and difficult. Specifically, the glacial and the periglacial environments are changing at fast and unprecedented rates. These changes in the mountain environments around the world lead, on the one hand, to the disappearance of some hazards, e.g., lack of ice falls in response to rapid glacier retreat, but on the other hand to the creation of new ones, such as instabilities due to glacial debuttressing or increased potential for glacier lake outburst floods, as new proglacial lakes form and mass movement activities increase. In addition, permafrost, which in many mountain regions around the world is typically discontinuous, in spatial terms, and warm, is expected to degrade further and disappear with time, affecting infrastructure foundations and slope stabilities. With the inability of using historic geohazard behaviour and processes to make projections about the future, e.g. the development of frequency magnitude correlations, new approaches are needed in the evaluation of geohazards in mountains environment in response to the rapidly changing cryosphere.

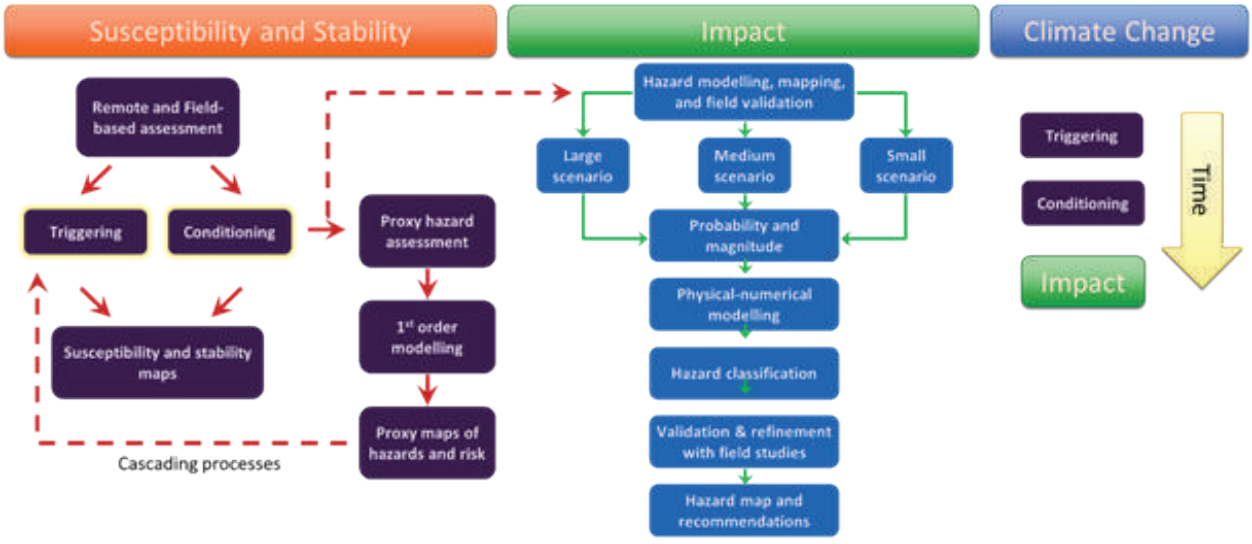

Figure 1: Framework for glacier and permafrost hazard assessment. Generally, the assessment of impacts is of most relevance for risk mitigation measure design and climate change adaptation planning (after GAPHAZ, 2017).

2. METHODOLOGY

In 2017, the Standing Group on Glacier and Permafrost Hazards in Mountains of the International Association of Cryospheric Sciences and the International Permafrost Association presented a guideline on how to assess hazards from glaciers and permafrost in mountain regions (GAPHAZ, 2017). This framework, which was expanded by explicitly adding climate change as shown in Figure 1, is a valuable tool for evaluating hazards in a changing mountain environment. It highlights key elements and necessities, such as the importance of remote and field based data collection and assessment, the iterative nature of the process, the use of different scenarios in the assessment and the value of modelling. Climate change impacts the triggering mechanisms and the conditioning factors. It is therefore important to evaluate how climate change impacts these factors and ultimately the hazards over time. Due to the natural dynamics of these environments it is challenging to project how some of these factors and elements behave in response to a changing climate. Hence, it is critical that a processes-based approach with multiple scenarios and appropriate probability langue is used when assessing geohazards or preparing geotechnical designs in areas that may be directly or indirectly impacted from changes in the cryosphere of mountain ranges. With cascading processes having impacts at large distances away from the initiation zone (triggering) expanding the region to be evaluated is important.

3. CONCLUDING REMARKS

Geotechnical engineers play a key role in evaluating geohazards in mountain environments in response to climate change because of their geophysical process understanding, systematic approaches and experience designing with uncertainties. They have the tools to calculate slope stabilities and provide guidance for site investigations that are necessary in order to understand the key parameter that control the triggering mechanisms and the conditioning factors.

ACKNOWLEDGEMENT

The author would like to thank the organizers of GeoMandu for the invitation to present this work.

REFERENCES

GAPHAZ 2017: Assessment of Glacier and Permafrost Hazards in Mountain Regions – Technical Guidance Document. Prepared by Allen, S., Frey, H., Huggel, C. et al. Standing Group on Glacier and Permafrost Hazards in Mountains (GAPHAZ) of the International Association of Cryospheric Sciences (IACS) and the International Permafrost Association (IPA). Zurich, Switzerland / Lima, Peru, 72 pp.

#Inv-2:

Steep Creek Hazards and the 2021 Flood Events on the Melamchi River

Hamish Weatherly[1]
[1]*BGC Engineering Inc.*

1. INTRODUCTION

Steep creek or hydrogeomorphic hazards are natural hazards that involve a mixture of water ("hydro") and debris or sediment ("geo"). Identifying and assessing hydrogeomorphic hazards is becoming increasingly important as populations increase in mountainous environments and climate change effects (e.g., glacier and permafrost melt exposing unconsolidated sediments, increased rainfall) impact their frequency and magnitude. This presentation provides an overview of steep creek hazards and how to differentiate between the processes based on topographic and geomorphic evidence. A case study of the Melamchi Water Supply Project (MWSP) is then discussed within this framework. The MWSP diverts water from Melamchi River to Kathmandu, Nepal through a 26 km long conveyance tunnel.

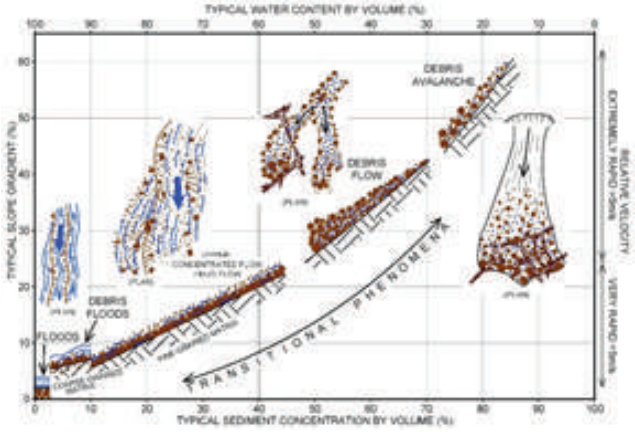

Figure 1: Hydrogeomorphic process classification by sediment concentration, gradient, velocity, and morphology.

2. HYDROGEOMORPHIC PROCESSES

Rivers in mountainous terrain are typically subject to a spectrum of processes ranging with increasing sediment concentration from clearwater floods to debris floods to debris flows (Figure 1). Debris floods most commonly occur in steep (>5%) mountain channels and on their alluvial fans but can also occur on gravel-bed rivers with watershed areas up to several thousand square kilometers (Church & Jakob, 2020). Debris flows dominate in steeper channels (>27%) with smaller watershed areas (typically < 10 km2).

Two broad levels of identification can be used to differentiate between hydrogeomorphic processes: the morphometry of the contributing watershed and the characteristics of channel/fan deposits. For the former, hydrogeomorphic processes can be initially differentiated based on the stream length and 'Melton Ratio' of the

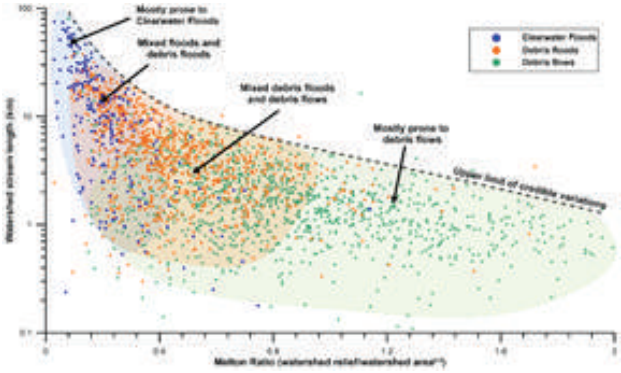

Figure 2: Dominant hydrogeomorphic processes as a function of Melton Ratio and stream length (after Church and Jakob, 2022).

drainage basin (Figure 2). The Melton Ratio is the dimensionless quotient of drainage relief (H) and area (A) (i.e., M= H/$\sqrt{A}$) and provides a measure of the steepness of the watershed.

Within the past 20 years, the English term 'debris flood' has come into use to describe severe floods involving exceptionally high rates of coarse bedload transport in steep channels. The onset of a debris flood is defined by

the exceedance of a critical shear stress threshold required to mobilize at least the D84 of bed material. Church and Jakob (2020) developed a three-fold typology for debris floods, which had previously not been defined well. In all cases, high bedload volume is triggered by the exceedance of a critical force acting on the bed. In a Type 1 debris flood, the flow exceedance occurs gradually in association with a storm hydrograph and the concomitant increase in flow depth and shear stress. Alternatively, a debris flood may develop abruptly through dilution from a debris flow in which the flow mechanics switch from visco-plastic to Newtonian (Type 2), or through the collapse of a moraine-, ice-, landslide-, beaver- or man-made dam (Type 3).

Hyperconcentrated flows are a special case of debris flood that can occur as Type 1, 2 or 3 debris floods. This term is reserved for volcanic or weak sedimentary fine-grained slurries, where the concentration of suspended fine sediments (~10-15%) is sufficient to impart yield strength to the fluid and maintain high fluid viscosity (Pierson, 2005). In such flows, sands and gravels are kept in suspension by turbulence and dynamic grain interactions

3. MELAMCHI RIVER 2021 FLOOD EVENTS

The Melamchi River has a catchment area of 324 km2 above its confluence with the Indrawati River at Melamchi Bazaar. At the diversion headworks site, the catchment area is 161 km2 at an elevation of 1430 m. Elevations reach a maximum of 5,916 m in the upper watershed.
Construction of the Melamchi River diversion headworks was underway, and scheduled to be complete in September 2021, when catastrophic floods impacted the headworks on June 15 and August 1, 2021. The floods inundated the headworks area, buried the headworks structures under a 15 to 25 m thickness of sediment, washed away roads, bridges, and construction camps, and killed more than 10 people.

Above the headworks site, the Melamchi River is generally confined for much of its length. During the June 15 event, up to 15 m of scour was observed in one bedrock-confined reach. Sediment was also sourced from ravelling colluvial sideslopes and numerous river-side landslides. The combined deposition volume of the June 15 and August 1 events was estimated to be 20 million m3 based on digital elevation model comparison by TA (2022).

Residents of Melamchi Bazaar reported that each event lasted about one day, with a long, gradual rise to the peak discharge. This description suggests that both events were a Type 1 debris flood. However, the situation is more complex and nuanced. Neither event can be characterized as a debris flow, as the channel gradient is approximately 10-15% for 15 km upstream of the headworks diversion, which is insufficiently steep for transport of a coarse-grained debris flow.

High-water marks observed at several locations suggest that the June 15 event had a maximum discharge of approximately 2,500 m3/s. In contrast, maximum annual daily flows are typically in the range of 40 to 80 m3/s at the headworks. Also, rainfall recorded at regional stations was not unusual for either 2021 flood event (TA, 2022), although there are no climate stations in the upper watershed.

The 2,500 m3/s peak discharge is likely best explained by a glacial lake outburst flood (GLOF), which is documented as having occurred in the upper watershed during the June 15 event (TA, 2022). It is hypothesized that the GLOF (Type 3 debris flood) was of sufficient magnitude to initiate transport of the D84 and destabilize the entire channel, allowing Type 1 debris flood conditions to persist for the better part of the day in its wake.

A landslide dam located about 15 km upstream of the headworks site was also destabilized during the June 15 event. The landslide dam is likely at least hundreds of years old and has infilled over time, creating the Bhemathan depositional plain with an estimated sediment volume of 21 million m3.

Based on eye-witness accounts, the August 1 event was of lower magnitude than the June 15 debris flood. However, this event was also associated with significant sediment transport rates. Because the entire channel had been destabilized by the June 15 event, initiation of a Type 1 debris flood would have been able to occur at a significantly lower discharge on August 1. Also, ongoing

erosion at the Bhemathan landslide dam resulted in significant retrogression into fine-grained deposits (sands and silts). Mobilization of these fine sediments would have enhanced sediment mobility, potentially creating hyperconcentrated flow conditions if suspended sediment concentrations were sufficiently high (~10-15% by volume). Available photographs of the August 1 event do suggest very high suspended sediment concentrations including large boulders that appear to be floating on top of the flow, consistent with a hyperconcentrated flow rheology.

4. CONCLUDING REMARKS

Following the 2021 debris floods, the Asian Development Bank (ADB) established a Technical Assistance Team to carry out a two-phase assessment of the Melamchi River catchment and the river diversion headworks. Phase 1, completed in July 2022, diagnosed the causes and triggers of the 2021 events, and examined the feasibility of stabilizing the catchment and river (TA, 2022). Phase 2, which is ongoing, includes assessing the impacts of the 2021 events on the river diversion headworks and identifying cost effective measures to rehabilitate and improve the functionality and sustainability of the headworks. BGC Engineering is a member of the TA Team.

ACKNOWLEDGEMENT

The author would like to acknowledge Saugata Dasgupta and Sujan Regmi of the ADB and the other members of the TA Team (Hans Enggrob, Sanjiv Shah, Gyanendra Shrestha, Mahesh Bhattari, Alex Strouth, Adrian Gygax and Daley Clohan).

REFERENCES

Church M and Jakob M. 2022. What is a debris flood? Water Resources Research, 56(8), e2020WR027144.

Pierson TC. 2005. Hyperconcentrated flow – Transitional process between water flow and debris flow. In M. Jakob, & O. Hungr (Eds.), Debris flows and related phenomena (p. 159–202). Heidelberg: Springer.

Technical Assistance 6596-NEP (TA). 2022. Damage Assessment of Melamchi Headworks and Hazard Mapping of the Catchment [Updated Final Report – Phase 1]. Prepared for Asian Development Bank.

#Inv-3:

Understanding Complex Cascading and Compounding Impacts of Natural Hazards

Bhesh Raj Thapa[1], Rocky Talchabhadel[2]

[1]Universal Engineering and Science College, Pokhara University, Lalitpur, Nepal

[2]Texas A&M AgriLife Research, Texas A&M University, El Paso, TX, USA

1. INTRODUCTION

Heavy downpours or/and prolonged precipitation in the upstream areas of the Himalayan region can lead to flash floods, landslides, debris flows, and river blockages. Rapid unplanned human activities compounded with climate change resulted in several cascading hazard-related disasters. Natural hazards and cascading failure are common in the Himalayan region due to extreme elevation gradient, young and fragile geology, extreme seasonal and spatial variation in rainfall, and diverse human impacts.

Recent events (such as 2012 Kharapani Debris/Flood, 2013 Uttarakhand Flood, 2014 Jure Landslide, 2021 Chamoli Landslide, and 2021 Melamchi Debris/Flood) have underscored the need to better understand the complex interactions between human, natural, and engineered systems in order to create effective disaster management strategies.

These cascading and compound hazards have severe economic, infrastructure, and livelihood repercussions, and often lead to acute and chronic disasters. To address this, it is necessary to create a comprehensive framework that identifies and tracks the links between the various factors and the associated risks in the Himalayan region. This study analyzed the 2021 Melamchi flood (June 15, 2021).

2. METHODOLOGY

W gather the periodic rainfall data. The land use land cover and soil-related data are used to estimate Curve Number values for hydrologic modeling. Rainfall-runoff modeling was conducted using the HEC-HMS, and the runoff-inundation was conducted using the HEC-RAS. We use an overtop dam break method in the HEC-HMS to predict peak discharge based on dam breach. Using the remotely sensed data, the landslide susceptibility was delineated using the Random Forest machine learning model. As the 2021 Melamchi disaster was caused by a combination of hydroclimatic and geomorphological processes, rather than simply one extreme event, we integrated remote sensing data, hydrologic and hydrodynamic modeling, and machine learning techniques.

3. RESULTS AND DISCUSSION

The landslide susceptibility is highly concentrated in the upstream regions (Melamchi, Yangri, and Larke basins). It is therefore essential to evaluate the resiliency of settlements and infrastructures in these areas to anticipate potential future landslides.

Following the 2015 Gorkha Earthquake, the Melamchi watershed experienced several damages, including landslides and fractures. While the rainfall during the event was not considered an extreme hydrometeorological event, such as a cloudburst, it was able to cause sediment disasters due to the transportation of landslide masses and high-altitude glacial deposits, resulting in debris flow. Water infiltration through the fractures may also lead to hillslope instability and mass failure.

Based on several damming scenarios, we find that 12- to 16-h obstruction seems more realistic than 8- and 10-h

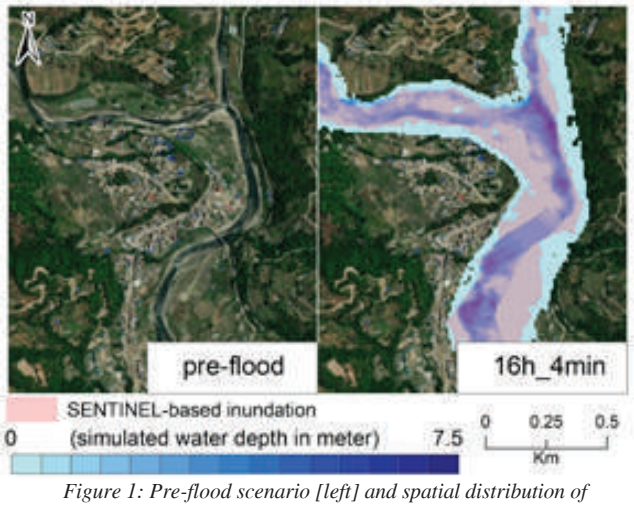

Figure 1: Pre-flood scenario [left] and spatial distribution of simulated inundation [right] overlaid over satellite-based inundation in Melamchi Bazar.

scenarios. We estimate nearly 2000 m3/s of peak discharge from the landslide damming location with a scenario of 16 h damming and a dam breaching time of 4 min (i.e., 16h_4min scenario, Figure 1).

We propose the development of a data-driven probabilistic model that integrates hydroclimatic models, remotely sensed data and non-traditional data streams (such as Citizen Science and expert knowledge). This model would serve as an operational decision support tool, allowing stakeholders to perform 'what-if' analyses and develop mitigation strategies. We also suggest establishing a cyberinfrastructure or mobile apps.

4. CONCLUDING REMARKS

The analysis revealed that the landslide dam's outburst, combined with heavy downpours, triggered a sudden release of large volumes of water, which flooded vast areas and caused damage up to Melamchi Bazar downstream.

This emphasizes the need to consider a series of non-extreme events when assessing risk, in addition to extreme events.

#Inv-4:

Escalating Highway Infrastructure Vulnerability in Nepal due to Climate Change Effects

Prabhat Kumar Jha[1]

[1]*Superintendent Engineer, Department of Roads, Ministry of Physical Infrastructure and Transport, Kathmandu, Nepal*
Email: geoprabhat@gmail.com

1. INTRODUCTION

The transportation industry holds immense potential to enhance the lives and livelihoods of billions of people. However, it is imperative that the sector not only meets the present needs of people but also prepares itself to cater to the expectations of future generations, which is the crux of sustainable development. In line with this, the government's policy for the transportation sector is to establish a dependable, cost-effective, safe, and sustainable transport system that contributes to environmental, social, and economic objectives.

Looking ahead, our long-term targets for 2100 encompass the development of all highways to meet the Asian Highway standard with 4 to 8 lanes, a multimodal transport system, and high-speed transport modes for travel between the federal capital, province capitals, and inter-provincial cities. Additionally, we aim to increase the road density from 0.55 Km per Sq.km (based on the year 2018) to 1.00 Km per Sq.km. Furthermore, we endeavor to expand the road network such that the percentage of families with access to motor transport within 30 minutes of travel, which currently stands at 82% (based on the year 2018), reaches 99% by 2043/44.

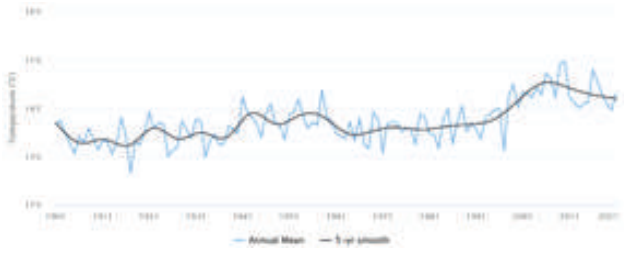

Figure 1: Observed Average Seasonal Mean Temperature (1901-2021)

2. OBSERVATIONAL EVIDENCE OF

Nepal's climate varies considerably both seasonally and according to altitude. Nepal can be divided into different climate zones according to altitude, ranging from the Terai region in the south at less than 500 m above sea level to the High Himalayan region in the north at over 5,000 m. Average temperatures decline from a peak of over 24°C in the south down to sub-zero temperatures in Nepal's highest mountains. Precipitation is spatially variable with some central and northerly pockets of the country receiving more than 3,000 millimeters (mm), the central and southern plains typically receiving 1,500 – 2,000 mm, and some high-altitude areas in the north receiving less than 1,000 mm.

3. IMPACT OF CLIMATE CHANGE ON HIGHWAY INFRASTRUCTURE

Given that transport infrastructure is essential for socioeconomic progress, it's no surprise that approximately one-third of the yearly development budget is dedicated to their development and upkeep. However, the onset of monsoon rains brings with it the threat of floods, landslides, and siltation, which often render these vital lifelines inoperable, requiring costly repairs and reconstruction efforts. Moreover, damaged infrastructure can hinder the functioning of other economic sectors for extended periods, resulting in significant economic losses. The Department of Roads manages an approximately 11,178 km national highway network worth an estimated 250 million USD, which experiences annual losses and damages amounting to around 15 million USD.

Table 1: Road Closure Data of Last 2 years (Major Road)

Code	Blockage in Year 20/21	Road Closure per Event (days)	Blockage in Year 21/22	Road Closure per Event (days)
NH01	8	8	9	65
NH13	18	3	15	14
NH17	5	36	19	3
NH25	24	81	17	237
NH34	29	44	35	64
NH47	19	10	19	12
NH58	35	9	6	8
NH63	10	239	3	122

4. ADAPTATION TO CLIMATE CHANGE

The adaptation strategies for the transportation sector can be categorized into two groups: engineering options, which involve structural changes such as subsurface

conditions, material specifications, cross-section and standard dimensions, drainage and erosion control, and protective engineering structures; and non-engineering options, which include maintenance planning and early warning systems, alignment, master planning and land use planning, and environmental management.

To address existing infrastructure, it may be necessary to increase maintenance contingency budgets in areas that are highly vulnerable to climate change impacts. This will allow for more rigorous supervision and monitoring of the most at-risk areas, reducing the occurrence of road closures and mitigating the severity of disasters. Maintenance planning systems can also incorporate early warning systems to predict extreme events, enabling crews and contractors to prepare for high rainfall events and potential landslides. While this may increase upfront capital costs, it can result in reduced operating expenditures and damages in the future. There is a trade-off between these costs and the potential benefits of preemptive road closures, which may limit property damage and save lives.

5. CONCLUDING REMARKS

As climate change and extreme weather events become increasingly prevalent, transportation systems must incorporate resilience planning to ensure long-term performance and reliability. To achieve this, a variety of tools and strategies are necessary, such as: (i) sectorial and spatial planning that takes into account risk and vulnerability; (ii) resilient infrastructure investments, including physical infrastructure, new technologies, and community-based adaptation; (iii) institutional and capacity support, awareness-raising, and finance to enhance stakeholder capabilities at the policy and regulatory level; and (iv) post-disaster risk and recovery assistance that incorporates climate change risk and resilience into rebuilding efforts.

REFERENCES

D ADPC 2012: Climate Data Digitization and Downscaling of Climate Change Projections in Nepal | TA 7173-NEP: Strengthening Capacity for Managing Climate Change and the Environment

WORLD BANK (June 2019). Improving the Resilience of Nepal's Strategic Roads Network (Criticality Assessment Report)

Government of Nepal, National Planning Commission, Kathmandu, Nepal (2011). Climate-Resilient Planning. [Working Document],

#Inv-5:

A Methodology for Road Cutting Design Guidelines

Ellen Robson[1,2], Andrea Agosti[2], Stefano Utili[2], David Milledge[2]
[1]Durham University (UK)
[2]Newcastle University (UK)

1. INTRODUCTION

One of the most common problems encountered in low and lower-middle income countries (LIC/LMICs) that have hilly topography and an annual 'wet seasons' is the failure of road-side cuttings. Cutting failures in these regions are commonly triggered by heavy rain (e.g., during monsoons or typhoons). However, natural landslide susceptibility is exacerbated by inadequate slope stabilisation design and construction. We believe that one of the reasons for this inadequate engineering is due to a lack of user-friendly but technically sound guidelines for the practitioners who design roadside cuttings (Robson et al. 2021).

Designing a roadside cutting is a trade-off between the desired safety margin against failure and the cost of excavation. In order to determine how steep a cutting can be whilst obtaining a desired safety margin, slope stability analyses are used. In high income countries (HICs), slope stability analyses are conducted for each individual cutting utilising data obtained through detailed and expensive site investigation. Geotechnical engineers use stability charts (e.g. Shen et al. 2013; Wyllie 2017) as a guide for preliminary design. In these stability charts the ground strength is characterised in terms of either the Generalised Hoek-Brown (G-H-B) (e.g. Li et al. 2008, Shen et al. 2013) or the Mohr-Coulomb (M-C) failure criterion (e.g. Wyllie, 2017). Intact rocks and jointed rock masses are best described by the G-H-B failure criterion, whereas highly weathered rocks, residual and alluvial soils are best described by the M-C criterion (Hoek & Brown, 2018).

In LIC/LMICs, it is often not feasible to conduct individual slope stability analyses for every road cutting due to constrained budgets. The existing simpler and cheaper stability charts are often not suitable for preliminary design as they require exact parameter values, and do not include guidelines on how these can be obtained. Therefore, many practitioners design roadside cuttings based on guidelines for cutting inclinations outlined in government and donor agency manuals (e.g. the Philippines: DPWH, 2007; Liberia: MPW, 2019; Nepal: DoR, 2013). However, these guidelines can lack rigor, and be difficult to use. Some ignore important characteristics of the cuttings such as: hardness of the geomaterial, rock weathering, seepage or weakening induced by excavation (e.g. MPW, 2019). They can lack in usability by not including suitable descriptions of rock or soil types (e.g. DPWH, 2007), and not including a description prone to inaccurate use (e.g. DoR, 2013).

In this paper we summarise our methodology presented in Robson, et al (2022) to develop stability guidelines for road cutting inclination design. We demonstrated this methodology by developing a set of road cutting guidelines for Nepal and Ethiopia. The guidelines consider cuttings made in hilly topography (i.e. inclined upslopes), and account for the impact of seepage.

2. METHODOLOGY

The guidelines are presented as tables that display recommended cutting inclinations within geomaterial groups. Common rock and soil types for the area of interest are assigned to these groups based on their strength characterised according to Generalised -Hoek -Brown (G-H-B) and Mohr-Coulomb (M-C) failure criterion, determined through a literature review. G-H-B is used in the majority of cases, whereas M-C is used for soils. The guidelines present the G-H-B parameters of disturbance caused by excavation (D), the structure and weathering state of the rock mass (Geological Strength Index, GSI), and the strength of the rock (Uniaxial Compressive Strength, UCS) as user inputs, alongside descriptions on how to estimate these in the field. The main geomaterial groups are classified according to UCS as this parameter plays a dominant role in defining rock strength (Hoek and Brown, 2019). The remaining parameters that are more difficult to estimate in the field, unit weight (γ) and material constant for intact rock (mi), are built into the table so they do not need to be defined by the user. Cutting heights and factor of safety (FoS) values are also given as user-inputs in the guidelines.

A low (L), intermediate (I) and high (H) value of GSI is defined for each rock grouping, as each rock type has a typical range of potential GSI values and the FoS is sensitive to GSI.

Two separate tables are presented in the guidelines to accommodate different disturbance scenarios: (1) For cuttings that have undergone mechanical excavation or controlled shallow blasting methods where negligible disturbance is caused (D=0), and (2) for cuttings that have been blasted in an uncontrolled manner causing disturbance (D>0). For the latter case, we implement a stepwise functional relationship for the decrease of D with distance from the slope surface (by imposing a parallel layer model, PLM) (Zuo & Shen, 2020).

As the G-H-B criterion has shown to be less accurate to characterise soils, the M-C failure criterion should be used in these cases (e.g. residual soils) (Hoek & Brown, 2018). To be consistent with the L, I, H categorisation adopted for GSI, L, I and H strength categories are defined for combinations of cohesion (c') and friction angle (φ') for soils. Local estimates of c' - φ' combinations are identified from published literature and are ranked in order of strength, with the lowest and highest strength combinations designated to the L and H categories, respectively, and the midpoint strength combination used as the c' - φ' pair for the I category.

Slope height is also a key parameter for the stability of a slope. A range of cutting heights should be included in the guidelines to represent the potential range for road cutting in the area of interest (e.g. for Nepal we used 5, 10, 20 and 30 m).

Where roads are heavily trafficked the economic and social consequence of failure becomes greater and, therefore, it is often desirable to design cuttings with higher FoS. If roads are less heavily trafficked, a lower FoS is desirable to conserve costs. Therefore, the guidelines should include at least two values of FoS to accommodate levels of social acceptability of risk: (1) a FoS value on roads where cutting failure carry low social and economic consequences and (2) a FoS value to represent road cuttings that carry greater social and economic consequences (i.e. more heavily trafficked). Based on literature, for Nepal, we chose to include FoS values of 1.3 for 'low consequences road cuttings' and 1.5 for 'high consequences road cuttings' cutting design.

Stability analyses are then conducted to determine cutting inclinations to achieve the desired FoS for every combination of parameters discussed i.e. both D scenarios for each hardness group (with their assigned values for UCS, γ and mi) for L, I and H GSI category (or c' - φ' combinations for soils) for every cutting height. We recommend performing stability analyses using the rigorous Morgenstern-Price (M-P) Limit Equilibrium Method (LEM).

To further improve the rigor of the guidelines, tables can be developed that include inclined upslope topography to represent roadside cuttings that are bounded on their upslope side by an inclined hillslope. To do so, the model domain for the stability analyses needs to be large enough in the horizontal direction to capture the critical failure mechanism. Hillslope inclinations of 15 and 30° were chosen to represent the topographic inclinations in Nepal.

So far, we have only discussed conducting stability analyses assuming dry conditions. Hydrological properties (e.g. hydraulic conductivity) are highly variable, and the saturation state of the cutting depends on rainfall history and upslope topography. Unfortunately, this information is not available in the vast majority of cases. In order to account for seepage, whilst avoiding adding unnecessary complexity to the guidelines, we recommend identifying the seepage conditions under which a dry analysis remains appropriate (i.e. where seepage does not affect the FoS) and thus where the guidelines remain applicable. To do so, Finite Element steady-state seepage analyses are conducted prior to the stability analyses, with the phreatic line of unconfined flow obtained as result of the analysis. To determine the critical seepage conditions, the total head is incrementally increased, starting from a height corresponding to the height of the cutting toe, until the resulting FoS deviates from that of the dry case by more than 1%. The depth of the phreatic surface from the ground surface is recorded at this point measured at a distance equal to the cutting height upslope of its crest. For scenarios where the slope is fully saturated at a distance H upslope from the cutting crest and the FoS is not affected, a pressure head equal to zero is applied along the uplsope ground surface (instead of imposing the total head along the ridge-side boundary). The extent of this zero-pressure zone is incrementally increased downslope until the FoS deviates from the values obtained in the dry case by more than 1%. In these cases, the distance from the cutting crest to the nearest saturated upslope ground surface point is recorded

3. RESULTS AND DISCUSSION

Guidelines developed following this methodology will include unique tables to represent different disturbance scenarios, sectioned by rock grouping, FoS and GSI (or c' - φ' combination). Each table includes guidance for the practitioner on how to select the appropriate rock grouping and GSI category for their cutting. Additional tables can

be developed for cuttings with inclined topography, and to address seepage.

The following trends are exhibited in the our guidelines, reflecting well know physical principles of slope stability: (1) steeper inclinations with increasing hardness; (2) steeper inclinations with higher GSI values (and combinations of c and φ'); (3) steeper inclinations with decreasing cutting height; and (4) steeper inclination with lower FoS. Where cutting inclinations recommended in the guidelines are below 30° (in the weakest rock groupings), significant excavation may be required. Where this is not feasible, slope stabilisation measures (e.g., walls, anchors or bioengineering) should be implemented to allow a steeper cutting inclination.

A key desirable property of our guidelines is the ability to quantify the error resulting from those uncertainties. To this end, a sensitivity analysis can be performed with the aim of determining the percentage and absolute difference in the cutting inclinations of adjacent categories to assess the sensitivity of the guidelines to the parameter choices that practitioners need to make. We found that the weaker categories were most sensitive to the choices that the practitioner makes, as well as to seepage.

It was also found that the tables for cuttings with inclined upslope did not differ greatly from cuttings

with horizontal upslope. Therefore, it may not be necessary to include these tables.

We tested our guidelines developed for Nepal against stability charts from literature for three slope scenarios (Table 1). Only Scenario 1 included results from Shen et al. (2013) since their charts are only applicable to cuttings of 45°.

Table 1: Comparing the inclinations (°) recommended by our guidelines against stability charts for three slope scenarios.

	Scenario 1	Scenario 2	Scenario 3
Our guidelines	44	60	60
Shen et al. 2013	45	-	-
Li et al. 2008	55	68	73
Wyllie 2017	43	60	57

The outcomes of our guidelines were further corroborated by the Carranza-Torres & Hormazabal (2018) method, with the predictions always within 1%. This test provides a robust validation for our method and lead us to recommend not to use Li et al. (2008) stability charts as a design tool for cuttings.

We also found that our guidelines improved on the usability of stability charts as a practitioner does not need to: make any calculations, nor determine parameter values by site investigation or additional sources. Our guidelines improve on the usability those in existing manuals as they are presented in a concise format, are transparent in the way that they were developed, can be adapted for locations exhibiting different geologies, and offer a choice on the resulting FoS.

Guidelines developed by conducting this methodology are designed to be an inexpensive approximate design tool for roadside cuttings. In cases where the design cutting inclinations are particularly sensitive to practitioner parameter choices, geotechnical investigation and numerical analysis are highly recommended. Uncertainties are also introduced by employing a numerical method. These uncertainties are difficult to quantify but are certainly small in relative terms. As these guidelines characterise rock according to the G-H-B (using GSI), they should only be used for intact and heavily fractured rock mass (not for those that exhibit a dominant structural orientation). GSI is based on the assumption that randomly orientated heavily fractured rock masses behave as an isotropic mass (Li et al. 2008).

4. CONCLUDING REMARKS

The usability of our guidelines is better than both existing guidelines and published stability charts due to their conciseness and use of descriptions of field tests to identify geomaterial categories. We also found that our Nepal guidelines are more robust than guidelines currently provided in manuals and are in close agreement with published stability charts. The guidelines can be used as a first approximation for road cutting design and as a tool to assess the stability of existing cuttings. The methodology can be used by geotechnical engineers to develop guidelines on road cuttings for any specific locality.

The methodology and guidelines presented by Robson et al. (2022) can be further improved by including additional categories for the weaker rock and soil and by adapting the guidelines to better suit engineers' knowledge and requirements.

ACKNOWLEDGEMENT

This research was supported by NERC IAPETUS Doctoral Training Partnership [grant number: NE/S007431/1].

REFERENCES

Carranza-Torres C and Hormazabal E, 2018. Computation tools for the determination of factor of safety and location of the critical circular failure surface for slopes in Mohr-Coulomb dry ground. Proc. Of the 2018 Int. Symp. of Slope Stability in Open Pit Mining and Civil Engineering.

DoR (Department of Roads), 2013. Nepal Road Standard 2070. Government of Nepal, Kathmandu.

DPWH (Department of Public Works and Highways), 2007. The study on risk management for sediment-related disaster on selected national highways in the Republic of the Philippines: Road Slope Protections. Japan International Cooperation Agency.

Hoek E and Brown ET, 2018. The Hoek-Brown failure criterion and GSI – 2018 edition. Journal of Rock Mechanics and Geotechnical Engineers. Vol. 11. pp. 445-463.

Li A-J, Merifield RD, and Lyamin AV, 2008. Stability charts for rock slopes based on the Hoek–Brown failure criterion. Int. Journal of Rock Mechanics and Mining Sciences. Vol. 45 pp. 689-700.

MPW (Ministry of Public Works), 2019. Manual for Low Volume Roads. Ministry of Public Works, Republic of Liberia.

Robson E, Utili S, Milledge D, 2021. Road slope stabilization in Nepal: stakeholder perspectives SCG-XIII Int. Symp. on Landslides, Cartagena.

Robson E, Agosti A, Utili S, and Milledge D, 2022. A methodology for road cutting design guidelines based on field observations. Engineering Geology. Vol. 207, 106771

Shen J, Karakis M, and Xu C, 2013. Chart-based slope stability assessment using the Generalised Hoek-Brown criterion. Int. Journal of Rock Mechanics and Mining Sciences. Vol. 64 pp. 210-219.

Wyllie DC, 2017. Rock slope engineering: Civil applications. 5th edition, CRC Press

Zuo J and Shen J, 2020. The effects of blast damage zone thickness on rock slope stability. The Hoek-Brown failure criterion – from theory to application. pp. 201-222.

#Inv-6:

Case studies on Shoring System Behaviour During Deep Excavations

Dr. Anil Joseph[1]

[1]*President, Indian Geotechnical Society and Managing Director, Geostructurals Pvt. Ltd. Cochin, Kerala, India*

1. EXTENDED ABSTRACT

With increasing cost of land in urban areas, vertical growth has become essential in city centres. With the requirement of service facilities like car parking and the restriction for height of buildings, construction of deep basement has become a necessity. Structures in the immediate vicinity of excavations, dense traffic scenario, presence of underground obstructions and utilities have made excavations a difficult task to execute. In this context, analysis and design of deep excavations and their supporting systems are essential. Even in complicated urban settings, deep retaining systems have been deployed successfully by overcoming construction challenges. For several infrastructure projects like metro rail, parking lots in commercial area, shopping malls etc. underground structures are preferred to preserve the landscaping in the area. This paper deals with two case studies of problems encountered in shoring systems and the solutions adopted. Case study one focusses on the analysis and review of touch pile system execution for a 3Basements+Ground+19 floors residential apartment building at Chennai, India and the second Case study is a forensic analysis of a touch pile system failure during deep excavation for a commercial building (3 basements, ground floor and 8 floors) near Metro Station Kaloor, Ernakulam, Kerala, India. From the forensic study of touch pile system failure, it was found that the failure is due to the fact that the strut system was inadequate to take up the lateral thrust from the touch piles and to provide the required stability. The soil at the dredge line has turned out to be very soft and has caused considerable loss of strength of the interface soil, high thrust from the shoring pile at the interface due to water seepage has caused yielding of this soil. Subsequent increase in unsupported length of pile is also a reason for the failure of pile in bending. It is true that the cellars are going deeper and deeper and floors going higher and higher. From the case studies on the shoring system behavior of deep excavation it is noted that accurate cost analysis is difficult to carry out as there is limited commonality to make comparisons between deep excavation projects. A great number of random and uncontrollable variances are likely to arise during the courses of work which makes planning and scheduling difficult. The actual effectiveness of works is highly depended on the as-constructed site environments. Quality of the management and the executing parties, as well as the problems solving ability of the frontline personnel, also seriously affects the performance and effectiveness of works. Dynamic layout arrangement is usually required for the removal of the excavated soil from the basement. This may involve forming of temporary ramp, provision of special equipment, or taking over of part of the completed building as temporary access. The construction industry is slowly getting attuned to modern design techniques and construction procedures. The trends cannot be discouraged but the authority should exercise greater caution and control when projects with such trends are approved.

#Inv-7:

Recent Development of Geotechnical Engineering in Sri Lanka

K.L.S. Sahabandu[1]
[1]*President, Srilankan Geotechnical Society*

Sri Lanka is an island nation located between northern latitude of 50 51' and 90 51' and eastern longitude of 790 40' and 810 55'. It occupies an area of nearly 65,000 square kilometers, stretching 435 km from north to south and 224 km from west to east.

Three distinct plains of denudation can be clearly recognized in Sri Lanka. The coastal plain, about 30 m above sea-level, an intermediate plain at about 500 m, and a third at 1,830 m above sea-level.

The country constitutes largely a continuation of the main geological formation of Southern India. Like the adjacent main land, the Island is composed almost entirely of crystalline metamorphic rocks of Archean or pre-Cambrian age. Miocene sedimentary rocks are located in the North and Northwestern coastal regions. In addition to those, some small faulted basins of Jurassic sedimentary rocks are also present in the Northwestern part of the country. Quaternary deposits composed of unconsolidated material of various grain sizes from clay to gravel are found along flood plains and terrace deposits of rivers, as residual soils or talus on hill slopes. On coastal plains they occur as marine and lacustrine deposits.

The most frequent natural hazards that affect Sri Lanka are floods, landslides, droughts, cyclones, vector borne epidemics and coastal erosion. Landslides which seconds only to flooding has been rain-triggered and have been causing massive damages from early days. The increase of this hazard has been identified to be resulting from undue human intervention such as bad land use and cropping practice, settlement in unstable areas, changes to natural drainage paths resulting in blockages, and non-engineered developments in hilly areas. Earthquakes and Tsunamis are infrequent but the latter have caused severe damage on the boxing day of 2004. Recent understanding of the tectonics of the Indian Ocean region indicates to an increasing risk of earthquake.

It would not be incorrect to say that the field of modern geotechnical engineering in Sri Lanka had been taking root in the island with its application to landslide risk reduction in early 1960s. Thanks to the efforts of the single person, the world renowned, Prof. A. Thurairajah, who introduced the full subject of Soil Mechanics into the Engineering degree curriculum in this country in the 1960's and eventually was called as the Father of Geotechnical Engineering in Sri Lanka.

It needs mention here that historical evidence however indicates that our forefathers have had a sound understanding of earth materials to put up a variety of spectacular and massive structures such as stupa, dams and ancillary structures which are standing vigorously even today.

In 1980s, the application of the field was focused on water resources sector towards utilizing the rich water resources of the country mainly by building 4 major dams such as Kotmale, Victoria, Randenigala, and Rantambe along the Mahaweli River, the longest river in Sri Lanka. Given the sound bedrock conditions, serious problems were not encountered for founding these dams and the ancillary structures. Yet, all dams were subject to geotechnical instrumentation to assess their performance from the construction stage to service stage. The experience and exposure offered by these mega projects helped advance the knowledge and working confidence in the field significantly!

It was during this decade that the Sri Lankan Geotechnical Society was formed, in response to the need felt by the scientists, engineers and geologists associated with Geotechnical Engineering to provide a forum for exchange and advancement of knowledge in the field of Geotechnical Engineering with the leadership of Prof. A. Thurairajah.

The area of foundation engineering including deep excavation with secant pile wall tied back by ground anchors and soil nails, and a hybrid shallow-deep foundation system with hand dug caissons was notably dealt with, first time in the country, in constructing the New Central Bank Building of Sri Lanka in mid 1990s including geotechnical instrumentation.

Infrastructure development projects comprising

significant components of ground engineering works got effected thereafter only beyond year 2000. Details of such nationally important projects by way of which the field of Geotechnical Engineering had a notable paradigm shift are briefed hereunder.

The Southern Expressway which is the, 222 km long, first–ever highway project in Sri Lanka connecting Colombo and down south involved extensive ground improvement work as many parts of the expressway traverses through flood plains and marshy ground consisting of peat, organic soils and soft clays. Depending on the ground conditions, various ground improvement methods including removal and replacement, preloading, preloading with vertical drains, dynamic compaction and vacuum consolidation were applied to improve the soft soil to build the embankments with heights varying from 2m to 12m. Further, the highway had several river and road crossings. Shallow and deep foundation systems were adopted for bridging these crossings. Deep foundations mainly comprising precast reinforced concrete driven piles and bored and cast in-situ piles were also demanded by the subsurface conditions encountered at some locations. Shallow foundation systems were also adoptable at several locations. Soft ground improvement techniques such as gravel compaction piles, vacuum consolidation method were also adopted in other highway projects.

The Construction of Eight Railway Bridges on Rail Track Extension, Phase 1, consisted of constructing four new bridges and replacement of superstructures at four existing bridge sites from the colonial era. The Superstructure of bridge consisted of steel truss construction and substructures consisted of reinforced concrete abutments and piers. Through a tradeoff analysis, micro piles which are steel pipes grouted with cement mortar extended into the bedrock were selected for the safe load transfer to the ground and due to other factors such as commercial reasons, site conditions etc.

The 26.7 km, Matara- Beliatta southern coastal railway line of Sri Lanka is the first phase of the proposed extension from Matara up to Hambantota. Geotechnical Engineering Design for the trace identified the same to comprise viaducts including railway underpass and overpass of 3000 m essentially on bored-and cast in-situ piles, tunnel sections of 850 m and the rest 23.5 km being embankments on normal as well as soft ground. Cut and cover and NATM Methods have been adopted for tunneling works. Soft ground improvement work involved preloading and DCM piles. Further, gravity and reinforced concrete retaining walls, soil nail walls, geo-grid walls etc. used for stabilizing of cut and fill slope.

Under the Metro Colombo Solid Waste Management Project, it is concurred that a Sanitary Landfill is the most appropriate long-term solution for the management of MSW generated in the MCR. The landfill is featured with modern day geosytheitc materials for different functional requirements.

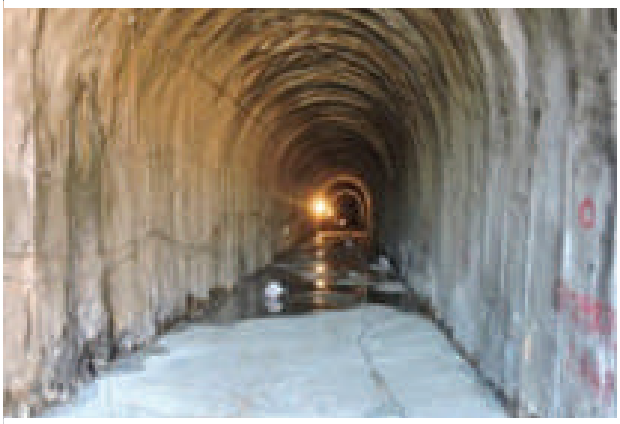

The Kalu Ganga Development Project is the last project of the five great reservoirs in the Mahaweli Master Plan. The Project consists of construction of a rockfill Main Dam with centre clay core, of height 76 m and crest length 524 m, having a gated (radial) spillway on left abutment, together with a 22 m high rockfill Saddle Dam some 4 km upstream of the Main Dam. Kasrtic features encountered in the subsurface condition posed problems in making the foundation watertight in this dam site.

Port-City Colombo is a brand-new city development which added 267 hectares of land for future residential and commercial development. The landfill and offshore breakwater which are the initial components of the development consist of elements such as 72 Million m2 of sand reclamation using Trailing Suction Hopper Dredgers, 4.383 km long Off-shore Breakwaters, Inner Breakwaters and Sand Barriers by Gravity rock fill Structures, 0.930km long revetment construction including rock inverted Filters, 5.454 km long up to 7m high Seawalls by plain

concrete blocks on vibro compacted around 20m thick sand fill, 2.654km long up to 3m high non reinforced concrete Retaining Walls on vibro compacted around 15m thick sand fill, over 20,000 points of 23m deep vibro compaction for ground improvement under retaining structures, over 65,000 points of dynamic compaction on roads and development land plots and over 1.6km long artificial beach.

In tandem with the infrastructure development in the country, there has been a significant development of landslide risk reduction and slope stabilization activities with soft engineering and structural measures in landslide prone areas.

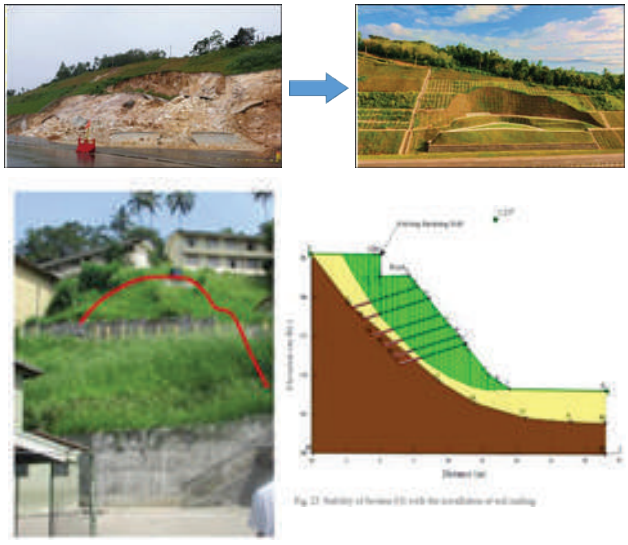

A number of Deep Excavations and Foundations particularly bored and cast insitu large diameter piles associated with high-rise building construction has been also being executed in recent past in commercial capital of Sri Lanka. Deep Excavations supported by secant pile walls and diaphragm walls facilitating maximum of five levels basements is becoming a common feature in most of high-rise construction. Presently high-rises in the Capital almost hit 100 story level found mostly on large diameter bored and cast insitu piles. Electronic Pile Integrity tests (PIT) such as low strain pulse echo method and cross hole sonic logging method, and Pile Driving Analyser (PDA) which is the pile load test virtually replacing the conventional static load test have become standard quality control tests associated with such pile construction.

#Inv-8:

Real-Time Monitoring of Active Landslide in Kalimpong, Darjeeling Himalayas

Neelima Satyam[1]

[1]*Department of Civil Engineering, Indian Institute of Technology Indore*
Madhya Pradesh, India, 453552

1. INTRODUCTION

Landslides are geomorphological processes those turn into disaster when interact with human environment. When rainfall is the primary triggering factor of landslides, the occurrence of landslides can be forecasted using a critical rainfall condition, known as the rainfall threshold.

The choice of rainfall parameters depends primarily on the typology of landslides. An approach, combining the effect of both long-term and short-term rainfall is more suitable, when a region is affected by both deep-seated and shallow landslides. Kalimpong in Darjeeling Himalayas is one such mountainous town, where multiple landslide types are observed. The town is in the West Bengal state and is frequently affected by landslides. Rainfall thresholds using several approaches (Satyam and Abraham, 2021). From these studies, it was found that the method studying both long-term and short-term rainfall is performing much better than the conventional approaches (Abraham et al., 2020). This has been done using SIGMA (Sistema Integrato Gestione Monitoraggion Allerta) model, which is an operational LEWS, originally developed for Italy. The model has over 20 years of operational experience, and is being updated and fine-tuned regularly for better performance. Apart from Italy, the model has been tested for Kalimpong in the Darjeeling Himalayas and Idukki in the Western Ghats.

The critically unstable slopes in Kalimpong town are monitored using MicroElectroMechanical Systems (MEMS) tilt meters and volumetric moisture content meters and the recent studies on updating rainfall threshold models have proved that the use of field-based data can improve the performance of conventional thresholds significantly. Hence this study is an attempt to update the SIGMA model for Kalimpong using latest rainfall and landslide data and explore the use of field-based monitoring data for improving the performance of SIGMA Model.

2. METHODOLOGY

The proposed approach is a modification in the SIGMA algorithm, integrating statistical distribution of rainfall data with the tilt sensor readings. While validating SIGMA model of Kalimpong, it was observed that the model issues false alarms with yellow alerts on days with no observed displacements as well. These alerts were counted as false alerts and such warnings will affect the response of people towards the LEWS. When the number of false alarms is increased, the credibility of LEWS is affected and the public might not respond positively to the instructions provided. Hence the yellow alerts predicted by SIGMA model will only be issued by the combined approach after verifying the tilt meter readings (Figure 3).

Figure 1. Decisional algorithm used for the calibration of combined approach (Abraham et al., 2021b)

In Figure 1, CR is the critical tilting rate, which can be customised for each region, using a trial-and-error approach. For Kalimpong, the value of CR has been calibrated as 0.03 o/h (Abraham et al., 2020a). Hence to issue a yellow alert, the algorithm first check if the

corresponding σ curve is crossed or not, as per the conventional SIGMA algorithm. If the threshold is crossed, it checks for the maximum tilting rate observed on the previous day. If the tilting rate is also greater than the threshold value, then yellow alert is issued, otherwise no warning is issued for the day.

3. RESULTS AND DISCUSSION

The slope failure and rainfall data from 2017 July to 2020 September were used to evaluate the performance of different models quantitatively. During the years 2017, 2018 and 2019, no major landslides are recorded near sensors, and the slope failures were in form of displacements and minor cracks in the roads near the installed sensors. All events were of minor criticality, where the authorities should observe the situations for any emergency. In 2020, multiple landslides have happened in Kalimpong along with major cracks in roads near sensor 2. The comparison of different models has been done using a confusion matrix. When the model has predicted a slope failure and such an incident is recorded in the database, it is counted as a true positive. Similarly, when the model predicts no slope failure and no such event has occurred as per the database, it is counted as a true negative (TN). Both TP and TN are true predictions and the more the true predictions, the better is the model. False predictions can be of two types: i) a slope failure is predicted by the model, but no such event is recorded in the database, which is termed as a false positive (FP) and ii) no slope recorded, termed as false negative (FN).

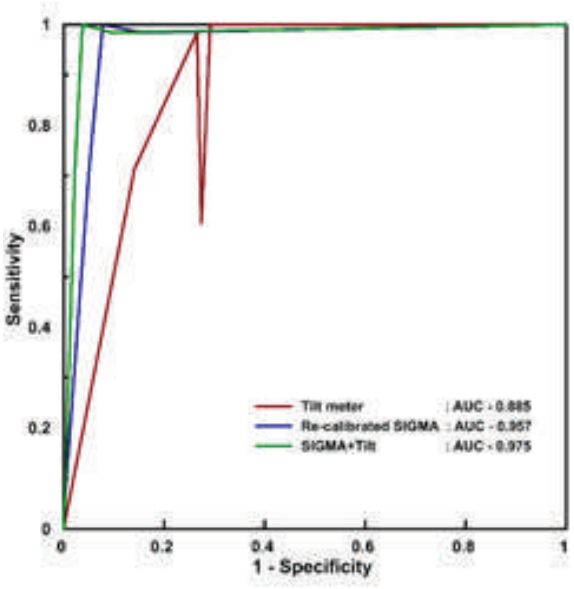

Figure 2. ROC curves for different models (Abraham et al., 2021)

It is noticed that the number of false predictions has noticeably reduced by using the combined approach. The number has reduced from 273 with tilt meters and 70 with re-calibrated SIGMA model, to 38, by using the combined approach.

Based on the attributes obtained from the confusion matrix, the sensitivity and specificity of the model can be calculated. Using the values of sensitivity and specificity, the performance of different models can be compared using a Receiver Operating Characteristic (ROC) curve. An ROC curve is a plot between sensitivity and 1 – specificity. The point (0,1) on the plot is called the perfect point.

In this study, the year wise performance of the three different models has been used to plot the ROC curve and compare the models quantitatively. The plot depicts that the combined approach with SIGMA+Tilt has the maximum value of AUC (0.975) and is the best performing, out of the three models. From Figure 2, it can be noted that the curve of combined approach is shifted towards the y axis, when compared to both the other models. This indicates that the model is more specific and issues a lesser number of false alarms. The points of tilt meter are at a larger distance from the y axis, indicating a higher number of false alarms. It should also be noted that the SIGMA model, and the combined approach have points closer to the perfect point and have a relatively consistent performance over the years, while the performance of tilt meter is highly varying every year. With the tilt meters, the major share of missed alarms has happened during the year 2018, where the field displacements were also minor. The events were not associated with heavy rainfalls and hence were missed by the SIGMA model as well.

While comparing the different threshold models proposed for Kalimpong, it is found that the new approach proposed in this study, which is a conceptual enhancement of the conventional SIGMA model, is performing better than the thresholds derived for the region so far. However, the model has certain limitations, which shall be rectified to convert this prototype to an operational LEWS.

4. CONCLUDING REMARKS

The results indicate that both the SIGMA model and the tilt meters, when used separately, issue several false alarms, which restricts their direct use in an LEWS. SIGMA model has also missed some of the alarms of minor criticality. The combined approach performs better than both the approaches when used independently. This

has been verified using an ROC approach, which indicated that the AUC values for SIGMA, tilt and combined approach were 0.957, 0.885 and 0.975 respectively. The proposed method was also compared with other rainfall thresholds derived for the region, and the results indicates that the combination of SIGMA and field based monitoring data is the best performing rainfall threshold derived for Kalimpong so far. The minor shortcomings of the method shall be rectified, and the model shall be fine-tuned, to be used as a potential tool for developing an LEWS for the region.

ACKNOWLEDGEMENT

The author acknowledges the financial support of Department of Science & Technology (DST), New Delhi, for funding the research project Grant No. (NRDMS/02/31/015(G)) and the support from Save The Hills (NGO) for carrying out the research.

REFERENCES

Abraham, M.T., Satyam, N., Kushal, S., Rosi, A., Pradhan, B., Segoni, S., 2020. Rainfall Threshold Estimation and Landslide Forecasting for Kalimpong, India Using SIGMA Model. Water 12, 1195. https://doi.org/10.3390/w12041195

Abraham, M.T., Satyam, N., Pradhan, B., Segoni, S., Alamri, A., 2021. Developing a prototype landslide early warning system for Darjeeling Himalayas using SIGMA model and real-time field monitoring. Geosciences Journal. https://doi.org/10.1007/s12303-021-0026-2

Satyam, N., Abraham, M.T., 2021. Development of Landslide Early Warning Using Rainfall Thresholds and Field Monitoring: A Case Study from Kalimpong, in: Garg, A., Solanki, C.H., Bogireddy, C., Liu, J. (Eds.), Proceedings of the 1st Indo-China Research Series in Geotechnical and Geoenvironmental Engineering. Springer, Singapore, pp. 153–173. https://doi.org/10.1007/978-981-33-4324-5_11

#Inv-9:

Ground Response and Liquefaction Analysis of Kathmandu City Based on 2015 Nepal Earthquake Data

Pradeep Acharya[1], Shiv Shankar Kumar[2], Pradeep Kumar Dammala[3], Murali Krishna Adapa[4]

[1]Politecnico di Milano, Italy, pradeep.acharya@mail.polimi.it

[2]National Institute of Technology Patna, India, k.shiv.ce@nitp.ac.in

[3]Indian Institute of Technology Jodhpur, India, pkdammala@iitj.ac.in

[4]Indian Institute of Technology Tirupati, India, amk@iittp.ac.in

1. INTRODUCTION

Nepal is one of the most seismically active regions in the world. The distribution of earthquakes in and around Nepal since 1990s has revealed the belt of intense micro seismic activities (Pandey et al. 1999). Kathmandu city being surrounded by several thrust fault such as Main Boundary Thrust and Main Central Thrust, had experienced many major earthquakes in the past, in particular the 2015 Nepal Earthquake (Mw 7.8). Several researchers studied the seismic vulnerability of the Kathmandu city and on the associated effects. This paper outlines one such study presented by Kumar et al. (2020) on the ground response and liquefaction analysis of the Kathmandu city.

2. METHODOLOGY

Non-linear ground response analyses of some typical sites of Kathmandu were conducted using DEEPSOIL v6.1 program (Hashash et al., 2016). Both the total stress approach and the effective stress approach, have been adopted. Ten boreholes, located in the vicinity of Kathmandu have been considered for the analysis. Chyasal (CHY), Jamal (JAM), Kalanki (KLK), Khulamanch (KHM), Kupandole (KUP), Mahaboudha (MBD), Nepal Airlines Office (NAC), Sundhara (SUN), Sundarighat (SDG) and Tokha (TOK). 2015 earthquake ground motion data recorded at five locations in Kathmandu were used for the input seismic data (Table 1). KTP (Kirtipur), PTN (Pulchowk), TVU (Kirtipur), THM (Thimi) and KATNP (Kanti Path). Liquefaction analyses were done using the analytical approaches to determine the factor of safety against liquefaction and liquefaction potential index (LPI).

3. RESULTS AND DISCUSSION

The results have been divided into three categories. First one deals with the effects of different ground motions on one chosen soil profile (SDG). The second one discusses the effects of soil stratifications in different locations, subjected to a single ground motion (KTP). Finally, third section deals with the liquefaction potential of the respective sites.

Figure 1 shows the effect of different strong motions on ground response at Sundarighat (SDG), in terms of PGA, maximum shear strain and pore pressure ratio.

Table 1: Strong motion data of 2015 Nepal Earthquake (after Kumar et al. 2020)

Parameters	Ground Motion Recording Stations				
	KATNP	KTP	PTN	THM	TVU
Site Geology	Unknown	Rock	Sediments	Sediments	Sediments
Epicentral distance (km)	76.86	75.78	80	81	77
PGA (g)	0.158	0.259	0.154	0.153	0.233
V_{s30}/A_{max} (s)	0.693	0.139	0.451	0.485	0.366
PIE Design acc* (g)	0.157	0.242	0.151	0.153	0.233
Predominant Period (s)	3.65	0.26	0.440	3.480	0.700
Mean Period (s)	1.893	0.387	1.171	2.822	1.693
Bracketed Duration (s)	24.01	42.32	27.31	37.52	50.78
Significant Duration (s)	53.76	38.13	37.78	38.94	47.87
Frequency Content	Low	High	Medium	Low	Medium

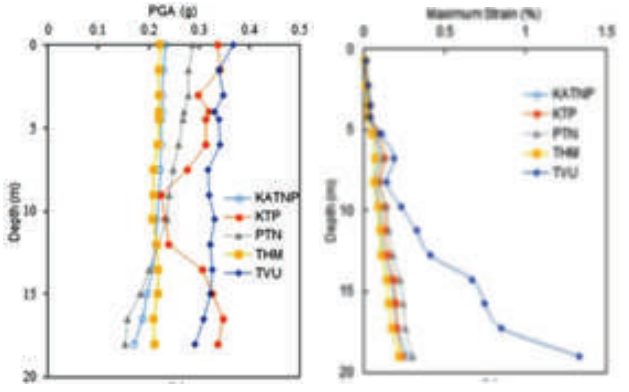

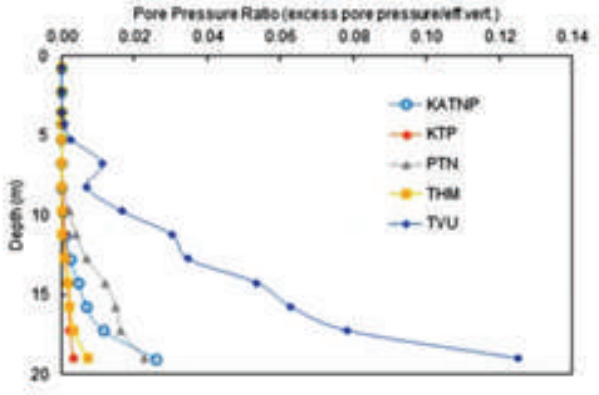

Figure 1: Effect of ground motions on the ground response at SDG location (modified after Kumar et al. 2020)

In a similar way, Figure 2 shows the effects of local soil conditions as site effects on ground response for a chosen earthquake ground motion data recorded at KTP station. Figure 3 presents the typical results of liquefaction analysis in terms of factor of

safety (FOS) against liquefaction at different sites for KTP strong motion data. Spectral acceleration responses obtained from the effective stress analysis at different locations for KTP ground motion is shown in Fig. 4.

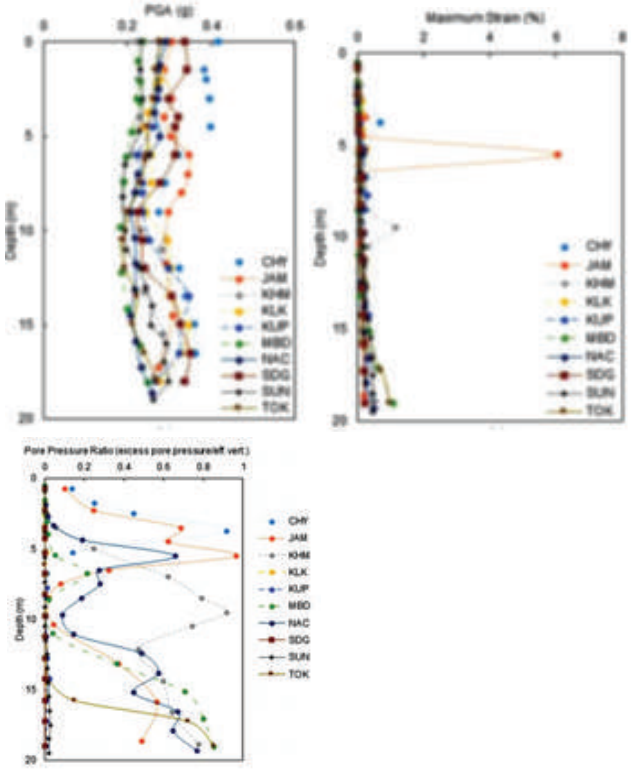

Figure 2: Site effects on the ground response for a chose earthquake ground motion recorded at KTP

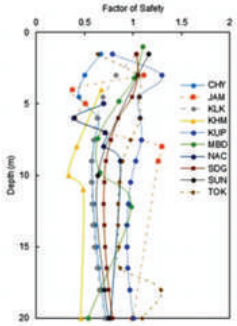

Figure 3: Variation of factor of safety against liquefaction along depth at different locations

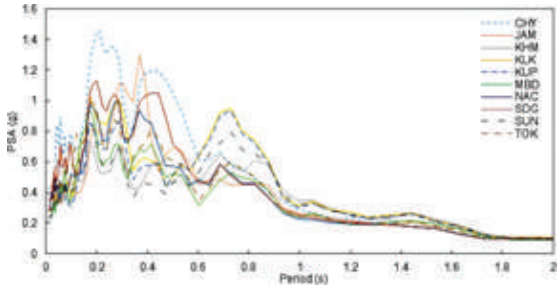

Figure 4: Spectral acceleration responses at different locations based on effective stress approach

4. CONCLUDING REMARKS

In general, it is observed that ground accelerations were amplified at the surface level of the considered ground motions. Input PGA of range 0.153g – 0.259g at SDG were amplified to surface PGA of range 0.233g-0.367g due to the variations in seismic parameters. Similarly, spatial variability also greatly affected the amplification. Seven out of ten chosen locations showed amplifications at the surface. The susceptibility of liquefaction has been found to be very high in most of the locations.

REFERENCES

Pandey MR, Tandukar RP, Avouac JP, Vergne J, and Héritier T, 1999. Seismotectonics of the Nepal Himalaya from a local seismic network. Journal of Asain Earthquake Science, Vol17, No.5-6, pp. 703–712.

Kumar SS, Acharya P, Dammala PK and Krishna AM, 2020. Characterization of Ground Response and Liquefaction for Kathmandu City Based on 2015 Earthquake Using Total Stress and Effective Stress Approach. Int'l Journal of Geotechnical Earthquake Engineering, Vol 11, No. 2, pp. 1-25.

Hashash YMA, Musgrove M, Park D, Tsai CC, Phillips C and Groholski D R. 2016. DEEPSOIL v6.1. Tutorial and User Manual. 129p.

#Inv-10:

Distress and Susceptible Behaviour of Calcium Based Stabilized Soils Due to Sulphate Contamination

Arvind Kumar Jha[1] Avadhesh Kumar[2]

[1]*Assistant Professor, Indian Institute of Technology Patna, Bihta-801103, Bihar, India*

[2]*Postgraduate Student, Indian Institute of Technology Patna, Bihta-801103, Bihar, India*

1. INTRODUCTION

Treatment of expansive soil with calcium-based stabilizer is an effective method due to the formation of stable pozzolanic compounds. Though, several cases of serious distress and heaving have been reported by the researchers in expansive soil comprising sulphates when treated with stabilizers of calcium-based additives (Hunter, 1988; Rajasekaran and Rao, 2005; Jha and Sivapullaiah, 2015; Puppala et al., 2018). Sulphates in the soil can occur through in-situ existence of any sulphatic compounds or from migration due to acid rain, soil contamination, soil pollution, surface water pollution, ground water contamination, river stream, chemical spillage, industrial wastes, mines residual slurry, etc. (Sharma and Kumar, 2020). The discharge released from industrial activities such as mines of coal and metals are highly acidic in nature, which is termed as "Acid Mine/Metalliferous Drainage (AMD)" (Moodley et al., 2018). In addition, the "Acid Rock Drainage (ARD) and Acid Sulphate Soil" (ASS)" are also natural phenomena responsible for accumulation of sulphates in soil causing contamination (Simate and Ndlovu, 2014). These processes occur through the weathering actions on rocks containing iron sulphides. These acid mine drainages or acid sulphate soils contain mainly sulphides and other heavy metals (Masindi and Muedi, 2018) which eventually leads to contaminate the soils.

Researchers reported frequent sources of sulphates in soil, such as CaSO4, Na2SO4, MgSO4 and K2SO4 having different solubility rates of 2.6 gm/L, 408 gm/L, 260 gm/L and 120 gm/L, respectively (Mitchel,1986; Jha and Sivapullaiah, 2016). When lime treatment is given to such soils, complex reactions take place among lime, sulphates and soil. This causes large volumetric expansion of soil, that leads to formation of heaves namely "Sulphate Induced Heaves" (Mitchell, 1986; Little et al., 2005). This excessive swell occurs due to production of extremely expansive compound such as Ettringite or Thaumasite, which can swell more than 137% of their own volume (Puppala et al., 2018). The phenomenon causing damage due to sulphates is generally known as Sulphate attack.
The present study has aimed to investigate the susceptible behavior of lime treated soil subjected to sulphates contamination and thereby induced distress to the stabilized soils. Further, mechanism of distress and susceptible behavior of the same has been brought out clearly in details.

2. METHODOLOGY

In order to achieve the objectives, various geotechnical investigations such physical properties, strength and volume change behavior are carried out to understand the behavior of lime treated expansive soil subjected to sulphate contamination. Further, physicochemical and micro-level analyses (XRD, SEM, EDAX, FTIRR) have been performed to elucidate the mechanism of lime treated soil subjected to sulphate contamination.

3. RESULTS AND DISCUSSION

It has been revealed that presence of sulphates and order of cations control the plasticity characteristics of lime treated soil greatly. The one-dimensional swelling percentage revealed that lime treated expansive soil with sodium sulphate shows the highest swelling percentage and magnesium sulphate shows lowest swelling percentage due to monovalent and divalent cations, respectively (Fig. 1). Further, the reduction in the strength of lime treated soil with sulphates at shorter curing periods is due to the rapid hydration and thereby formation of cracks and void within the samples (Table 1). Microanalyses of lime treated expansive soil have been determined by scanning electron microscope (SEM), X-ray diffraction (XRD), energy dispersive X-ray spectroscopy (EDAX) test. Formation of ettringite and cementitious compounds in the lime treated soil depend on the types and content of metal sulphates that lead to affect the behaviour of lime treated soil subjected to different metal sulphates.

Table 1: Unconfined Compressive Strength at different curing period

Combination	UCS (kPa) at curing periods (days)		
	7	14	28
Soil (S)	358	989	358
S+ L	2250	2777	2231
S+L+2G	2360	1600	3125
S+L+4G	2675	2450	3188
S+L+6G	1915	2005	3566
S+L+8G	1885	2191	3573
S+L+2SS	1945	1335	2231
S+L+4SS	1805	1884	3103
S+L+6SS	1690	1975	3846
S+L+8SS	1795	1981	2886
S+L+2MS	2340	1603	3376
S+L+4MS	2160	1335	2231
S+L+6MS	1815	1979	3261
S+L+8MS	1235	1344	2596
S+L+2KS	2045	1560	3465
S+L+4KS	1850	983	2163
S+L+6KS	1160	1335	2231
S+L+8KS	865	2725	2730

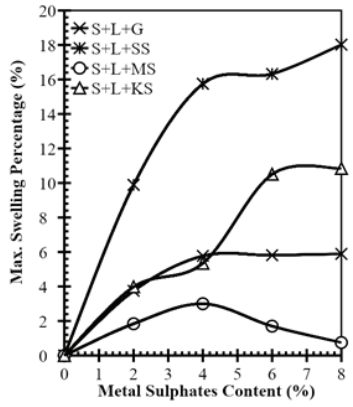

Figure 1: Effect of metal sulphate on the maximum swelling percentage of lime treated soil.

4. CONCLUDING REMARKS

Followings are the key outcomes that can be drawn from present study:

1. Maximum swelling percentage in lime treated soil with metal sulphates reveals that monovalent metal sulphates cause more detrimental induced swelling in the lime treated soil in comparison to divalent sulphates. The increasing order of maximum swelling percentage at 8% of metals sulphates in lime treated soil is observed to be 0.75% (Mg++)>5.89% (Ca++)>10.84% (K+) and 18.02% (Na+).
2. The strength of lime treated soil reduces with the presence of lower metal sulphates of gypsum, sodium sulphate and magnesium sulphate at lower curing periods of 14 days. However, the long-term strength of lime treated soil is further enhanced with gypsum, sodium sulphate and magnesium sulphate. However, the presence of potassium sulphate accelerates the strength at shorter curing period and is found to be constant afterward at longer curing periods. But overall strength of lime treated soil in the presence of potassium sulphate reduces with curing period in comparison to lime treated soil. It can be concluded that lower metal sulphates are observed to detrimental at shorter curing period but are beneficial in strength gain at longer periods.

REFERENCES

Hunter, D., 1988. Lime-induced heave in sulfate-bearing clay soils. Journal of geotechnical engineering, 114(2), pp.150-167.

Rajasekaran, G. and Narasimha Rao, S., 2005. Sulphate attack in lime-treated marine clay. Marine Georesources and Geotechnology, 23(1-2), pp.93-116.

Jha, A.K. and Sivapullaiah, P.V., 2015. Susceptibility of strength development by lime in gypsiferous soil—A micro mechanistic study. Applied Clay Science, 115, pp.39-50.

Puppala, A.J., Talluri, N., Congress, S.S.C. and Gaily, A., 2018. Ettringite induced heaving in stabilized high sulfate soils. Innovative Infrastructure Solutions, 3, pp.1-12.

Sharma, M.K. and Kumar, M., 2020. Sulphate contamination in groundwater and its remediation: an overview. Environmental monitoring and assessment, 192, pp.1-10.

Simate, G.S. and Ndlovu, S., 2014. Acid mine drainage: Challenges and opportunities. Journal of environmental chemical engineering, 2(3), pp.1785-1803.

Mitchell, J.K., 1986. Practical problems from surprising soil behaviour. J. of Geotech. Engrg., 112(3), pp.259-289.

Jha, A.K. and Sivapullaiah, P.V., 2016. Volume change behavior of lime treated gypseous soil—influence of mineralogy and microstructure. Applied Clay Science, 119, pp.202-212.

Little, D.N., Nair, S. and Herbert, B., 2010. Addressing sulfate-induced heave in lime treated soils. Journal of geotechnical and geoenvironmental engineering, 136(1), pp.110-118.

Society NG and Nepal GS, 2022. GeoMandu, an international conference series of Nepal Geotechnical Society, Int'l Journal of NGS, Vol1. No.2, pp.112-123.

Nepal GS, Geotechnical, SN, and Society NG, 2014. Geohazards and Geoinformation: An international conference by Nepal Geotechnical Society, Int'l Journal of NGS, Vol1. No.12, pp.10-20.

#Spl-1:

Effect of Soil Strata on Peak Characteristics of H/V Spectra of the Ground Ambient Vibration -A Case of Kathmandu Valley Ground-

Netra Prakash Bhandary[1] and Youb Raj Paudyal[2]

[1]*Faculty of Collaborative Regional Innovation, Ehime University, Japan*

[2]*Department of Urban Development and Building Construction, Government of Nepal*

1. INTRODUCTION

Recording microtremors and interpreting the FFT (Fast Fourier Transformation) data for understanding ground shaking behavior and predicting structural damage during earthquakes have been in use for the past several years. Estimating dominant frequencies of a ground and a building or structure help predict potential structural damage level. In case of ground, the predominant frequency is primarily governed by the material type and the depth of deposit. Especially in a lacustrine deposit like in the Kathmandu Valley, this effect is prominent because the material depth is high in the middle and material type in terms of soft clay layers variates spatially.

It is often necessary to adopt a simple method to assess the ground. Interpretation of the microtremor or ambient noise data is one easy method of understanding ground shaking behavior during earthquakes. The fine or coarse material stratification and the depth of each stratum in the ground govern the dominant frequency or the dominant period of shaking. A diagrammatic depiction of such ground behavior is shown in Fig. 1. So far, most research work in these issues have focused on the relation between the overall depth of the deposit and the dominant frequency of shaking (e.g., Paudyal et al., 2013), but it is equally important to understand the effect of material stratification pattern and its depth on the H/V spectral peak characteristics.

In this study we focus on the characteristics of the H/V Fourier Spectrum peak and compare them with the ground stratification interpreted from the available borehole logs.

2. METHODOLOGY

Before the 2015 Earthquake in Nepal, we conducted a microtremor survey at 170 points in the Kathmandu Valley and did an assessment of the seismic ground shaking behavior based on the H/V spectra obtained out of Fast Fourier Transform analysis (Nakamura 1989) of the recorded ambient ground vibration. In this study, we have used all those data to interpret the peaks of H/V spectra. In addition, the H/V spectral peak characteristics are analyzed on the basis of available material stratification interpreted from the existing borehole logs nearest to the microtremor survey points in the valley. The microtremor survey locations are shown in Fig. 2 and a set of microtremor data interpretation in three typical peak characteristics (i.e., clear peak, multi peak, and no clear peak) is show in Fig. 3.

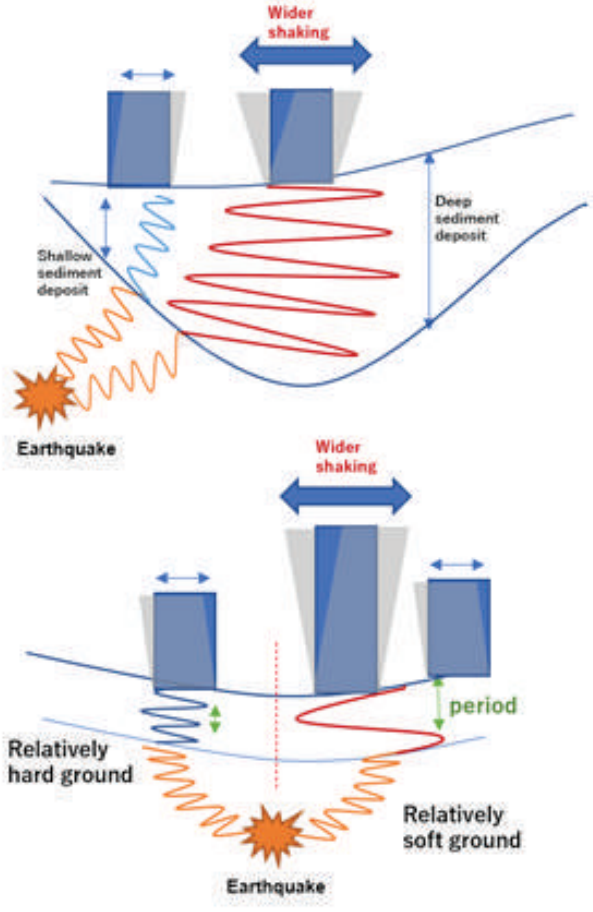

Figure 1: An image of the effect of depth ground deposit and material type on the shaking behavior.

Figure 2: Location of the microtremor survey points

3. RESULTS AND DISCUSSION

The ambient noise data analysis has resulted in three typical types of H/V spectral peak characteristics: 1) clear peaks, 2) multi peaks, and 3) no clear peaks (as shows in Fig. 3).

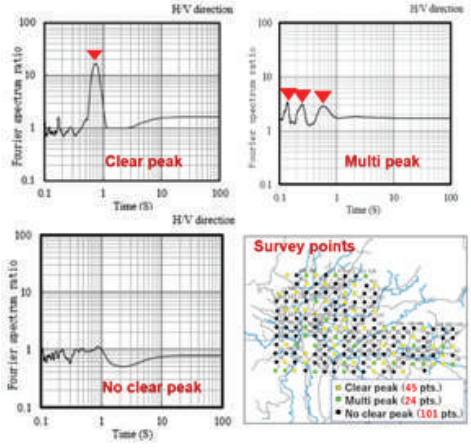

Figure 3: Interpretations of the ambient noise data in three typical H/V spectral peak forms.

of the 170 data acquisition points, 45 points showed clear peaks, 24 points showed multi peaks, and 101 points showed no clear peaks. The spatial distribution of the points is not quite well patterned but is quite mixed. A closer spatial analysis, however, makes it clear that the 'clear peak' points are denser on the northern part and the 'multi peak' points are denser in the middle.

Due to space constraint, it is not possible to include the diagrammatic details of all the comparisons between the H/V spectral peak patterns and the features of borehole log-interpreted material strata, but a preliminary understanding is that the 'clear peak' ground points are composed of thick layer clayey material over stiffer (sandy/gravelly) strata, the 'multi peak' ground points are composed of alternating soft (clayey) and stiff (sandy and gravelly) layers, and the 'no clear peak' ground points are composed of thicker layers of alternating sandy/gravelly layers with thinner clayey layers (Fig. 4, Fig. 5, and Fig. 6). This understanding may be an index to predict the ground structure out of ambient noise data analysis although the data reliability still needs to be increased through a large number of verification survey.

4. CONCLUDING REMARKS

Interpretation of ground ambient noise record data in terms of dominant frequency or dominant period helps assess ground shaking during earthquakes. In this study we have conducted a preliminary comparison of H/V spectral peak patterns of the ground structure. Our understanding from the ground ambient noise data analysis in the Kathmandu Valley is that there are typically three H/V spectral peak features: clear peak representing deep soft layers over harder strata, multi peak representing alternating clayey and sandy/gravelly layers, and no clear peak representing more alternative sandy/gravelly layers with thinner clayey layers.

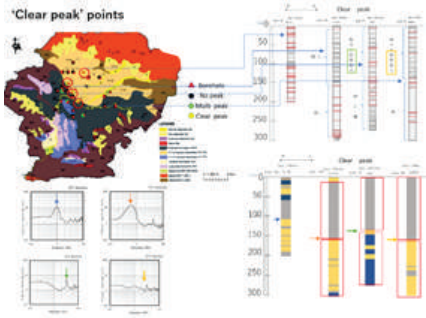

Figure 5: A few typical cases of comparison between the peak patterns of 'multi peak' points and the nearest borehole logs.

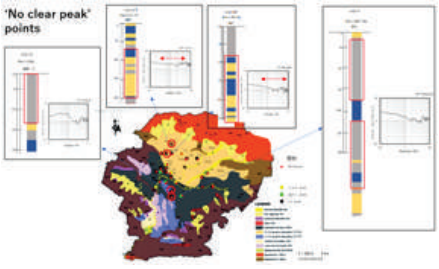

Figure 6: A few typical cases of comparison between the peak patterns of 'no clear peak' points and the nearest borehole logs.

REFERENCES

Nakamura Y, 1989. A method for dynamic characteristics estimation of subsurface using microtremor on the ground surface, Quarterly Report of the Railway Technical Research Institute, 30, 25-33.

Paudyal YR, Yatabe R, Bhandary NP, Dahal RK, 2013. Basement topography of the Kathmandu Basin using microtremor observation, Journal of Asian Earth Sciences, 62, 627-637.

#Spl-2:

Mapping Resilient Kathmandu: Intersecting Geo-Hazard Analysis and Urban Planning

Ar. Apil K C[1], Dr. Mandip Subedi[2]
[1]Institute of Engineering, Thapathali Campus, Kathmandu, Nepal
[2]Nepal Geotechnical Society, Kathmandu, Nepal)

1. INTRODUCTION

The cultural and historical center of Nepal, the Kathmandu Valley, is located in a region with significant seismic activity. The valley's current urban morphology can be dated to ancient times, where early inhabitants of Kathmandu were capable of spotting places that were less susceptible to hazards. Numerous recent catastrophes in the valley, including the earthquakes of 1934 and 2015, have made it clear that geo-hazard analysis should be incorporated into the tools used to make urban planning decisions, especially considering the rapid urbanization pattern in last few decades.

Despite the national development of hazard maps, these maps are not systematically incorporated into city planning level beyond the level of individual buildings. Hence, the need to integrate geo-hazard analysis in the urban planning decision-making process for open spaces, new settlements, and big infrastructures is of utmost importance.The study explores the gaps in policies and pracitces in urban planning through the lens of geo-hazard analysis.

2. METHODOLOGY

This study compares plans, policies, and development patterns of Kathmandu valley using GIS maps of liquefaction hazard analysis and urban settlement growth patterns. The hazard analysis identifies high-risk areas for liquefaction during an earthquake, while the settlement growth pattern is analyzed using satellite images to identify significant changes over time. Along with, the GIS maps are then overlaid to identify areas of high growth potential and high liquefaction risk. This allows for the identification of areas that are at high risk of disasters, and areas that could potentially be developed in the future. Existing plans and policies at local, regional, and national levels are examined, along with the plans of the Kathmandu Valley Development Authority for city development. However, the study only considers the Liquefaction as the only hazard indicator while making the evaluation.

3. RESULTS AND DISCUSSION

The comparison analysis's findings and the GIS maps' findings demonstrate that the Kathmandu valley's present urban planning decisions are not supported by a thorough comprehension of geo-hazard analysis.

The study revealed that geo-hazard analysis is not integrated into urban planning decisions in Kathmandu Valley, leading to vulnerable settlement development in high-risk areas. The lack of consideration for site analysis during decision-making is exemplified by the Balaju liquefaction zone, which was developed into housing despite its potential hazards, resulting in building collapses during the 2015 earthquake. Additionally, open spaces are not planned with evacuation centers in mind, which further exacerbates the population's vulnerability to natural disasters.

The findings highlight the need to incorporate geo-hazard analysis into decision-making for open spaces, new settlements, and big infrastructures to ensure safer and more sustainable urban development. Unfortunately, current decision-making is guided by private developers and abrupt political decisions that ignore potential hazards. This is exemplified by the Kathmandu Valley Development Authority's (KVDA) proposal to make new cities along the four cardinal directions of Kathmandu, planning more than one lakh ropani of lands without adequate consideration for site analysis. Several places in the valley are at a high risk of liquefaction during an earthquake, according to the GIS maps. These are also the regions that have grown significantly over the past few years. Analysis reveals that the potential risks connected with development in these areas are not taken into account during the decision-making process as it stands.

4. CONCLUDING REMARKS

In conclusion, it is critical for the safety of the residents of the Kathmandu valley that geo-hazard analysis be included in the decision-making process for open areas,

new settlements, and large infrastructures. Planners could create spaces and structures that are secure for the occupants by identifying areas that are less susceptible to hazards. However, there are obstacles that must be overcome for the execution of this strategy to be successful. The lack of consideration given to site analysis during decision-making, including making new cities and developing open spaces without evacuation centers, highlights the need for a more comprehensive approach to urban planning in Kathmandu Valley.

5. ACKNOWLEDGEMENT

The authors thank Dr. Mandip Subedi for providing the liquefaction geo-hazard data used in this study. Dr. Subedi's Ph.D. research on hazard mapping in Kathmandu valley laid the groundwork for this study.

REFERENCES

1. Bhattarai, K., & Conway, D. (2010). Urban Vulnerabilities in the Kathmandu Valley, Nepal: Visualizations of Human/Hazard Interactions. In Journal of Geographic Information System (Vol. 02, Issue 02, pp. 63–84). Scientific Research Publishing, Inc. https://doi.org/10.4236/jgis.2010.22012

2. Subedi, M., & Acharya, I. P. (2022). Liquefaction hazard assessment and ground failure probability analysis in the Kathmandu Valley of Nepal. In Geoenvironmental Disasters (Vol. 9, Issue 1). Springer Science and Business Media LLC. https://doi.org/10.1186/s40677-021-00203-0

3. Mesta, C., Cremen, G., & Galasso, C. (2022). Urban growth modelling and social vulnerability assessment for a hazardous Kathmandu Valley. In Scientific Reports (Vol. 12, Issue 1). Springer Science and Business Media LLC. https://doi.org/10.1038/s41598-022-09347-x

#Spl-3:

Development of a Digital Monitoring Device for Smart Rockfall Barriers

Dennis Gross[1], Manuel Eicher[1], Helene Lanter[1]
[1]Geobrugg AG, Romanshorn, Switzerland

1. INTRODUCTION

Without detection and lack of maintenance of flexible steel protection systems against natural hazards, appropriate protection of the assets below cannot be guaranteed. On the other hand, establishing regular controls despite the difficulty of access exposes personnel to unnecessary risks and isn't cost-efficient, as excessive routine checks will turn out to be unnecessary.

The second target, next to the monitoring of flexible steel protection systems against dynamic impacts, is to allow to pass from repair and preventive maintenance to predictive maintenance in the future by evaluating the local corrosivity with a digital twin. The presented digital device is equipped amongst others with an accelerometer and a specially developed corrosion sensor. Following an impact from a rockfall or debris flow, the device will send out a signal, enabling targeted maintenance. The development of the corrosion sensor is further described by Hofmann et al (2019).

This contribution focuses on the first results of the accelerometer embedded in the digital device, tested on a rockfall barrier in real terrain and not in a lab-style setup such as the rockfall barrier test sites. The working principle is that an impact of a rock with a certain kinetic energy into a flexible rockfall barrier will transmit this energy to the barrier which can be measured as an acceleration of the barrier itself.

2. METHODOLOGY

The very first prototype was tested at the flexible steel net supplier's test site, measuring the dynamic acceleration close to an energy-dissipating device. Different energy classes of rockfall barriers were tested with accelerometers, for example, a 100 kJ barrier without energy-dissipating devices, up to a 10'000 kJ barrier. This field test in a controlled environment allowed to set off a pre-triggering time and define an activation level of the sensor. The accelerometer needs to be able to detect a rockfall impact but shouldn't trigger a signal during a thunderstorm or the passing of wildlife (Wendeler et al., 2019).

3. RESULTS AND DISCUSSION

The Chant Sura test site is situated close to the Flüelapass, in the canton of Grisons, in Switzerland. It was initially used by the WSL Institute for Snow and Avalanche Research (SLF) for real rockfall experiments in order to calibrate the 3D rockfall simulation software RAMMS::ROCKFALL®.

In May 2019 an Innosuisse project (Swiss Innovation Fund) was granted to the SLF and Geobrugg for testing fully instrumented rockfall barriers in natural terrain with instrumented blocks (Sanchez et al., 2020). As the tests are fully instrumented good control of the energy of the rocks themselves is given and the actual loads transmitted to the boxes are known. Therefore, four digital devices were installed onto the barrier to calibrate them with the field results. The digital devices were installed on the upper support rope, the remaining ropes close to the post head and on the bottom support rope (see Fig.1).

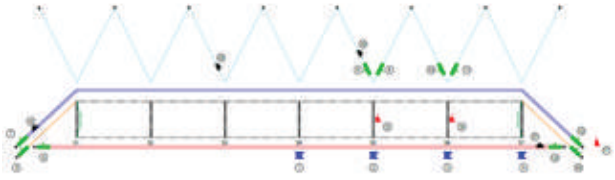

Figure 1: Technical drawing of the rockfall barrier at the test site. The digital devices are labelled in black by the numbers 18, 19, 20 and 21.

In total 6 impacts/accelerations were recorded for a total of 9 true impacts in the barrier. For the analysis and interpretation of the data, the focus will be set on Test number 8, with a wheel-shaped EOTA-style block 221, with a weight of 2'600 kg.

For rockfall dynamics results and interpretation see Sanchez et al., 2020. Figure 2 illustrates the total acceleration measured by the digital device 20 (see Fig.1). A peak total acceleration of 50.04g was recorded upon

impact with the EOTA wheel. This value is approximately half of the acceleration recorded by the block upon impact with the barrier.

These results were satisfactory for a proof of concept. Further tests were led in 2019 and 2020, developing the sensor further. Then the sensor got deployed all over Europe, gathering further experience (see Figure 3 for an example of an installed device).

An example of a real case is highlighted here, further case studies will be presented at the conference. Figure 4 illustrates an impacted rockfall barrier and its associated acceleration graph, recorded by the digital device. The impact was beyond the design energy of the barrier as well as the design jump height. The boulder sectioned the support rope, impacted the road below and ended up in a stream further down. The values of 196 and 120g triggered immediate control by the road maintenance crew, enabling the road to be closed until emergency repairs were done to the rockfall barrier.

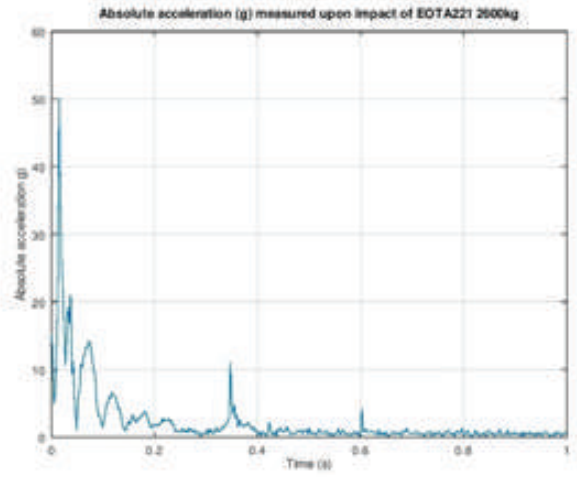

Fig. 2: Acceleration of the digital device upon impact

Figure 3: Example of an installed digital device called Geobrugg GUARD.

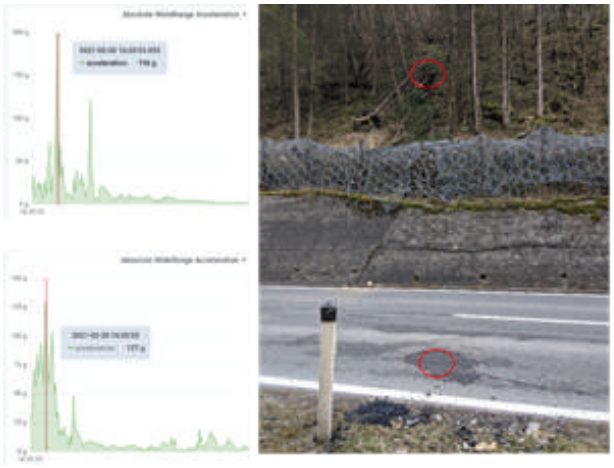

Figure 4: Example of an overload impact recorded by two digital devices.

4. CONCLUDING REMARKS

To summarise: the first steps into a digital monitoring concept for rockfall barriers, in a simple way, have been shown. This sensor concept can, in future, also be used for other applications such as flexible facings or debris flow barriers with the aim to minimize maintenance costs for the customer as much as possible. Continuous monitoring will allow us to refine the different corrosion classes with the obtained results.

REFERENCES

Hofmann, H., Sorg, M., Hörtnagl, A., Vogel, A., von Wartburg, J., "Development of a digital device for monitoring and predictive maintenance of flexible steel protection systems against natural hazards", extended abstract submitted to 14th Congress INTERPRAEVENT 2020, Bergen, Norway, 2019.

Wendeler, C., Svetlicic, S., Vogel, A., Sorg, M., "Smart Barrier Box for Monitoring and Sate Conditions of Evaluation of Rockfall Barrier Systems" International Conference on Information technology in Geo-Engineering, Portugal, 2019.

Sanchez, M.A., Lanter, A., Caviezel, A., Bartelt, P., Christen, M., Lu, G., Ringenbach, A., "Full-scale Testing of Flexible Rockfall Barriers under Realistic Conditions" submitted to 7th Interdisciplinary Workshop on Rockfall Protection, Sapporo, Japan, 2020.

#Spl-4:

Geotechnical Challenges in the Foundation Design of Mechi Bridge

Dr. A.P. Singh[1]
[1]*Honorary Secretary, Indian Geotechnical Society, New Delhi*
Director, Explore Engineering Consultants Pvt. Ltd., Noida, India, 201301
E mail: apsingh@exploreconsultants.com

1. INTRODUCTION

River Mechi, originated from the hills of Mahabharata range of Nepal and flows through Nepal forming the boundary between India and Nepal and then flows through the Indian state of Bihar to join the Mahananda in Kishanganj district of Bihar (India). The Mechi-Mahananda interfluve is a transitional area between the hills and the plains and exhibits a wide range of topographical variations.

The six-lane Mechi Bridge connects Panitanki in Darjeeling district of India with Kakarvitta in Jhapa District of Nepal. The new bridge is part of up-gradation of the Kakarvitta (Nepal) to Panitanki Bypass (India) on NH 327B covering a length of 1,500 meters including a six-lane approach road of 825 meters. This bridge is considered an Eastern Trade point between India and Nepal.

Figure 1. Location of the bridge

2. SITE CHARACTERIZATION

For the proposed construction of the six-lane bridge between the connecting points across river Mechi, suitable foundation system need to be proposed, designed and constructed. To reach the suitable and optimum design, the foremost important activity is to characterise the subsoil strata by conducting geotechnical investigation. To cover the entire stretch of the bridge, investigation was performed by making ten boreholes with depth of investigation as 40m below the existing ground surface. (Figure 2).

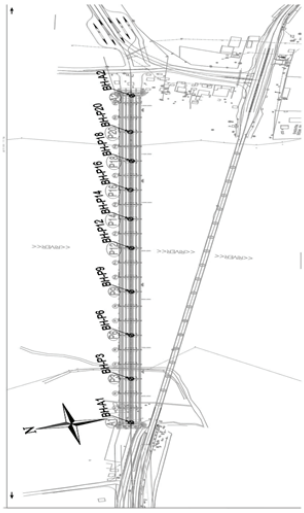

Figure 2. Bore holes location for investigation

From investigation in the field and the soil sample testing in the laboratory, it is found that the subsoil strata is Boulder, Cobble, Pebble with Sand Matrix and Sandy Silt with Gravel (ML-CL) throughout the explored depth. (Figure-3). Liquefaction potential analysis were done for the entire strata and it was found that the subsurface strata is not susceptible to liquefaction in seismic condition. Water table was considered at surface for all design

purposes. From hydrological study using the discharge regime and soil profile, it was recommended to consider scouring depth as 3.0m for abutment and 7.0m for Pier locations.

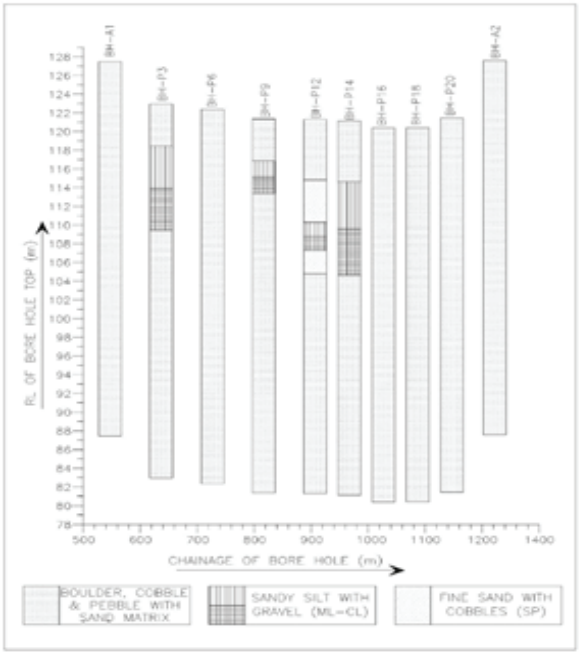

Figure 3. Sub surface strata profile

3. FOUNDATION PROPOSAL

In view of the findings & results obtained during the field and laboratory investigations and the analysis carried out thereafter, isolated foundation as well as cast in situ bored piles were recommended as the suitable foundation for the proposed bridge construction. The allowable bearing capacity for the isolated square footing of different sizes and founding levels and load carrying capacity for pile of 1000mm diameter and different lengths were calculated as per IS code and recommended as per given in table 1 and table 2.

Table 1- Recommended value for isolated foundation

Founding Level Below EGL (m)	Size of Foundation (m)	$q_{allowable}$ (t/m²)
5.00 (Abutment)	8.0 X 8.0	32.50
	10.0 X 10.0	32.75
6.00 (Abutment)	8.0 X 8.0	34.50
	10.0 X 10.0	33.75
6.00 (Pier)	8.0 X 8.0	33.00
	10.0 X 10.0	32.75
7.00 (Pier)	8.0 X 8.0	34.50
	10.0 X 10.0	33.75

Table 2- Recommended value for pile foundation

Effective Length (m)	Safe Axial Capacity (t)		Safe Lateral Capacity (t)	
	Comp.	Uplift	Free Head	Fixed Head
23.0	275	180	8.5	31.0
25.0	300	200	8.5	31.0
27.0	330	230	8.5	31.0

The above recommendations were made for the foundation design and construction. Initially, pile of recommended diameter and capacity were adopted for construction. Initial pile load test was designed and planned to be carried out. While doing the pile installation, there was so much aquifer pressure that the piling work could not be done properly. Hence it was decided to abandon the design of pile foundation as the suitable foundation system for the project. The next adopted foundation system was shallow square foundation of the determined size and founding level below the scouring depth. This foundation was successfully adopted and executed for the proposed bridge structure.

4. CONCLUDING REMARKS

From this investigation and findings of the project, it is found that subsurface strata, hydrological condition, and scouring depth play very important role in successful design and construction of the project. At this site, deep foundation was not executed due to practically adverse site situation for piling. Hence open shallow foundation was adopted and executed.

ACKNOWLEDGEMENT

Thanks are owed to M/s ASC Infratech Pvt Ltd. Noida and Mr Ajay Srivastava in person who is designer for the project for providing all technical project data and support. Thanks to M/s Explore Engineering Consultants Pvt. Ltd. Noida also for sharing the geotechnical investigation report of the project.

REFERENCES

1. IS:1893 (Part-1) : 2016 – Criteria for earthquake design of structures
2. IS:2911 (Part I / Sec.2) : 2010 : Design and construction of pile foundations
3. IS: 6403-1981: Code of practice for determination of bearing capacity of shallow foundations
4. IS: 8009-1976 (Part-1) Code of practice for calculation of settlements of foundations: Shallow foundations subjected to symmetrical static vertical loads (Amendment 2)
5. Geotechnical Investigation report by M/s Explore Engineering Consultants Pvt. Ltd Noida (Ref. : 17123388)

#Spl-5:

Slope Stability Analysis of Waste Dump in Sisdol, Nepal for Post-closure Plan and Sustainable Utilization of Land

Dhundi Raj Pathak[1] and Manab Rijal[2]

[1]*Engineering Study & Research Centre, Kathmandu, Nepal*

[2]*Maccaferri (Nepal) Pvt. Ltd., Kathmandu, Nepal*

1. INTRODUCTION

The quantity of solid waste has immensely increased in Kathmandu Valley (KTMV), Nepal due to rapid urbanization and economic development. In 2020, more than 60% (~800 tons per day) of municipal solid waste (MSW) generated in the KTMV was disposed of at the Sisdol dumpsite. It was initially a sanitary landfill site but turned into a vulnerable dumpsite due to a lack of minimum landfill elements and poor operation for more than 13 years, which created multiple environmental problems in surrounding areas. Now, the height of the waste dump has reached to more than 80 meters when extending nearly 300 meters horizontal distance. As the Sisdol dumpsite has already been saturated and overloaded, its post-closure management is needed and should be carried out soonest possible. For this purpose, stabilizing the steep slope of the Sisdol dumpsite is required. Therefore, this paper applies the SLOPE/W to carry out the slope stability analysis (SSA) of the Sisdol dumpsite.

2. METHODOLOGY

To analyze the stability of the slope, geometry for the SSA in SLOPE/W was prepared based on the recent topographic survey of the dumpsite. We divided the subsurface strata into three regions in the model; fresh MSW, old MSW, and natural ground. As no field and laboratory tests have been conducted on the MSW, literature review, judgment and experience with similar materials have been used to adopt the pertinent shear strength properties of the MSW. The groundwater table was modeled drawing the phreatic line in the SLOPE/W based on the observation made on the site. The SSA was carried out for both normal groundwater table (NGWT) and elevated groundwater table (EGWT). As we know the effective cohesion of the soil decreases when the soil gets saturated, different sets of shear strength parameters has been adopted for NGWT and EGWT.

3. RESULTS AND DISCUSSION

From the SSA result, we can observe that the factor of safety (FoS) of the waste slope decreases when MSW is saturated. And, this result justifies the site condition during the monsoon season. During the monsoon season, the mass movement has been frequently observed after MSW gets saturated. As presented in Table 1, the slope profiles along alignment-1 and alignment-2, FoS is above 1 for both NGWT and EGWT. For alignment-3, the FoS for NGWT is marginally above 1, and for EGWT is less than 1. And, for alignment-4 and alignment-5, the FoS is less than 1 for both NGWT and EGWT conditions, which is also in compliance with the observation made at the site. It supports the assumption of the shear strength parameters of the landfill material. However, the properties of dump materials change with depth and time along with the geometry of the slope modeled in course of time. So, the SSA in this study indicates the risk of sliding off the dumpsite along the road connecting the proposed Bancharedanda landfill, which needs to be analyzed in detail to design the proper stabilization measures before post-closure and sustainable utilization of land in the Sisdol dumpsite.

Table 1: Summary of the FoS of SSA

Alignment	FoS: option -1	FoS: option- 2
Alignment - 1	1.61	1.33
Alignment - 2	1.54	1.35
Alignment - 3	1.04	0.89
Alignment - 4	0.93	0.81
Alignment - 5	0.96	0.80

4. CONCLUDING REMARKS

This paper presents the result of the SSA of the Sisdol dumpsite before developing a post-closure and land utilization plan. For this purpose, the FoS was calculated in five critical sections. The FoS obtained in Alignment-4 and Alignment-5 for both NGWT and EGWT from the analysis confirms the slope is unstable and the risk of sliding of the dumpsite along the road connecting the new Bancharedanda landfill, which is also in compliance with the observation made at the site. The analysis helps to design proper stabilization measures before post-closure plan and sustainable utilization of land in the Sisdol dumpsite.

REFERENCES

Babu, G. S., Chouksey, S. K., & Lakshmikanthan, P. (2012). Study of engineering properties of MSW of Bangalore city. In Proceedings of Indian Geotechnical Conference.

Caicedo, B., Yamin, L., Giraldo, E., Coronado, O. (2002a). Geomechanical properties of municipal solid waste in Dona Juana sanitary landfill. In: Proceedings of the Fourth International Congress on Environmental Geotechnics, Brazil, vol. 1, pp. 177–18

#Gen-1:

Engineering Geological and Geochemical Investigation of Black Clay Deposits of Dang Valley Lumbini Province, Nepal

Madan Oli[1], Adesh Atreya[1], Manoj Thapa[1], and Megh Raj Dhital[1]
[1]Department of Geology, Tri-Chandra Multiple Campus
Tribhuvan University, Kathmandu, Nepal

1. INTRODUCTION

Clays are naturally occurring fine-grained soils with particle size less than 2µm that are generally plastic at a suitable range of water content and hardens when subjected to high temperature (Dogan et. al., 2002). The nature of clay and its mineralogical composition regulates its quality, commercial use, and engineering behavior. The engineering perspective of clay is influenced by mineralogical constituents and physical properties such as particle size distribution, non-clay mineral composition, organic content, and geologic history of formation (Grim, 1968). These properties of clay determine their commercial use depending on various types admixed, the percentage and composition of non-clay minerals present, and other factors.

The Dang valley is comprised of Pleistocene to Holocene fluvial sediments and the southern territory is dominated by lacustrine deposits comprising dark gray to black silt and clay. Therefore, the primary objectives of this research are to prepare the soil map and to characterize the properties of black clay for industrial applications in the southern end of the Dang Valley.

2. METHODOLOGY

This study followed the qualitative approach in the case of soil mapping and the quantitative concerning soil properties. At first, fieldwork was accomplished with two main stages- description of soil type locality and collection of soil samples for laboratory testing. It included specific coordinates, respective soil categories and its description, a columnar section of the soil profile, and soil texture information. Further, soil samples were collected from sites generally from a depth of about 1 meter by pushing the hollow circular rubber pipe with a nominal internal diameter of 90 millimeters into the soil supported by a hammer to thrust inside.

Apart from mineralogical and chemical analysis, the soil sample was tested for engineering geological characteristics that include specific gravity, natural moisture content, particle size distribution, Atterberg limits, and Hydrometer analysis. On the other hand, the chemical analysis includes the determination of the percentage of various oxides (SiO2, Al2O3, Fe2O3, K2O, CaO, and MgO) with loss of ignition.

3. RESULTS AND DISCUSSION

Eight varieties of soil based on the raw color of soil were identified in the field and are presented in the map as shown in Figure 1. It shows predominant red

soil in the northern and eastern parts of the valley whereas, the southern marginal area is dominated by yellow silty clay where the thickness was observed to be greater than 20 m. The southern-central to southern- eastern part features black clay with a thickness greater than 10 m and grey-brown to yellow clay is distributed in the central part of the valley. The columnar section in the maps shows the decreasing grain size from north to south.

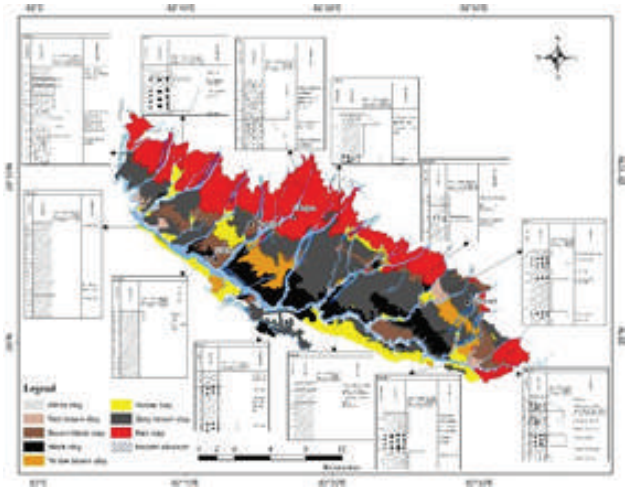

Figure 1: Soil map of the Dang Valley

In regards to index properties of the soil, samples resulted have lower moisture content, particularly less than 15%, and only nine samples manifested the specific gravity to lie between the range 2.3-2.7. In terms of grain size analysis, almost all samples account for 90-96% of clay and silt

and the grain size classification of raw clay sample is presented in Winkler's diagram as shown in Figure 2. The plasticity index count ranges from 9-30% and the liquid limit of the samples has values from 23-55% respectively, and the plot is presented in the Bain and Highley diagram as shown in Figure 3. Further, the shrinkage percentage, loss of ignition (LOI), modulus of rupture (MOR), water absorption percentage, water of plasticity, total dissolved solids (TDS), residue 240 mesh, and optical properties are shown in Table 1.

Among the percentage of chief oxides (SiO2, Al2O3, Fe2O3, K2O, CaO, Na2O, and MgO), SiO2 varies from about 40 % to 90 % with most of the samples containing SiO2 ranging in between 50 to 70% whereas, TiO2 and Na2O, the variation is smaller and content are less than 1 %. A ternary plot of chemical constituents with SiO2, Al2O3, and the sum of the remaining oxides present in the raw clays in each axis is shown in Figure 4.

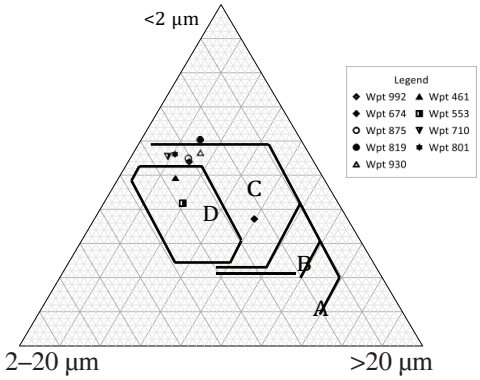

Figure 2: Grain size distribution of raw clay in Winkler's diagram. Domains: (A) common bricks, (B) vertically perforated bricks, (C)roofing tiles and masonry bricks, and (D) hollow products

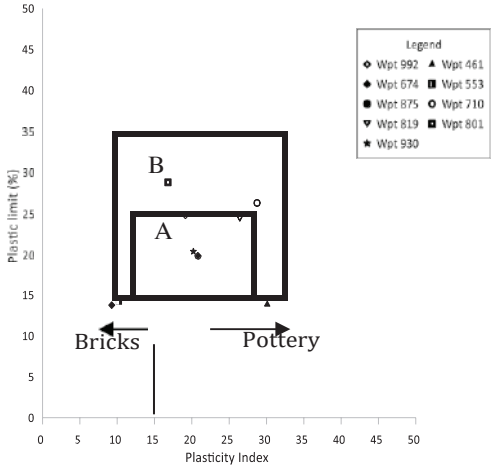

Figure 3: Diagram of Bain and Highley representing Atterberg limits of raw clay showing domains for clay shaping by extrusion. (A) optimum and (B) acceptable

Table 1: Test result of soil properties

Samples	Physical Properties												
	Shrinkage (%)	LOI (%)	Dry MOR kg/cm²	Fired MOR kg/cm²	Water abs. (%)	Water of plasticity (%)	T.D.S	Residue 240 (%)	L*	a*	b*	White-ness	Fired color
Wpt 728	O.F	8.33	26.8	O.F	O.F	32	480	0.92	38.34	6.84	7.88	10.06	Dark brown
Wpt 729	3.62	12.38	23.4	172.2	11.48	26.6	525	4.47	59.41	8.68	19.61	27.68	Light yellow
Wpt 730	9.89	6.75	28.7	282.2	0.45	32.4	480	0.54	40.97	12.02	12.93	12.25	Brown
Wpt 731	6.52	5.84	26.4	271.2	1.36	28.2	380	1.12	42.44	14.39	16.43	12.87	Brown
Wpt 732	5.84	17.92	26.9	182.8	9.92	32.4	515	1.31	56.22	8.36	23.78	23.57	Light yellow
Wpt 733	6.45	6.52	26.5	275.7	2.75	30.2	380	0.81	39.07	9.78	10.84	11.05	Brown
Wpt 734	2.09	3.24	23.8	173.2	10.63	22.6	605	2.37	50.62	20.12	25.59	19.26	Light red
Wpt 735	0.07	1.44	ND*	124.2	19.73	ND*	80	14.62	59.75	21.57	30.15	27.95	Yellow
Wpt 736	O.F	9.87	28.7	O.F	O.F	37.2	465	0.88	42.94	12.46	14.66	13.84	Brown
Wpt 737	O.F	7.35	27.3	O.F	O.F	32.5	1200	0.72	41.33	12.04	14.25	11.61	Dark brown
Wpt 738	2.62	11.47	29.5	228.2	6.82	34	950	1.85	48.42	15.73	18.46	16.99	Light brown
Wpt 739	4.25	10.85	27.1	241.2	6.59	32.8	610	1.52	45.89	13.61	17.05	15.44	Light brown
Wpt 740	9.28	4.35	28.6	342.2	0.75	32.4	280	0.68	41.98	12.07	13.28	12.72	Brown
Wpt 741	4.58	7.47	23.6	193.2	9.23	24.2	265	8.08	50.32	8.92	15.98	17.36	Greyish brown
Wpt 742	6.26	4.63	25.4	318.2	4.97	28.2	230	0.71	43.93	17.19	19.49	14.22	Light red
Wpt 743	2.96	17.19	26.7	152.2	14.19	33.4	340	0.55	71.07	8.49	27.32	42.05	Yellowish white
Wpt 744	5.42	11.63	26.2	224.4	5.25	31.4	215	4.63	51.66	9.85	17.19	19.72	Light brown
Wpt 755	7.82	5.65	26.8	267.7	5.11	34.4	210	0.52	43.81	17.87	20.25	13.65	Reddish brown
Wpt 756	5.84	6.07	26.5	287.2	4.65	33.2	155	0.75	45.11	18.83	22.54	14.56	Reddish brown
Wpt 757	3.67	4.75	25.1	202.5	9.31	31.2	120	1.35	46.32	19.53	24.03	15.82	Light red

The different color of the soils represents various depositional sediments such as gravelly soils in the northern valley which appear red whereas, clay is dominant in the southeastern part of the valley which appears as grey-brown to black. The central part consists of a mix of gravel, sand, and fine which appear to be yellow to grey-brown. Soils with less clay content can be subjected narrowly to particular use in ceramics contrary to soils with a fair amount of coarse- sized particles used in the coarser ceramic products (Singer & Singer, 1963).

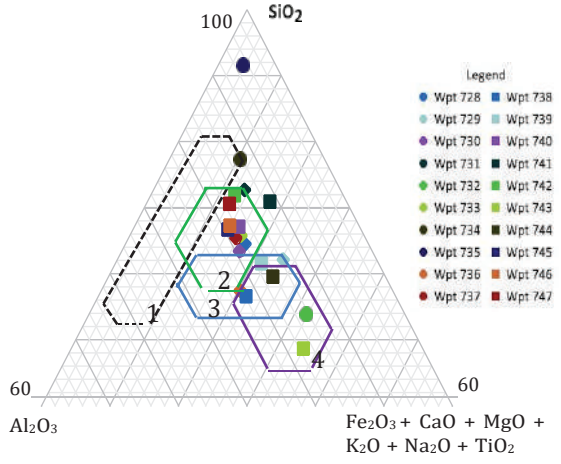

Figure 4: Ternary diagrams presenting the chemical composition of raw clays and domains for application. stoneware tiles :(1) white bodies, (2) red bodies, and (3 and 4) porous tiles

The Al2O3/ Fe2O3 ratio range of Clay from Dang is

2.1 – 3.3 indicating iron-rich clay indicating the relevance of clay for building materials and table wares. The high proportion of fines in the clay makes most of the clay convenient for pottery also as supported by the plot of Atterberg limits in the diagram of Bain and Highley. Clays with PI values greater than 10% are preferred for ceramic products to avoid risks of cracks.

4. CONCLUDING REMARKS

In conclusion, the dominant grey to black clay with greater organic content and abundant mollusc shell indicates the prehistoric lacustrine environment. These soils can be used in roofing tiles, light blocks as well as thin-walled hollow bricks and blocks along a higher proportion of clay making it suitable for pottery also as indicated by particle size distribution and the plasticity index values pointed to its usefulness in structural ceramics. The clay can also be utilized as raw materials in tiles, fired bricks, red stoneware tiles, and red porous tiles.

ACKNOWLEDGMENT

The researchers are indebted to the University Grants Commission (UGC) for financially supporting the work. We are grateful to the Department of Geology, Tri-Chandra Multiple Campus, and Planet Test Pvt. Ltd. for providing the environment and assisting with laboratory work.

REFERENCES

Dogan, C. P. et al., 2002. Improved refractory materials for slagging coal gasifiers. Florida, USA, s.n., pp. 1167 - 1176.

Grim, R. E., 1968. Clay Mineralogy. 2nd ed. New

York: McGraw-Hill Book Company.

Singer, F. & Singer, S. S., 1963. Industrial ceramics.

1st ed. London: Chapman & Hall.

#Gen-2:

Rockfall Hazard Mitigation along Main Approach Road of Z-Morh Tunnel Jammu & Kashmir, India

Prakash Ravindran[1], Deepak Manjunath[2] and Saikat Chatterjee[3]

[1]*Assistant Manager, Reinforced Earth India Pvt. Ltd (Terre Armeè), Bengaluru, 560094, India*

[2]*Head-Engineering Operations, Reinforced Earth India Pvt. Ltd (Terre Armeè), 110044 New Delhi, India*

[3]*Assistant Vice President, Reinforced Earth India Pvt. Ltd (Terre Armeè), New Delhi, 110044, India*

1. INTRODUCTION

A natural phenomenon that results in a threat to human safety or that induces damage to infrastructure is broadly classified as a geohazard. Rockfall is a type of geohazard that results when varying sizes of rock are detached from the parent rock mass. Depending on the steepness of the hill slope, the detached rock mass either rolls, bounces or falls down the hill slope. The joint orientation of rock mass, bedding dip direction, extent of weathering and steepness of the slope are some parameters that determine the type and severity of rockfall events. Natural freeze thaw cycles, earthquakes and some human induced forces like blasting and excavation of hill slopes comprising rock masses also trigger rockfall events. This paper presents a case study that validates the performance and functional advantages provided by rockfall barrier systems when used to arrest falling rock during excavation works for construction of the main approach road leading to the Z-Morh tunnel in Sonamarg, Jammu and Kashmir, India.

Fig. 1 Rockfall Barrier

2. ROCKFALL BARRIER SYSTEM

Rockfall barriers typically comprise steel posts and a flexible net supported by wire ropes. The systems are anchored to the ground using rock or soil anchors. There are two primary styles of rockfall catchment fence system viz., fixed, and hinged connection. Fixed post systems are much heavier than hinged ones with the same energy capacity because the hinged system distributes forces from the post head directly to anchors via upslope retained ropes. These barriers use steel components and steel wire ropes made from high quality materials, following a stringent quality assurance program.

Given the high risk posed to commuters on the operational Srinagar-Leh Highway (NH1) and several

residential buildings down the hill and in close vicinity to the construction area of the hill road, the rockfall barrier system was designed by considering Consequence Class 3 of the Austrian guideline ONR 24810. An EAD (formerly known as ETAG 27) certified, hinged rockfall barrier system having Maximum Energy Level (MEL) capacity of 500 kJ and characterized by a combination of High Energy Absorbing (HEA) posts, galvanized cable rope Omega Net, retaining, bearing, side stabilization ropes and spring type brake elements was designed and installed along a 2 km stretch.

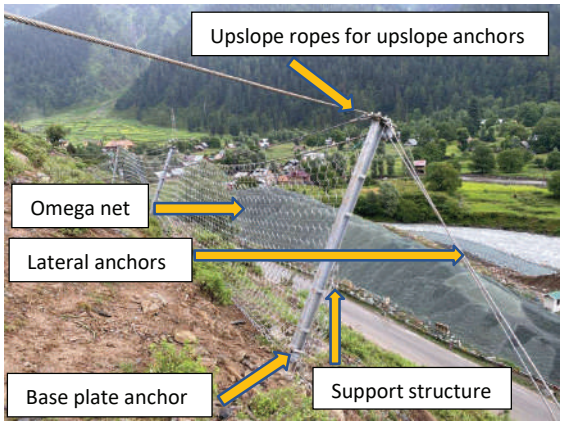

Fig. 2 Components of Rockfall Barrier

3. DESIGN PHILOSOPHY

In order to evaluate the rock fall hazard and to propose adequate measures, the rock fall potential has to be analyzed in detail. A comprehensive understanding of

Rockfall trajectories is the key to effectively control Rockfall hazards. An important characteristic that distinguishes different rockfall models is the presentation of the rock block in the model. Lumped mass models represent rock as a dimensionless point, while rigid body models can consider block geometry in rockfall simulation. The detailed design analysis for this project was done by Lump Mass method using the RocFall2 simulation program from Rocscience Inc.

The program produces two kinds of "envelopes" namely: the kinetic energy envelope and the velocity envelope. Each envelope is defined by the maximum value (e.g., maximum velocity) at a number of evenly spaced horizontal locations along the slope profile. The kinetic energy envelope measures the highest kinetic

energy that any rock attains while passing each horizontal location. The velocity envelope measures the highest velocity that any rock attains while passing each horizontal location.

The location of the rock endpoints is, arguably, the most important single piece of output from the program. The location of the rock endpoints is presented as a distribution.

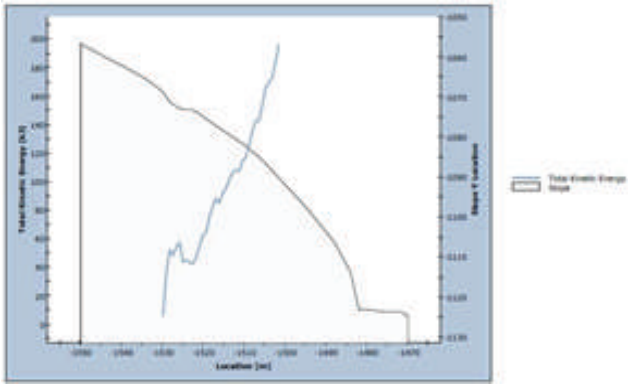

Fig. 3 Total Kinetic energy on Slope

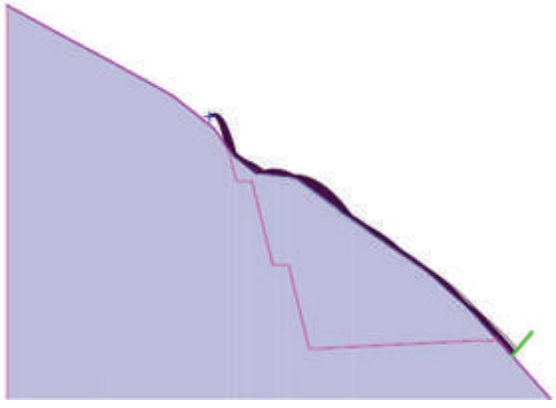

Fig. 4 Rockfall simulation output

DESIGN CONSIDERATIONS:

- As per site condition, the maximum diameter of the boulder considered for analysis was 0.5m.
- The density of the boulder is considered as 2,500 kg/cu.m.
- The source was considered in the excavation zone for road construction from where potential rockfall events were envisaged to be initiated.
- The objective was to position the rockfall barrier above the village area to protect the human lives and infrastructure like buildings and service roads. Trumer's online design tool "TheRockStopsHere"

was used in the selection of appropriate anchorage by verifying the acting kinetic energy, bounce height and anchor forces against the resisting criteria of the structure and anchors based on input parameters obtained during site investigation and further modelling.

4. CONCLUSION

The 500 kJ TSC-500-ZD rockfall barrier was installed along a 2 km stretch out of a 3.5 km stretch of the main approach road leading towards the western portal of the Z-Morh tunnel. The maximum estimated impact energy on the rockfall barrier at various design chainages as per the design considerations is summarised as below:

Table 1: Summary of Calculated Maximum Impact Energy

Design chainage (Km.)	Max. Kinetic Energy (kJ)
1+010	270
2+240	254
3+010	306
4+350	223

The installed rockfall barrier having a maximum impact absorption capacity as 500KJ was successful in mitigating the rockfall hazards during the construction of the Main approach road. There is no doubt that guidelines, standardization, and certification of hazard mitigation products is necessary and beneficial.

REFERENCES

1) Bichler, A. and Stelzer, G. (2014) Special solutions in hazard mitigation. Proceedings of GeoHazards 6, Kingston, Ontario, Canada, 15-18 June 2014.

2) Stelzer, G. and Bichler, A. (2013) ONR 24810 – A comprehensive guideline for building better rockfall protection structures. Proceedings of the 64th Highway Geology Symposium, North Conway, New Hampshire, USA, 9-12 September 2013.

#Gen-3:

Restoration of Riverbank and Prevention of Further Soil Erosion Using Tech Revetment® at U/S of Dikchu Bridge along the Left Bank of Reservoir from EL-570m to 580m and RD ±20m to ±100m at Teesta-V Power Station Sikkim. (Package-I), North Sikkim, India

Hirak Dutta[1], Sunip Barman[2] and Prasanna Gangaler[3]

[1]Head - Special Projects, Reinforced Earth India Pvt. Ltd. (Terre Armée India), New Delhi, 110044, India.
[2]Business Development Manager, Reinforced Earth India Pvt. Ltd. (Terre Armée India), Kolkata, 700071, India.
[3]Design Manager, Reinforced Earth India Pvt. Ltd. (Terre Armée India), Bengaluru 560094, India.

1. INTRODUCTION

This paper presents a case study that validates the performance and functional advantages offered by TechRevetment® – an engineered, factory customised, durable and flexible geosynthetic fabric form grouted mattress system that was successfully adopted for erosion control and scour protection in a riverine hydraulic setting for a reservoir of Hydro Electric Power (HEP) Project in India.

Keywords: *Concrete, fabric, grouted mattress system, restoration, reinforcement, riverbank protection, soil erosion.*

2. BRIEF BACKGROUND

The 2019 monsoon season was characterized by several high intensity rainfall events, which resulted in large scale riverbed scouring and erosion along the left bank of reservoir of Teesta-V Power Station in Sikkim, India. In one stretch, a portion of the riverbank was washed away due to the high-water discharge. The structural integrity of the Dikchu bridge abutment that connects East Sikkim to North Sikkim was at risk due to severe soil erosion. Heavy erosion also resulted in partial collapse of the adjoining highway (NH 310A); see Figs.1, 2 & 3.

Fig. 1. Initial condition (a). at Site

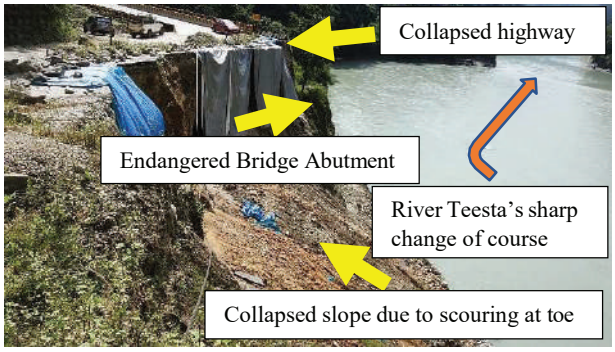

Fig. 2. Initial condition (b). at Site

Fig. 3. Initial condition (c). at Site

3. PROPOSAL FOR RESTORATION

Restoring the damage was critical, especially since National Hydro Electric Power Corporation (NHPC) 3x170 MW power generation station, i.e., Teesta-V was located upstream of the river. Teesta-V was commissioned in 2008 to harness the hydro power potential of the River Teesta. Keeping in mind the interruption of power generation and direct revenue loss for NHPC in the event of a temporary stoppage of power generation, Terre Armée India proposed a unique solution that would be implemented in underwater conditions without stopping the operation of NHPC. This solution involved the proposed lining of bi-directional TechRevetment® mattress along a 70m stretch of the riverbank to protect it

from further soil erosion during the lean period (by March 2020) when the velocity and depth of water are relatively low. The design was carried out by Terre Armee India keeping in mind the recommendations of IRC-SP-113:2018 and FHWA-NHI-09-112 (Hydraulic Engineering Circular No. 23).

4. CRITICALITY

There were several critical factors that were taken into account while executing this task. Keeping in mind the River Teesta's flow velocity of around 4 m/sec., a team of professional divers was deployed for rapid underwater installation during low water level. The Terre Armée team was able to effectively carry out work for only 4 -5 hours a day since they had to keep in mind the draw-down aspect of the water level. During the divers' initial dive and subsequent analysis, it was understood that the gabions that were earlier installed at this location had partially collapsed, and so was the road section. The crash barriers that were provided at the edge of the road also feel in the river during collapse of the road resulting in the formation of an undulated riverbed that was unsuitable for the laying of the TechRevetment® mattress. Also, the divers noticed that there were deep undercuts in the river, and the riverbed was also at a steep angle. These factors made the process of laying our TechRevetment® mattress a bigger challenge. Therefore, a gentle profile of the riverbed was prepared by placing boulders and laying soil bags with the help of divers and the boat carrying these construction materials. Transporting sandbags and boulders to the process for bed preparation was also an onerous task. Two other factors, namely the extremely cold water and the rapid flow of water in the river meant that the divers could work under water only 15 minutes at a time.

5. SEQUENCE

The primary step in the restoration work involved arranging boats and putting in place the requisite safety measures to enable a team of divers to investigate the existing underwater profile; see Fig. 4.

Fig. 4. Restoration work underway

Based on the divers' understanding of the underwater situation, the design mix for fine aggregate concrete was established after checking the flowability and compressive strength as per specifications. Subsequently a flatter slope on the riverbed was prepared, and voids that were caused due to deep scouring were filled with boulders and sandbags. Submerged sharp projections that occured due to the result of gabion wires and submerged concrete debris were either removed or covered since these, if left unattended could possibly rupture the TechRevetment® mattress. A layer of non-woven geotextile was then laid and secured. TerraAnchorsTM were then driven into the existing reiver bank or gabion lining, as per actual site conditions; see Fig. 5. The first portion of the TechRevetment® mattress was then laid, and the high-tensile wires pre-installed within the mattress were connected to the TerraAnchorsTM; see Fig. 6.

Fig. 5. Laying of NGT and TechRevetment® mattress

Fig. 6. Connecting TerraAnchorTM strand to HT strand of TechRevetment® mattress

Concrete pump and other necessary tools were placed at a suitable location. Subsequently, fine aggregate concrete was filled into the mattress. While doing so, the team ensured that this activity started from the upstream end and gradually progressed towards the downstream end. Subsequent mattresses were connected one after the other using an industrial zipper and fine aggregate concrete was carefully pumped into those, one after the other and completed; see Fig. 7.

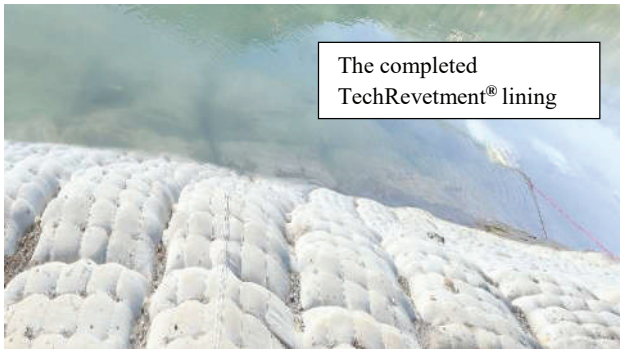

Fig. 7. The completed TechRevetment® mattress as seen from the surface

6. RESOURCES DEPLOYED

The contractor deployed a team of professional divers equipped with all the necessary protection gears and boats for the purpose as per recommendation of Terre Armee India. Self-loading concrete mixers were pressed into service, in addition to concrete pump and requisite accessories. Driving equipment, used for the installation of TerraAnchorsTM were also used in this operation. Terre Armée's trained technical experts provided full time (24x7) technical assistance to the contractor's installation team during activities like bed preparation, fabric laying and concrete filling.

7. CONCLUSION

The TechRevetment® grouted mattress system with bi-directional cable reinforcement that was installed at the left bank of reservoir of Teesta-V Power Station in 2020 is performing well and continues to provide optimum protection to the riverbank, thereby preventing further soil erosion, and protecting the highway from further damage. After successful commissioning of the project, we can conclude the following points;

- TechRevetment® mattress is custom made at factory as per geometry and dimensions of the project site. Adjacent panels are joined by using industrial zipper. Hence, there was no sewing or manual stitching at site. This made the entire work very easy and faster.
- TechRevetment® technology due to its custom design and site-specific factory production ensured uniform thickness with high standard of quality without any major manual intervention.
- TechRevetment® can be used underwater for important HEPs without stopping the power generation operation, thus without any revenue loss to the project owner.
- Use of high strength cables as reinforcement ensures the integrity of the mattress, which guarantees high performance under turbulent hydraulic force and rapid draw down conditions. The cables improves the flexibility of the mattress and prevents allows the launching of the apron under riverbed scouring without individual disintegration of the blocks. This also ensures high performance against uplift as compared to mattress systems without cables.
- It is critical to protect the hill toes, especially that are adjacent to riverbank or reservoirs to prevent land slide or slope failures and for protection of infrastructure.
- Trained and efficient divers are important for carrying out this type of projects.
- An experienced engineering team is also necessary to guide the contractor during installation and to manage site-specific unforeseen problems.

REFERENCES

1) FHWA-NHI-09-112, Hydraulic Engineering Circular No.23: "Bridge Scour and Stream Instability Countermeasures: Experience, Selection, and Design Guidance-Third Edition- Volume 2" published September 2009.

2) IRC 89 (1998): "Guidelines on flood disaster mitigation for highway engineers".

3) IRC-SP-113-2018: "Guidelines on Flood Disaster Mitigation for Highway Engineers"

#Gen-4:

Effect of Forest on Debris Flows

Sandeep Shrestha[1], Prof. Rao Martand Singh[2], Prof. Vikas Thakur[3]
[1,2,3]Norwegian University of Science and Technology
(NTNU, Trondheim, Norway)

1. INTRODUCTION

Debris flows cause tremendous risks for damage and destruction of the infrastructures and risk of casualties in mountainous and hilly regions around the world. They impose such danger due to their combination of high velocity, impact forces, long run-out distance and difficulties in the prediction phenomena (Jakob, M., Hungr, O., and Jakob, D. M., 2005). They contain a mixture of rock, water and soil and are driven/steered by gravity (Iverson, 1997). They are usually triggered through the means of small or large landslides, short-duration intense rainfall, long-duration rainfall, surface runoff from colluvium and bedrock. (Coe, J. A., Kinner, D. A., and Godt, J. W., 2008). They are serious geohazards because of their prediction difficulty, their high flow velocity and their long runout distances (Chen, H., & Lee, C. F., 2004).

Numerical modelling methods are very useful to both back-calculate the documented debris flows and forward calculate the consequence of possible hazard scenarios. However, their application creates several new challenges to geotechnical engineers (Shrestha, 2020). A long-standing problem in the study of debris flows is to understand how forests interact with debris flows. Studies show small and medium debris flows are decelerated and, in some cases, stopped by the forest stands. Whereas, large debris flows break, uproot and overturn trees causing damage to the forests as trees fail to withstand tremendous energy carried by the large and fast-moving debris flows. The trees and branches of the forest area that are entrained by the debris flows might impede the flow. However, it might also increase the flow height which subsequently might increase the erosion downslope as well. Since forests are enormously present in the mountainous regions, it is very important to understand how trees affect debris flow in terms of their flow behavior and runout distance. The major objective of this paper is to observe the effect of forest area on debris flow using a numerical modelling tool “RAMMS::DF”.

2. METHODOLOGY

The parameters that have been studied are the flow velocity, flow height, runout distance, and energy loss due to the presence of forest area on the small-scale flume model. To achieve the main objective firstly the calibration of Voellmy friction parameters (Mu and Xi) of the model are necessary and they are back calculated to obtain similar results given by the physical modelling tests. Forest area is then introduced into the program and its effect on flow velocity, flow height, Froude number and runout distance are observed and analyzed.

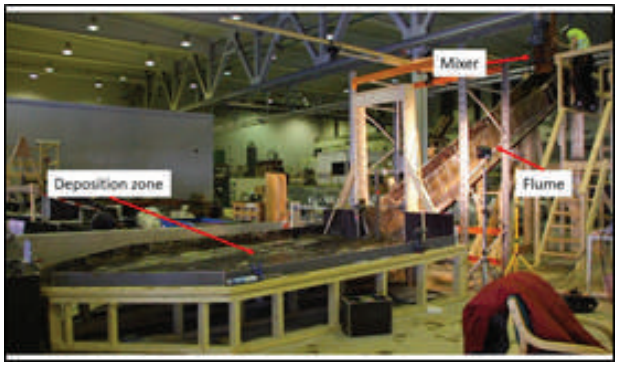

Figure 1 The flume model used in the experiments for the physical modelling experiments of debris flows (Vicari, 2018)

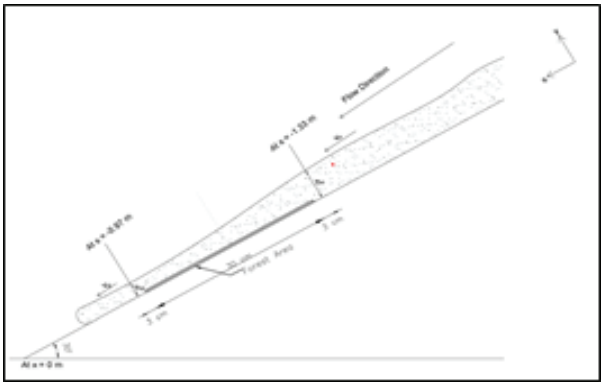

Figure 2 Principle sketch of the debris flow path in the flume model with the forest length of 60cm delineated between x= -1m to x= -1.60m. The flow parameters and energy loss due to flow impedance by forest are analyzed 3cm upstream and downstream of the forest. (Shrestha, 2020)

6. RESULTS AND DISCUSSION

The parameter calibration of the model reveals that the software is able to well simulate the physical modelling in small scale experiments when the Voellmy parameters of the model are Mu = 0.07 and Xi = 1000 m/s2. The observation shows that the Coulomb type friction coefficient (Mu) controls the depositional behavior of the flow, and the turbulent friction coefficient (Xi) mainly affects the flow velocity. The forest areas are delineated in the model using the friction approach, where the Voellmy friction coefficients are modified and assigned to the desired area. This allows creating the braking effect on the flow by the assigned forest area. The forest area of two lengths; 30cm and 60cm are selected for analysis and the Coulomb type friction coefficient (Mu) of the forest is increased between 50% and 300% of the calibrated Mu value of the model. Whereas the turbulent type friction coefficient (Xi) of the forest area is significantly reduced and are set to 200 m/s2 and 400 m/s2. The analysis reveals that flow height, flow velocity, Froude number and energy loss are significantly affected more by the Xi value, then by the length of the forest and comparatively least by the Mu value of the forest. Although for the runout distance, the same trend was observed, the difference between the Xi value, length and Mu value of forest was not as high.

Flow interaction with the forest exhibits a sharp reduction in Froude number. The Froude number decreases significantly with smaller Xi values of the forest and it decreases with the increasing Mu value of the forest.

The runout distance is shortened after the forest is placed in the flume. Both Xi and Mu values of forest have a significant influence on the runout distance. However, Xi value has more dominating effect as the runout distance is least for smaller Xi value of forest. The value of Mu has an inverse effect, the runout distance decreases with an increasing Mu value of forest. Likewise, forest length also plays an influential role in the debris flow runout, the longer the forest length, the shorter is the runout distance. The quantitative values, figures, charts and discussions will be published in the full paper.

7. CONCLUDING REMARKS

The forest area of two different lengths 30cm and 60cm are delineated in the model. The forest area has been placed in the model using the friction approach. In this approach, the modified values of the Voellmy friction parameters (Mu and Xi) are assigned to the desired area to create the braking effect on flow by the forest area. It was observed that the flow height, flow velocity and Froude number are to a larger extent affected by the friction coefficient Xi of the forest than by the friction coefficient Mu of the forest. The length of the forest also significantly impedes the flow in the downstream of the forest area. The longer is the length of the forest area, the more is the reduction in flow velocity. Furthermore, an evaluation of energy loss due to forest area shows that the energy loss is more sensitive to the Xi value of the forest area, followed by the length of the forest and less sensitive to the Mu value of the forest.

REFERENCES

Chen, H., & Lee, C. F. (2004). Geohazards of slope mass movement and its prevention in Hong Kong. Engineering Geology, 76(1-2), 3-25.

Coe, J. A., Kinner, D. A., and Godt, J. W. (2008). Initiation conditions for debris flows generated by runoff at chalk cliffs, central colorado. Geomorphology, 96(3-4):270–297.

Iverson, R. M. (1997). The physics of debris flows. Reviews of geophysics, 35(3):245–296.

Jakob, M., Hungr, O., and Jakob, D. M. (2005). Debris-flow hazards and related phenomena, volume 739. Springer.

Shrestha, S. (2020). Effect of forest on debros flows. Norway: Norwegian University of Science and Technology (NTNU) Masters Thesis.

Vicari, H. (2018). Physical and numerical modelling of debris flows. . Master's thesis, Politecnico.

#Gen-5:

Geotechnical Investigation: A Slope Stability Assessment of Pathibhara Cable Car Project

Sandeep Shrestha[1], Sulabh Majgainya[2]
[1]*Akara Material Testing Laboratory Pvt. Ltd.*
[2]*Tribhuwan University*

1. INTRODUCTION

Despite the improvements in recognition, prediction, and mitigative measures, landslides are still a severe social, economic, and environmental catastrophe in mountainous regions. Analysis of the stability of landslides is very important for slope failure. Moreover, rapid urban development and man-made change contribute to landslides. In this paper, the slope stability at the proposed cable car site location for visiting Pathibhara Devi Temple in the Taplejung District in Province 1 state of Nepal is analyzed, and corrective methods are recommended.

2. METHODOLOGY

2.1 Field Investigation

Thirty-six boreholes were drilled for a total length of 475 meters by using rotary drilling for the geotechnical investigation at the project site. Further the standard penetration test (SPT) and dynamic cone penetration test (DCPT) at different depths depending on the soil layer encountered during the drilling of the boreholes for accessing the in-situ soil parameters. The samples collected during the drilling were also tested in the laboratory to determine various soil parameters. As well as the geophysical investigation an ERT survey has been conducted to access the 2D profile of the in-situ soil deposit.

2.2 Slope Stability Analysis

As per the soil strength parameters obtained from the geotechnical investigation, the slope stability assessment was conducted using the Equilibrium Method (LEM) or method of slices. The slip/failure surface position is revealed once the slope has already failed. Otherwise, the location and shape of the most critical slip surface are unknown. The shape of the undetermined surface is assumed while determining the location. If the shape of the slip surface is either a circular arc (the slope is not homogeneous) or partly circular and partly linear, a grid of centers is selected, with the radius varying at each center and covering all possible conditions. The shape of the slip surface of layered soil can be shallow, elongated, deep with sharp breaks, or convex

Two techniques for calculating slope stability are common. Only used under the conditions of plastic rupture (CHEN, 1975).

5. Limit equilibrium method (LEM)
6. Analytical methods of limit constraints

LEM are still currently most used for slope stability studies. These methods consist in cutting the slope into fine slices so that their base can be comparable with a straight line and then writing the equilibrium equations (Göktepe, F., & Keskin, I., 2018).

3. RESULTS AND DISCUSSION

The different analysis method submits different factor of safety. Although it is to be acknowledged that the Bishop method of slope stability calculations is considered to be the most realistic one for the hilly regions and in our case.

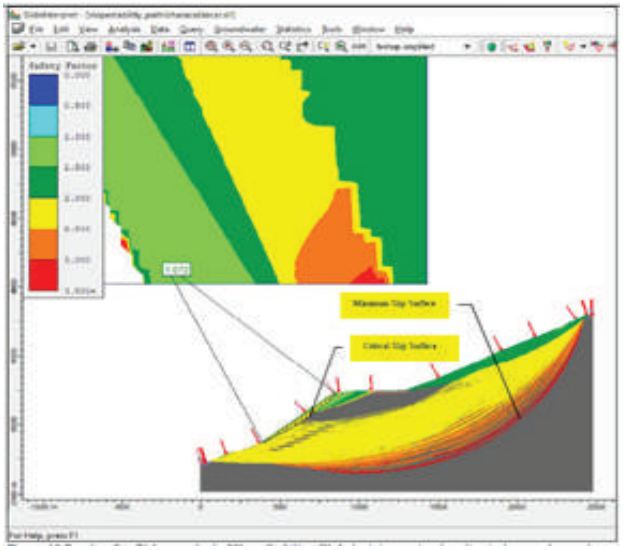

Figure 1: Result after Bishop Method of slope stability. Global minimum circular slip circles are shown along with FoS.

As from the analysis, all other slopes are stable except for the ones between the proposed towers 4 and 7 (FoS > 1.5). However, the slope between the proposed towers 4 and 7 requires attention since the FoS is below 1.5 and above 1 (1 < FoS < 1.5).

4. CONCLUDING REMARKS

The comparison with the safety factors calculated by using the methods of the Limit equilibrium (LEM) and different slice methods confirms that the results obtained are similar. This study shows that the natural slope cross section between the proposed towers 4 and 7 should be paid attention (1 < FoS < 1.5). Whereas other slope cross-sections seem to be stable (FoS > 1.5). Regarding safety factors calculated using the different numerical solutions confirm that the results obtained are similar.

REFERENCES

Bishop, A.W. (1955). The use of the slip circle in the stability analysis of slopes. Geotechnique 5 (1): 7-17.

British Standards Institution, BS 1377-9:1990 Methods of test for soils for civil engineering purposes. In-situ tests

Göktepe, F., & Keskin, I. (2018). A comparison study between traditional and finite element methods for slope stability evaluations. Journal of the Geological Society of India, 91(3), 373-379.

Ameratunga, J., Sivakugan, N., & Das, B. M. (2016). Correlations of soil and rock properties in geotechnical engineering.

Chowdhury, R. N. (1978) "Slope analysis". Developments in geotechnical engineering vol.22, Elsevier, Amsterdam.

#Gen-6:

Rainfall Triggered Landslides and Roadblock Locations in Sindupalchowk District of Nepal

Unisha Ghimire[1], Kaushal Gnyawali[2]

[1]Khwopa College of Engineering, Tribhuvan University, Bhaktapur, Nepal

[2]Himalayan Risk Research Institute, Bhaktapur, Nepal

1. INTRODUCTION

Rainfall-triggered landslides block mountainous roads frequently in Nepal, hindering mobility from a few days to months. Nepal's hilly and mountainous areas cover 76.9% of the country, making it particularly susceptible to landslides. The impact on transportation infrastructure in Nepal is significant, with roads impacted by landslides, particularly in the monsoon season (June- September) (Dahal et al., 2006). It is essential to map road blockade locations in Nepal and the time taken for reopening the route to identify critical road sections needing alternative route planning.

Sindupalchowk is a mountaineous district located in central Nepal with an area of 2,542 km². It is one of the most landslide hazard prone road networks in Nepal because of its fragile geology, intense precipitation and prevailing non-engineered road constructions practices (McAdoo et al., 2018). In this study, we demonstrate the relationship between rainfall-triggered landslides and the road network in Sindhupalchowk and identify the duration of road blockade and the following reopening at those locations. The findings are relevant to identify critical road network sections in the district that are relevant for further investigations to build the resiliency of the overall road network for sustainable mobility.

2. METHODOLOGY

We use secondary data and desk study to assess the relationship between landslides and roads in Sindhupalchowk. Then we build an original inventory of landslide-blocked road sections by interpreting local news archives. The inventory includes road location, blockade and reopening date, and approximate dimensions of landslides. The locations have been confirmed from Google Earth's historical satellite imagery.

3. RESULTS AND DISCUSSION

A total of 4359 rainfall-triggered landslides occurred in the Sindhupalchowk district between 2016-2020 and before 2016. The landslide locations are shown in Fig. 1, taken from the recent landslide inventory by Gnyawali et al. (2023). The landslide distribution is widespread in the district. Factors such as high-intensity precipitation, weak geology, and the area being hit severely by the recent large earthquake (Mw= 7.9) in the year 2015 could potentially be the cause of the widespread landslides.

Figure 1 Rainfall triggered landslide locations in Sindhupalchowk. Data taken from Gnyawali et al., 2023.

The rainfall-triggered landslide susceptibility map shows that most of the southern part of the district is exposed to high and very high landslide susceptibility, Fig. 2.

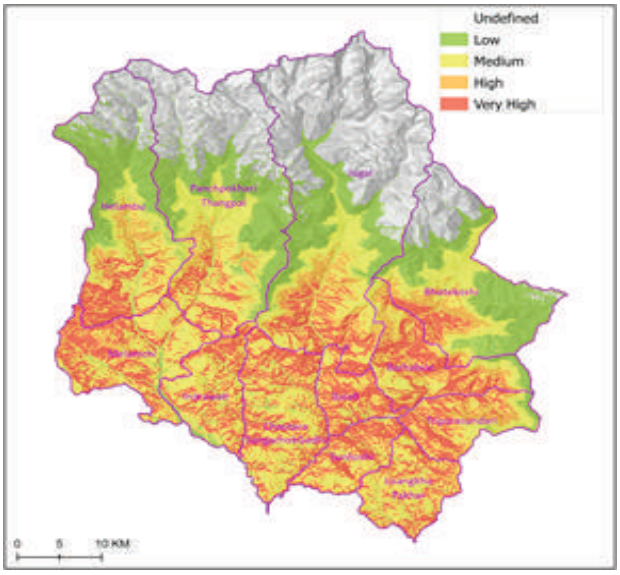

Figure 2 Rainfall triggered landslide susceptibility map of Sindhupalchowk. Data taken from Gnyawali et al., 2023

The road network of Sindhupalchok is dense, with 457 nodes and 557 edges. Its roads are primarily categorized into six types: Highway, Feeder Road, District Road, Main trails and Other roads, Fig. 3. Most of the secondary road network is earthen and operable seasonally in the summer. The main highway Araniko highway, was the primary trade route to China before 2015.

We prepared an inventory of road blockade locations in the Sindhupalchowk district. The following table shows the identified landslide locations, their area, approximate dimensions (height and width), and the number of days of road blockade.

Table 1: Landslide road blockade locations inventory verified in Google Earth

SN	Area (m^2)	Dimensions (H×W m)	Days blocked	Location
1	3312	35×90	90	Barhabise
2	18744	100×200	90	Barhabise
3	17620	151×90	90	Bhotekoshi
4	5572	220×25	90	Bhotekoshi
5	3950	58×80	24	Bhotekoshi
6	850000	1400×980	90	Barhabise
7	455	13×22	1	Melamchi
8	2692	130×20	2	Melamchi
9	3700	60×60	30	Helambu
10	1200	19×55	30	Helambu
11	5863	75×80	30	Helambu
12	3990	90×70	30	Helambu
13	7980	23×210	-	Helambu

Figure 3 shows these locations on the map and the corresponding road network. The exact location of every landslide could not be ascertained with the available information, and thus, some of the landslides were approximately located within the road section.

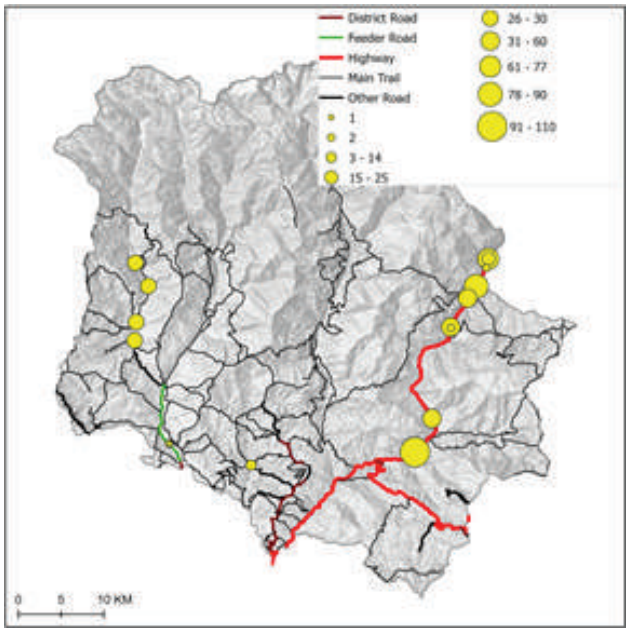

Figure 3 Road network and landslide-road blockade locations (yellow dots) in Sindhupalchowk. The size of the dots represents the number of days taken to re-open the road section after the landslide impact.

Figure 5 shows two representative landslides verified in Google Earth Imagery from historical imagery.

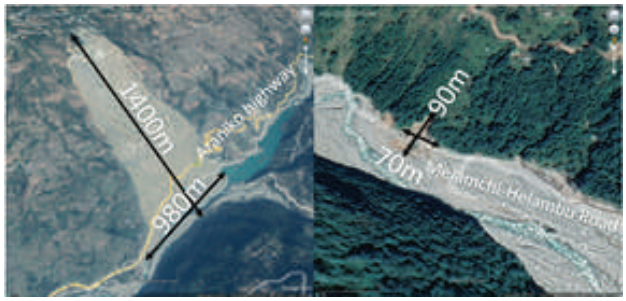

Figure 4 Landslide blockage locations at roadsides seen in Google Earth historical imagery.

In total, 13 landslides were located in Google Earth, of which 4 were found to have occurred after the Gorkha earthquake in 2015, and 4 were found to have occurred following the devastating Melamchi flood of June 15, 2021.

In table 1, landslides 1-6 occurred on the Araniko highway, including the Jure landslide with a total area of

850,000 m2 on August 2, 2014, and blocked the road for three months. Landslides 7 and 8 occurred on the Melamchi highway (Zero-kilo to Melamchi bazar) and blocked the road for a comparatively shorter duration. Landslides 9-13 occurred on the Melamchi-Helambu highway, with most of them occurring after the Melamchi flood on June 15, 2021, and blocking the road for two months. In the case of landslide 13, the specific days of traffic blockage could not be ascertained. The results indicate that the major roads in the region are highly vulnerable to landslides and lack resilience against such disasters that occur frequently in the area.

The results show that the district's Araniko highway and Melamchi-Helambu Road are highly susceptible to landslides. These roads, situated in the vicinity of the Bhotekoshi river and Melamchi river, were found to have a greater concentration of landslides compared to other roads in the study area. Specifically, out of the total of 20 landslides located in the study (we were not able to pinpoint several landslide locations in Google Earth, but we found them in news reports and thus included them in this analysis), 18 were recorded along these two roads. In comparison, the remaining two landslides were found on the Pachkhal-Melamchi road. Fig. 3 shows the approximate location of all the recorded landslides.

3. CONCLUDING REMARKS

This study identifies the relationship of rainfall triggered landlsides and road blockades in Sindhupalchowk district of Nepal. We identified that Araniko Highway and Melamchi-Helambu road as the roads exposed to long-duration road blockades due to large landslides. The results of this case study can be utilized by various stakeholders for the effective development of transportation systems in the Sindupalchowk district. Future research is needed to understand the resilience of these road networks with more granular data and spatial analysis for alternative route planning.

REFERENCES

Dahal, R. K., Hasegawa, S., Masuda, T., & Yamanaka, M. (2006). Roadside slope failures in Nepal during torrential rainfall and their mitigation. Disaster mitigation of debris flows, slope failures and landslides, 503-514.

Gnyawali, K., Dahal, K., Talchabhadel, R., & Nirandjan, S. (2023). Framework for rainfall-triggered landslide-prone critical infrastructure zonation. Science of The Total Environment, 162242.

McAdoo, B. G., Quak, M., Gnyawali, K. R., Adhikari, B. R., Devkota, S., Rajbhandari, P. L., & Sudmeier-Rieux, K. (2018). Roads and landslides in Nepal: how development<? xmltex\break?> affects environmental risk. Natural Hazards and Earth System Sciences, 18(12), 3203-3210.

#Gen-7:

Strength Variation of Rocks from Weak to Hard Anisotropic Rocks: An Example from Nepal Himalaya

[1]Anada Gupta, [2]Suman Panthee*
[1]Lincon University, Malaysia
[2]Central Department of Geology, Tribhuvan University, Nepal
*Corresponding Author: sumanpanthee@gmail.com

ABSTRACT

Rock strength values are important in rock engineering because they are required for creating structures within or on top of rocks. When examined from any angle, certain rocks show quite small, nearly unnoticeable variations in their strength, while others show very significant variations. This study covers the strength variation of weak to hard anisotropic rocks from the Nepal Himalayas. With the smallest strength value happening between 30° and 45° degrees and the biggest value occurring between 0° and 90°, this research demonstrates the nature of how rocks react to varied loading angles in UCS. However, the point load diametral test shows the maximum value is obtained at 0° and the minimum is obtained at 90°. The results obtained show that when the rock material is squeezed under specific conditions when a force is applied and more energy is required for a fracture to develop between layers of bands, the strength is at its maximum.

Keywords: *Rock strength, Uniaxial compressive strength, Point load index, and Strength anisotropy*

1. INTRODUCTION

Rocks are concerned with the design of excavation, underground spaces, and mining research laboratory examinations of their isotropic and anisotropic parameters are fundamental for source rock fracturing in crude oil mining, safe designs, and any excavations. The mechanical properties of rock depend on its rock type and mineral composition, grain size, bounding, arrangement of the mineral grains, and also the stress and joints (crack and fracture) that have developed during tectonic processes. Due to the reason, rock types are inhomogeneous the degree can determine the anisotropic level. Anisotropy of the strength and deformation behaviors of fractured rock masses is a crucial issue for design and stability assessments of rock engineering structures, due mainly to the non-uniform and non-regular geometries of the fracture systems (Bidgoli and Jing, 2014) and the stress and strain responsible for the development of foliation so the influence of the stress effects on the strength of the rock. Schist specimens that fail along foliations show low strength whereas specimens failed through material result in high strength (Basu et. al 2013).

Rock is used to depict blocks of modestly small volume, which are aggregates of minerals of practically relative composition and geological structure. The stress and strain are responsible for the development of foliation (anisotropy) molded due to deformation or crystal growth in the rock so the influence of the stress affects results in the strength of the rock so the examination will be occupied with the strength anisotropy of the rock by index tests. These types of the study were done in the Nepal Himalayas by examining the strength anisotropy and failure behavior of rocks in the point load index test and uniaxial compressive strength test (Acharya et al. 2021a; Acharya and Panthee 2019). Similarly, Acharya et. al (2022) developed the correlation between point load index and uniaxial compressive strength with respect to loading angle.

This study reveals the nature of rocks' response in different loading angles where the minimum strength value is obtained between 30° to 45° degrees and the maximum value is obtained between 0° and 90° degrees. Analyzing weak to hard types of anisotropic rocks' strengths as shown by point load index tests, uniaxial compressive strength tests, and fracture propagation in uniaxial compressive strength tests was the study's main objective.

2. METHODOLOGY

For analyzing different grades of the anisotropic rocks in uniaxial compressive strength, Tensile strength, and point

load index test, the selection of anisotropic rocks depends on the geology of the study area.

To accomplish the objectives, different methods like desk study, field study, laboratory testing, and analysis were adopted. The suggested method for uniaxial compressive strength is suggested by ISRM (1985) and the suggested method for the point load index test is suggested by ISRM (1979). In the study, the Uniaxial compressive strength test and point load strength test were done with varying anisotropic angles (0˚, 15˚, 30˚, 45˚, 60˚, 75˚ and 90˚) with respect to the plane of different rocks in which rock types are Augen gneiss, Migmatic gneiss and slate from different rock form the Lesser and Higher Himalaya of Central Nepal were sampled and tested for this study. During this study, the points explained by Acharya et. al (2021b) were carefully done for this study.

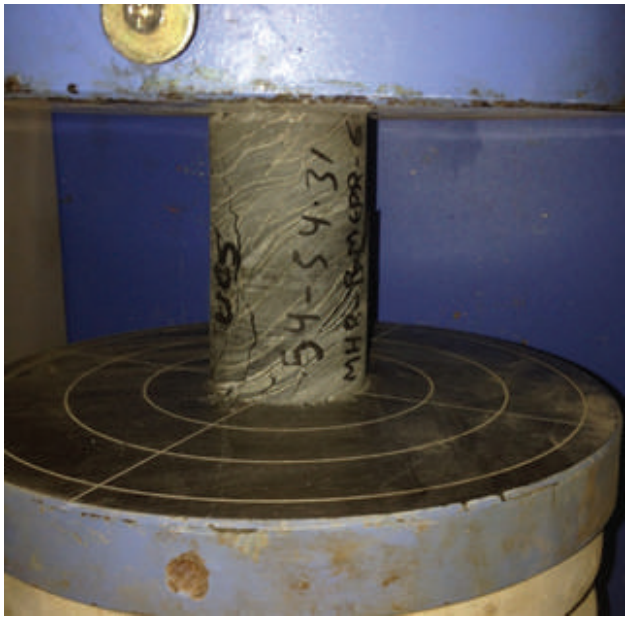

Figure 1: Rock fracturing after UCS testing

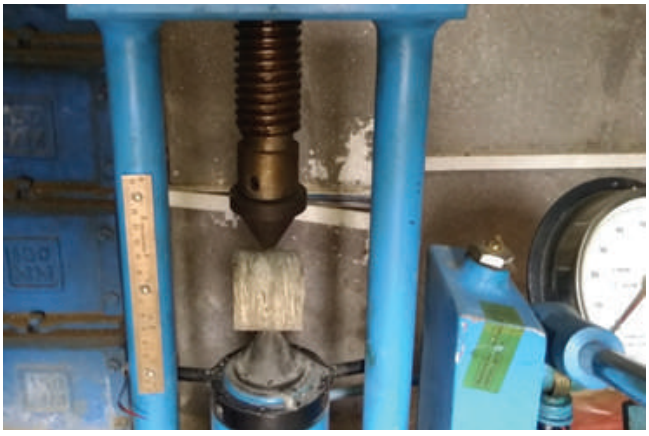

Figure 2: Point load testing.

Well-defined anisotropy is especially to be found among sedimentary and metamorphic rocks, where the bedding or the foliation normally is clearly visible. Igneous rocks may often look very homogeneous and isotropic, but testing reveals that many of their material properties vary with the direction of testing. Although at the material scale mineralogy and geometric arrangements of particles and voids and/or micro-cracks together control rock mechanical behaviors.

The obtained results from the tests are analyzed with Ramamurthy's (1993) strength anisotropy relationship (Equation 1) as the variation in strength under uniaxial loading conditions of intact rock with respect to the loading angle.

$$R_C = \frac{\sigma_{ci\,(90)}}{\sigma_{ci\,(min)}} \ldots\ldots\ldots\ldots\ldots\ldots (1)$$

where σci(min) is the minimum value of ci derived from oriented under uniaxial compression, often occurring when the loading axis forms an angle to the foliation between = 30 and 45. σci(90) is the uniaxial compressive strength perpendicular to the planes of anisotropy.

3. RESULTS

Cylindrical core samples of augen gneiss were loaded in a uniaxial direction at the laboratory (Photograph 5) at varying anisotropy angles (foliation angle) 0o, 30o, 45o, 60o, and 90o. Three series of tests were carried out, testing three samples for each angle in total the obtained results are shown below in table (Table 1) and the nature of the graph showing the relation between compressive strength and anisotropy angle (β) is presented below (Figure 5).

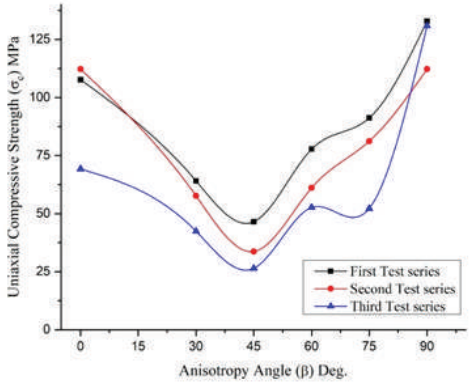

Figure 3: The graph obtained by UCS to loading angle in different rock types.

The trend line obtained from the scatter plot of all data from the three-test series is depicted in the graph above Figure 3. The equation derived from the generalized relationship between UCS and the anisotropy angle is given in Figure 4.

It has been proven that slate samples are classified as moderately anisotropy rocks based on the value obtained in Table 3 (Ramamurthy, 1993). The variance between UCS and anisotropy orientation of the slates is shown in Figure 4 and it's also been proved that the highest strengths are obtained when the applied stress is perpendicular to the foliation. On the other hand, the minimum strengths of slates are calculated when the angle of foliation and applied load equals around 45º degrees. The variance of UCS versus loading direction had shown a U-Shaped and nearly wavy-shaped curve pattern, as shown in Figure 4.

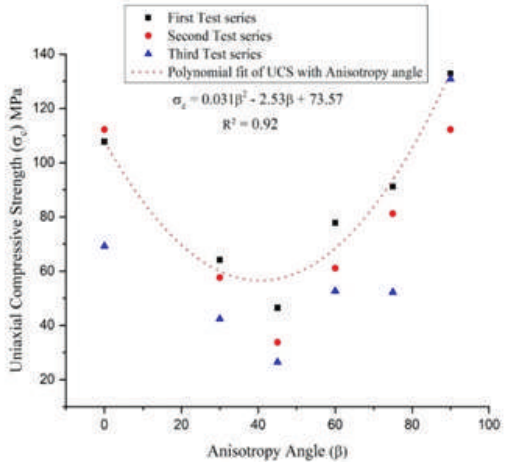

Figure 4: Scatter plot and trend line from three-test series and its generalized equation

As a result, the generalized strength anisotropy equation for Slate specimens is deduced from the graph (Figure 4). Through analysis of the testing data available, an empirical relationship has been established between rock strength and anisotropy angle which is expressed in the following Equation 2.

$\sigma_c = 0.031\beta^2 - 2.53\beta + 73.57$……..... (Equation 2)

Where, σ_c = Uniaxial compressive strength and, β= anisotropy angle.

The polynomial relationship between the compressive strength and oriented rock specimen can be plotted based on the data in Figure 3 and Figure 4, and the expressions for these lines can be obtained by fitting. It can be seen from Figure 4, strength gradually decreased with an increase in loading angle becoming minimum at 45º, and gradually increasing up to 90º by making U shaped curve and broadly positively correlated. Figure 4 gives the empirical formulas relating to the compressive strength and orientation of the slate rock samples, where y represents compressive strength and x represents orientation. How strength varies with orientation is reflected by the slope of the fit line, known as the proportionality factor.

Therefore, the positive correlation between σc and orientation is very high. The fitting coefficient R2 is 0.92, R2 ≥ 0.90σc, and orientation thus shows a very obvious Polynomial relationship under these processing conditions. To achieve better fits, the trial of the different fits other than the polynomial function relating to σc and β has been done but a satisfactory result isn't obtained. Comparing the other function with the polynomial function, the polynomial function achieves a better description of the relationship between the σc and the β than other functions, and therefore, it is more accurate to predict the coefficient of anisotropy value using this function. From the above analysis, it can be concluded that the Compressive strength is strongly correlated with the anisotropy angle.

Additionally, for the anisotropic study, two types of foliated metamorphic rock were taken from different locations and different formations with different grain sizes and the test were the diametral test and axial test. The study includes the effect of anisotropy of both rock samples: Augen gneiss and migmatitic gneiss in the diametral test.

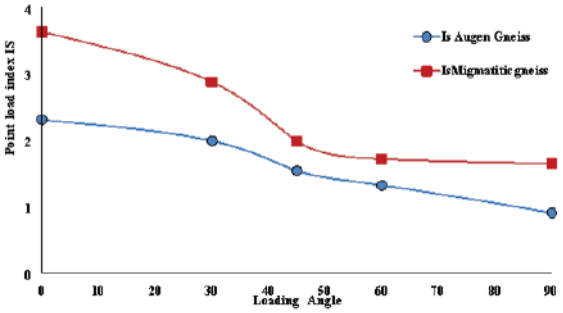

Figure 5:Is(50) Vs Loading angle(º)

The minimum strength value from the point load strength index is achieved at an anisotropic angle of 90°, and the maximum value is obtained at an anisotropic angle of 0°, which is perpendicular to the plane.

Table 1: Strength anisotropy index obtained according to diametral test

S.N.	Rock Type	Anisotropic index
1	Augen gneiss	2.55
2	Migmatitic gneis	2.21

The fracturing pattern in the diametral test depends on the weakest plane. In Augen gneiss the mineral grain of feldspar, quartz and dark mineral biotite, muscovite. Augen gneiss is highly influenced by its grain size the presence of feldspar grain with dark mineral i.e. mica developed anistropy which influence the strength.

4. DISCUSSIONS

Comparing obtained strength anisotropic values with anisotropy classification according to uniaxial compressive strength Table 3.

Table 2: Strength anisotropy classification by Uniaxial compressive strength test, (Ramamurthy, 1993).

Degree of compressive strength anisotropy, $I\sigma_c$	Descriptive term
1.0-1.1	Isotropic
1.1-2.0	Fairly anisotropic
2.0-4.0	Moderately anisotropic
4.0-6.0	High anisotropic
>6.0	Very highly anisotropic

Table 3: Strength anisotropy classification by Point load index test, (ISRM, 1972)

Degree of Point load strength anisotropy, $I_{a(50)}$	Descriptive term
1	Isotropic
1-2	Fairly- moderately anisotropic
2-4	Highly anisotropic
>4	Very highly anisotropic

From Table 2 and Table 3, the rock types are moderately anisotropic to highly anisotropic. The peak stress is the actual strength of the rock. The compressive strength of rock is a function of the confining pressure. As the confining pressure increases so does the strength but when anisotropic angles are 30º to 45º.

5. CONCLUSION AND RECOMMENDATIONS

The result shows anisotropic behavior is followed at each test in different orientations gaining maximum strength at β=90º and minimum at β=45º. The strength decreased for samples tested at 00, and slightly decreased with increasing the anisotropic angle 30º, and became a minimum strength value at 45º, then increased to 60º, and finally became a maximum strength value at 90º. The strength has decreased by a small amount (1-2 times on average) for samples of =30º, 45º, and 60º, but has increased significantly at 75º and 90º compared to the strength value at =30º, 45º, and 60º. In general, the UCS value for Slate has increased and reached a maximum value at =0º and 90º. The strength gradually decreased with an increase in loading angle becoming minimum at 45º, and gradually increased up to 90º by making U shaped curve and broadly positively correlated.

From the diametral test, the nature of the result shows the maximum value obtained when loading is perpendicular to the loading angle and the minimum value parallel to the loading angle of foliation planes both in Augen gneiss and migmatitic gneiss at room temperature. The strength is maximum because at that condition when the load applied to the rock material is compressed and develops a crack between the layers of bands which requires more energy. The minimum strength obtained when parallel to the foliation plane in that condition the stress applied to turn up to perpendicular to both foliation and force direction which split from the foliation plane. The pattern of both graphs is similar and influenced by the angle of the weakness plane between the axis of the core. The strength classification of the two rocks sample in which the nature of Augen gneiss is strongly foliated and the strength anisotropy obtained is 2.55 and the rock is described as highly anisotropic rock and the sample of migmatitic gneiss has a nature of moderately foliated and value obtained is 2.21 rock is described as moderately anisotropic.

6. ACKNOWLEDGEMENT

We are grateful for the assistance provided by our professors and are very thankful for our friends' special thanks to Durga Acharya, Ajita Bhandari, and Sujan Karki, Central Department of Geology, Nepal for their help and support in lab and fieldwork.

REFERENCES

Basu, A., Mishra, D. A., Roychowdhury, K., 2013. Rock failure modes under Uniaxial Compression, Brazilian, and Point Load tests. Bulletin of Engineering Geology and the Environment v. 72. pp. 457–475.

Bidgoli, M.N., Jing, L., 2014. Anisotropy of strength and deformability of fractured rocks. Journal of Rock Mechanics and Geotechnical Engineering, v. 6, pp. 156-164.

ISRM (International Society for Rock Mechanics), 1985. Suggested method for determining point load strength. International Journal of Rock Mechanics and Mining Sciences &Geomechanics Abstracts, v. 22, pp. 51–60

ISRM, 1979, Suggested methods for determining the Uniaxial Compressive Strength and deformability of rock materials. International Journal of Rock Mechanics and Mining Sciences &Geomechanics Abstracts v. 16(2), pp. 135-140.

Ramamurthy, T., 1993. Strength and modulus responses of anisotropic rocks. In: Hudson J. A. (Eds.), Comprehensive rock engineering, Oxford: Pergamon Press, pp. 313–29.

Acharya D., Panthee S. (2019) Study about the failure and the strength behavior of rocks in point load index test with respect to loading angle. In: 14th International Congress on Rock Mechanics and Rock Engineering (ISRM 2019). pp. 1958–1963. CRC Press, Taylor & Francis Group

Acharya D., Panthee S., Raina A.K., Dhakal S. (2021)(a) Analysis of failure behaviour of the anisotropic rocks in the point load index test. IOP Conf. Ser. Earth Environ. Sci. 833, 012193. https://doi.org/10.1088/1755-1315/833/1/012193

Acharya D., Raina A.K., Panthee S. (2021)(b) Challenges to study the Anisotropic Rocks using index tests in the Himalaya Region: A review from the Nepal Himalaya. IOP Conf. Ser. Earth Environ. Sci. 861, 022050. https://doi.org/10.1088/1755-1315/861/2/022050

Acharya D., Raina A.K., Panthee S. (2022) Relationship between point load index and compressive strength of foliated metamorphic rocks at different loading angles. Arab. J. Geosci. 2022 156. 15, 1–18. https://doi.org/10.1007/S12517-022-09745-5

#Gen-8:

A Tale of Reinforced Soil Slope: Penstock Slope Alignment of Middle Tamor Hydropower Project

Manab Rijal[1], Basu Dev Pokhrel[1], Manoj Adhikari[1], Aarakshya Kandel[2]
[1]Maccaferri (Nepal) Pvt. Ltd., Kathmandu, Nepal
[2]Sanima Hydro and Engineering Pvt.Ltd., Kathmandu, Nepal

1. INTRODUCTION

Most of the hydropower project development faces the challenge of slope stability in the headworks and powerhouse location. In these locations of the project the original ground is heavily disturbed by excavating for the construction of the structures. In the Middle Tamer Hydropower Project (MTHP), the stability of the penstock slope alignment was disturbed by the excavation of the slope to the design level for the construction of the saddle slab and the anchor blocks. The subsurface stratum of the penstock slope consists of coarse-grained soil (Silty Sand with Gravel) deposited by the kholsi flowing along the slope. This approximately 90 m high penstock slope consists of two anchor blocks, one each at the crest and toe with the saddle slab throughout the slope. Initially the penstock slope was excavated up to the design level for the construction of the saddle slab, but with the exposure of the cut slope to the monsoon rainfall, deposition of the tunnel muck at the crest, elevated groundwater profile, steep slope etc. resulted the slope mass to creep. And thus, the ground profile of the slope deformed from the design level. Considering the timeline for the construction and bringing back the deformed ground profile to the design level, backfilling the slope with the soil reinforcement (high strength geogrid Paralink) was selected. This enabled the construction of the saddle slab simultaneously with backfilling and hence saving the construction time considerably.

2. METHODOLOGY

After the failure of the slope different options (series of retaining wall, soil nailing, reinforces slope) of stabilizing and maintaining the design grade for penstock pipe alignment were explored. The option of using high strength geogrid (Paralink) as soil reinforcement during backfilling was opted as it helped to expedite the construction process and was more economical and met the required factor of safety. Initially all the slide mass and lose soils were removed from the slope alignment. After reaching the good/undisturbed foundation strata, the topographical survey and geotechnical exploration of the penstock slope alignment were carried out. The deepest excavated portion of the slope was approximately 8 m high. The required length, spacing, and strength of geogrid were analyzed using the SLOPE/W of GeoStudio suite.

3. RESULTS AND DISCUSSION

The stability assessment of the penstock slope alignment was carried out for existing condition, during construction and end of construction to capture

the critical stage. was selected for the critical stage. The critical stage was seismic loading scenario. So, the design strength, vertical spacing and length of the geogrid was selected based on this loading scenario. Table 1 presents the summary of the Factor of Safety (FoS).

Table 1: Summary of Factor of Safety for different loading scenario.

Design Stage	Obtained FoS	Required FoS
Existing Slope	1.1	1.0
During Construction (half)	1.4	1.1
Completed w/o pipe	1.4	1.3
Completed with pipe	1.3	1.3
Completed with pipe (seismic)	1.1	1.1

As per the analysis the high strength geogrid (Paralink) of 100 kN/m at the vertical spacing of 1m was selected as the soil reinforcement for stabilization and backfilling the slope to the design level. The wrapping around technique

was used to lock the geogrid on the front side of the backfill. And, as we know the ground water is one of the prominent reason to destabilize the slope, the use of drainage composite (MacDrain) was used at the interface of the natural ground and structural fill on the hill side.

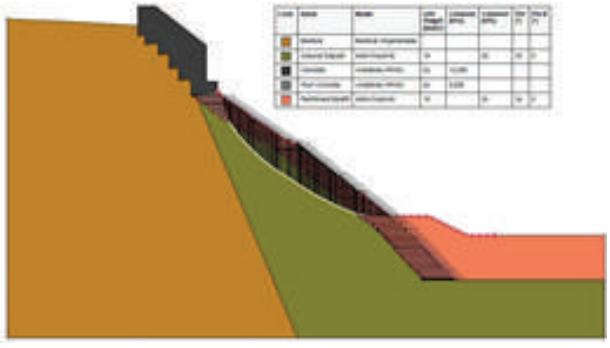

Figure 1: SLOPE/W Analysis of the penstock slope alignment after the use of high strength geogrid (Paralink) as soil reinforcement.

4. CONCLUDING REMARKS

The use of the high strength geogrid (Paralink) can be used as soil reinforcement in backfilling the slope to the design level and achieving the stabilization requirement.

REFERENCES

Duncan MJ, Wright SJ, and Brandon LT, 2014, Soil strength and Slope Stability, 2nd Etd., John Wiley and Son Inc.

BS 8006-1 2010, Code of Practice for Strengthened/Reinforced Soils and other Fills.

#Gen-9:

Understanding the dynamics of Chure River Systems: Implications for Integrated Management of Watersheds and Fluvial Disasters

Saroj Karki[1], Bhesh Raj Thapa[2], Sanjay Giri[3], Nagendra Kayastha[4], Keshab Sharma[5]

[1]Ministry of Water-Supply, Irrigation and Energy, Province-1, Biratnagar, Nepal

[2]Universal Engineering and Science College, Lalitpur, Nepal

[3]Royal HaskoningDHV, Netherlands

[4]Independent Specialist, Netherlands 5 BGC Engineering Inc., Fredericton, Canada

** sarojioe@gmail.com*

with every event. The Chure region receives one of the highest rainfalls across the country.

1. INTRODUCTION

The Chure region, the youngest member of the Himalayan range, is considered to be the most fragile region in Nepal from a geomorphological standpoint, and it faces multifaceted challenges. These challenges range from environmental issues such as land degradation, poor water resources management (both surface and groundwater), deforestation, and loss of biodiversity to social challenges such as increasing hardships for marginalized communities and migration induced by natural disasters. The region's inhabitants face numerous difficulties in sustaining their livelihoods, and addressing these issues is crucial for the long-term well-being of the region. The Chure region, the southernmost hills of the Nepal Himalayas, spans over 2400 km beyond Nepal's borders, forming a continuous belt from the Brahmaputra in the east to the Sindh River in the west. At the northern end of the Terai, the topography abruptly rises, marking the beginning of the Siwalik hills. In Nepal, the Siwalik hills are commonly referred to as the Chure range, covering around 13% of the total area of Nepal with elevations ranging from 200 masl to 1000 masl or even higher at some locations. However, the majority of the rivers originating from and flowing through the Chure region are ephemeral in nature due to the low groundwater levels.

2. CHURE-TERAI RIVER SYSTEMS

The Siwalik or Chure hills of Nepal, which are considered the most fragile regions in terms of geology, are particularly susceptible to soil erosion and land degradation and sediment transport. Based on SRTM90m DEM, there are 168 rivers that predominantly originate in Chure-Terai region as seen in Figure 1. The catchment area varies from over 2000 sq. km to less than 0.1 sq. km. The stream density is highest across Chure-Terai which is illustrated in Figure 3. Rivers originating from these hills are predominantly ephemeral, flowing only in direct response to rainfall events. The water table is generally below the river bed level. Flash floods occur frequently, affecting the channel morphology with every event. The Chure region receives one of the highest rainfalls across the country.

River gradient drop significantly as the river approaches Terai from Chure and Mahabharat which

can be clearly depicted from Figure 2. The significant aggradation in the upper reaches (at the foothills) is caused by the low sediment carrying capacity due to reduced bed slope. Usually, braided planform, wide floodplain, avulsion, and channel shifting are common, and bed morphology changes with every flood event.

The demand for construction materials has accelerated the mining of riverbed materials such as sand and gravel in

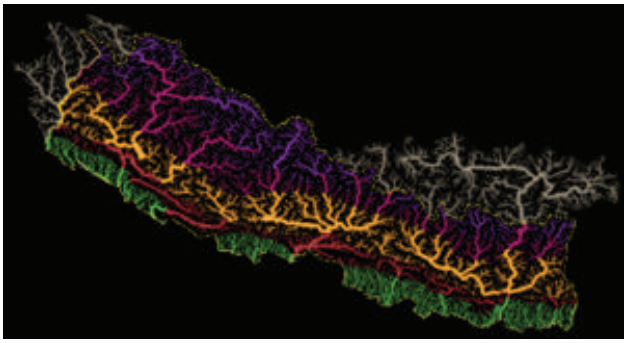

Figure 1: River systems across physiographic regions of Nepal

recent years. This unscientific mining has not only affected river morphology, but it has also jeopardized the safety and performance of irrigation systems and river training structures. The problem of sand mining is particularly severe in the Chure/Siwalik region.

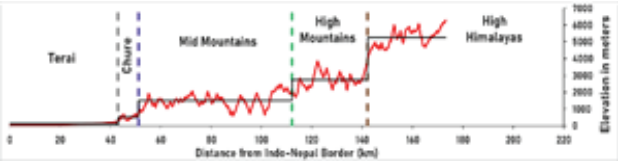

Figure 2: Typical elevation profile across North-South

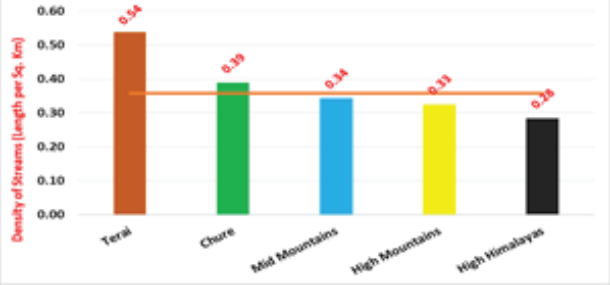

Figure 3: Stream density across physiographic region

3. CASE OF BAKRA RIVER

Bakra River shown in Figure 4, originates in the Northern part of Morang district of Miklajung VDC which is a typical example of Chure River. Bakra River was embanked nearly two decades ago on both banks, right from the foothills to the Indian border in the south measuring more than 50 kilometers. However, the design of the embankment didn't anticipate the excessive influx of sediment. In the present scenario, above the East-West Highway, the embankment in some reaches has been completely buried below the river bed while partially in some reach, mainly due to the excessive sediment deposition. The deposition is so severe that now the adjacent village is well below the river bed level and prone to inundation even with a small flood (Figure 5). While below the East-West Highway, severe erosion of the river banks can be observed.

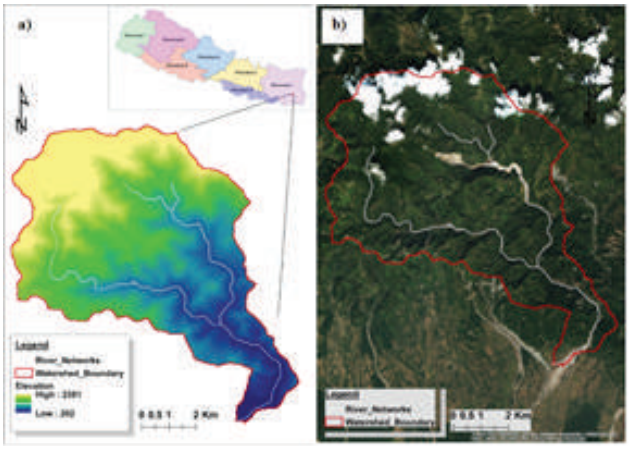

Figure 4(a and b): Bakra River Basin

Figure 5: Aerial view of Bakra River showing aggraded river bed and mining

Some of the issues concerning Bakra River system are;

1. Excessive influx of sediment from catchment
2. Implementation of River training works without considering the sediment transport phenomena.
3. Unpredictability in river flow path with frequent channel shifting and avulsion.
4. Lack of discharge measurement (Ungauged) due to the temporary nature of the stream hinders the research and development.
5. Haphazard sand mining further exacerbates the fluvial problems.
6. Rapidly increasing population in the floodplain.

4. MANAGEMENT OF CHURE RIVERS

Chure-Terai river systems and their watershed are vital for the sustainability of livelihoods including water resources, food and agricultural systems and other resources management. Therefore, management of these river systems should be given a high priority.

Downstream flood control measures without considering upstream watershed dynamics won't be sustainable. The main factor contributing to the increased flood risk is the excessive of influx of sediment through erosion. Countermeasures should focus on minimizing the erosion loss from the upstream including river improvement works in the downstream. Management of Chure-Terai river systems needs coordinated effort of multiple-stakeholders. Some of the measures for sustainable management of Chure river systems are;

3. Prioritizing watershed/sediment management works and improving land-use practice.
4. Suitable protection measures should be considered while constructing roads and other infrastructures in the watershed areas.
5. Development of buffer zones along the river banks.
6. Sediment management works including the detention basin, construction of sediment trap structures like check dam, small ponds, etc.
7. Prioritizing alternative countermeasures incorporating local materials and local technology

5. CONCLUDING REMARKS

The Chure river sytem plays a critical role in the socio-economic and environmental harmony of the Terai. To ensure its sustainability, multiple stakeholders need to make planned and persistent efforts rather than taking haphazard actions and short-sighted policies. Stringent laws must be enforced to regulate land use practices, river management, watershed conservation, water management, scientific riverbed mining, and geo-technically appropriate infrastructure development in the hills. Policies for conservation should align with emerging challenges and sustainable solutions, and research activities should be prioritized.

#Gen-10:

GIS-based MCDA–AHP modelling for avalanche susceptibility mapping of Sagarmatha National Park in Nepal

Madan Pokhrel[1]

[1]*Department of Civil Engineering, IOE-Paschimanchal Campus, Pokhara 33700*

1. INTRODUCTION

Steep creek or hydrogeomorphic hazards are natural Sagarmatha National Park is a prime location for hikers and mountaineers, attracting visitors with its stunning attractions such as Mount Everest and various challenging high-mountain trekking routes, including the Everest Base Camp Trek and the Gokyo Lake Trek. Despite its popularity, it's important to acknowledge that this great destination also comes with some risks, as every year, many trekkers and climbers lose their lives or suffer injuries due to natural disasters such as avalanches, which are a result of the park's high altitude and rough terrain. Despite the frequency of high-altitude avalanches in the region, studies on the subject have been limited. This study applied the Multi-Criteria Decision Analysis-Analytical Hierarchical Process method to map the avalanche susceptibility of the area. The Aster GDEM and snow cover data from the High Mountain Asia (HMA) were utilized to create the susceptibility map, which was then validated using previous recorded avalanche incidents in the region.

2. METHODOLOGY

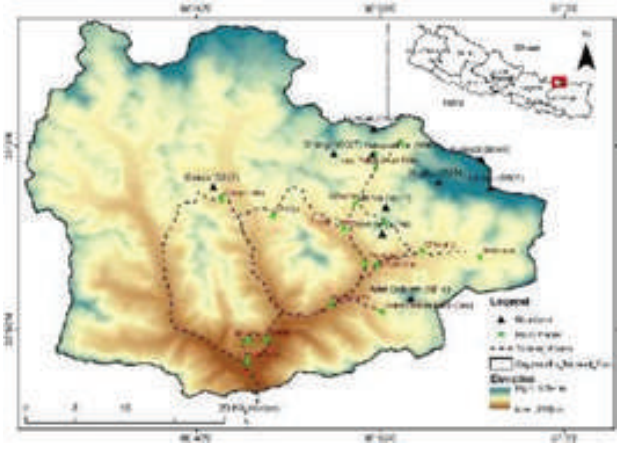

Figure 1: Study area map: Sagarmatha Naional park

Figure 2 illustrates the methodological diagram of the

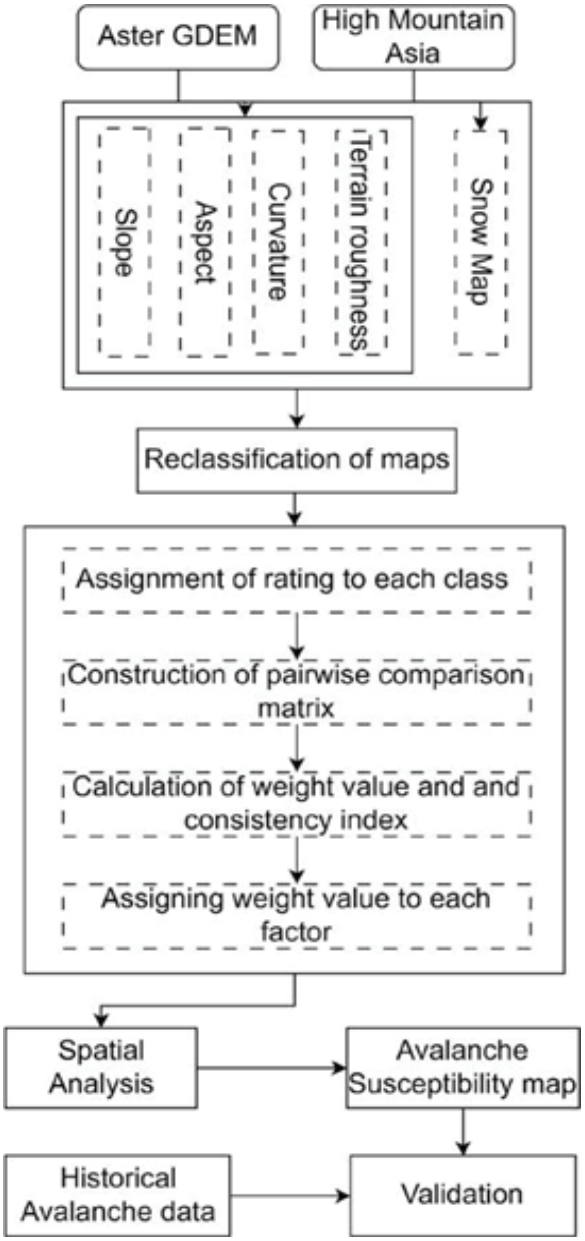

Figure 2: Methodological diagram (Kumar, Srivastava, and Snehmani 2017)

study. The digital elevation model was acquired from ASTER GDEM, while the snow map from High Mountain Asia was utilized as the primary source of data for analysis. Several GIS tools were employed to generate maps of slope, aspect, curvature, and terrain roughness based on the DEM data shown in Figure 3. These maps were then classified

into various categories according to the relevant literatures.

To assign weights for each category, a pairwise comparison matrix was constructed. Subsequently, spatial analysis was conducted to generate an avalanche susceptibility map of the region, which was validated using records of previously occurring avalanche events.

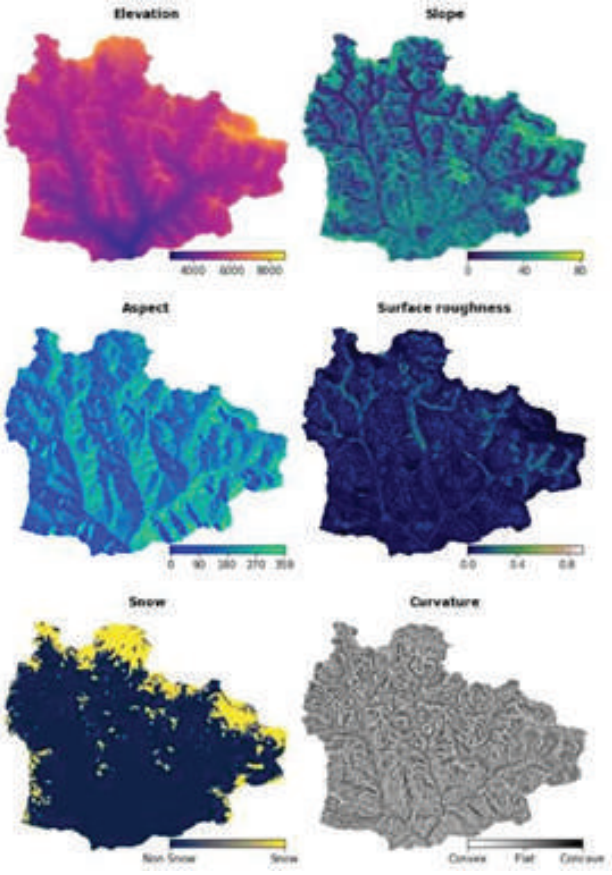

Figure 3: Input parameters for the study

3. RESULTS AND DISCUSSION

Figure 4 displays the avalanche susceptibility map of Sagarmatha National Park. The study findings indicate that the region is prone to avalanches, with around 40% of the area falling into the high and very high susceptibility categories. Notably, not only the higher peaks but also areas with seasonal snowfall are highly susceptible to avalanche events.

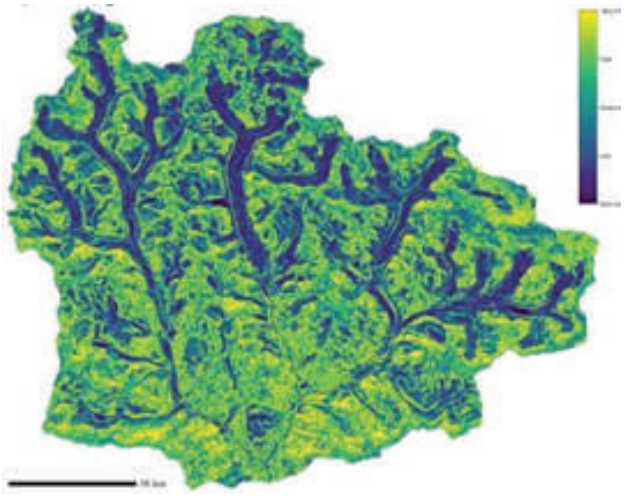

Figure 4: Avalanche susceptibility map of the region

SN	Avalanche Susceptibility	Area(Km^2)	Percentage
1	Very Low	96.5	8.51
2	Low	279.16	24.63
3	Moderate	297.36	26.24
4	High	213.58	18.84
5	Very High	246.84	21.78

The avalanche susceptibility map also indicates that the relatively flat, glacierized regions in the area have a low susceptibility to avalanches due to their level terrain

Table 1: Events used for validation

SN	Year	Event	Lat	Lon
1	1982	1982 Avalanche during Swiss expedition in Lhotse face	27.9702	86.9083
2	1970	Ice-fall avalanche in the Khumbu Icefall between Base Camp and Camp I	27.9960	86.8729
3	1981	Avalanche in West CWM	27.9820	86.8958
4	1989	Avalanche in W. ridge	28.0085	86.8255
5	1989	Pumori's exposed slope	27.9958	86.8941
6	1995	Numerous avalanches in the Khumbu region	27.9208	86.7094
7	2006	Due to a massive serac Collapsing at the Khumbu icefall	27.9965	86.8774
8	2007	Everest region	28.0066	86.8694
9	2014	Avalanche western spur	27.9922	86.8755
10	2015	Shaking from earthquake	28.0155	86.8705

The study's results were validated by examining 10 previous avalanche events. Among these events, 4 occurred in the very highly susceptible region, 4 occurred in the highly susceptible region, and the remaining 3 occurred in the moderately susceptible region. Based on the validation, the prepared susceptibility map demonstrated a high level of accuracy.

4. CONCLUDING REMARKS

Using a GIS-based Multi-Criteria Decision Analysis-Analytical Hierarchical Process, an avalanche susceptibility map was created for Sagarmatha National Park. Past events were used to validate the map, which revealed a significant portion of the area to be highly susceptible to avalanches.

To gain a deeper understanding of avalanche-related vulnerability, it would be beneficial to overlay the prepared map with major trekking and climbing routes, as well as settlements. This could be an attractive topic for future studies analyzing avalanche hazards and vulnerability.

Due to limited data, the map was validated using only a few incidents. However, establishing a data monitoring and preparing repository could enhance future studies on avalanches in the region

REFERENCES

Kumar, Satish, Pankaj Kumar Srivastava, and Snehmani. 2017. “GIS-Based MCDA–AHP Modelling for Avalanche Susceptibility Mapping of Nubra Valley Region, Indian Himalaya.” Geocarto International 32(11):1254–67. doi: 10.1080/10106049.2016.1206626.

#Gen-12:

Rainfall Thresholds for Shallow Landslides in Kavre District and Sediment Dynamics of Roshi River, Nepal

Suman Shrestha[1],*, Prachand Man Pradhan[1], and Hari Krishna Shrestha[2]

[1]*Department of Civil Engineering, Kathmandu University, Dhulikhel, Kavre, Nepal*

[2]*Nepal Engineering College, Changunarayan, Bhaktapur, Nepal*

**suman.shrestha@ku.edu.np*

1. INTRODUCTION

Kavre district experiences a huge number of shallow landslides in the monsoon season. The hydrologic characteristics of a watershed like discharge and sediment play an important role in river morphology and sedimentation. Dahal et al. 2008 conducted research 2008 on rainfall threshold affirming exceeding 144mm of daily rainfall increase the risk of landslides high in the Himalayan mountain [1]. Shrestha, H.K. et al., 2008 researched creeping landslide for effective use in the planning and execution of slope stability enhancement measures in Otoyo town, Shikoku, western Japan utilizing a three-dimensional model [2]. Chhetri A. et al. 2016 researched the sediment of River Langtang of Rasuwa, Nepal calculating the concentration of suspended sediment and then generating the sediment rating curve [3]. This study aims to determine the rainfall threshold for the initiation of shallow landslides in the Kavre district, Nepal. It also includes the hydrological study of discharge and sediment dynamics of Roshi River with the development of a suspended sediment rating curve.

2. METHODOLOGY

Khopasi rain gauge station was taken as a base station. Landslides data of the Kavre district was downloaded from Desinventar. From 113 landslide events, 15 landslide events were extracted and used for establishing rainfall thresholds. The antecedent rainfall and the landslide occurrence event were also analyzed. The statistical analysis was carried out and the best-fit regression line was drawn. The rainfall intensity I (mm/h), and duration D (h) relationship is developed by using the power law, $I = \alpha * D\beta$. The analysis also incorporates the drawing of the lower boundary which is the average rainfall intensity for the initiation of landslide in the Kavre district.

The primary hydrological data includes the collection of field data from Roshi River that includes the measurement of discharge and suspended sediment sampling followed by suspended sediment analysis in the laboratory. The discharge and suspended measurement was carried out for 31 days in the month of monsoon August-September, 2022.

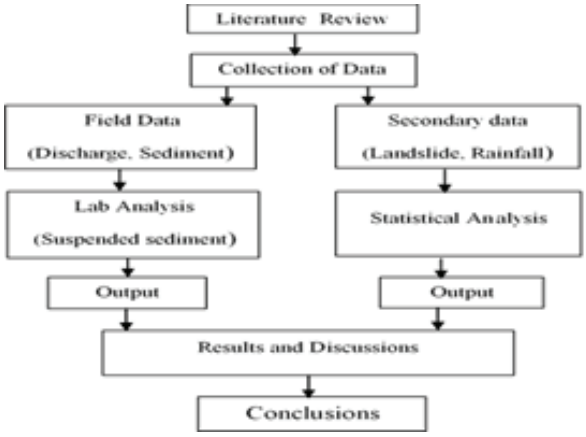

Figure 1: Methodology flow chart

Figure 2: Suspended sediment sampling and lab analysis setup

3. RESULTS AND DISCUSSION

3.1 Rainfall Threshold

The statistical analysis of the rainfall and landslide yielded rainfall thresholds with the creation of the best-suited regression line having a coefficient of determination R2 =

0.1461. Equation 1 illustrates the relation between rainfall duration (D) in hours and intensity (I) in mm/h.

$I = 9.5869 * D^{-0.866}$

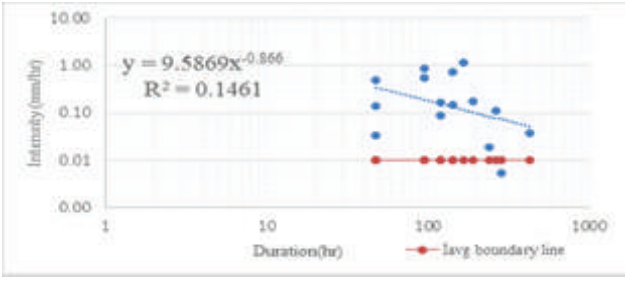

Figure 3: Rainfall intensity threshold for landslide

The average intensity above which the risk of landslide initiation is high in the Kavre district is 0.01mm/h. The rainfall intensity at 24 and 48 h duration at which the risk of occurrence of landslide is high are 0.61mm/h and 0.34mm/h

3.2 Antecedent Rainfall

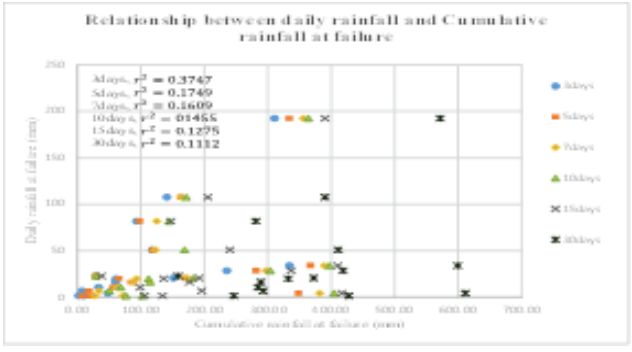

Figure 4: Relationship between daily rainfall and cumulative rainfall at failure

The daily rainfall (mm) and cumulative rainfall (mm) at failure were plotted in an arithmetic graph. The cumulative rainfall duration considered for the study is 3 days, 5 days, 7 days, 10 days, 15 days, and 30 days. The graph plotted shows the coefficient of correlation between daily rainfall at failure and cumulative rainfall at failure with r2 = 0.375, 0.175, 0.161, 0.146, 0.128, and 0.111 for 3 days, 5 days, 7 days, 10 days, 15 days, and 30 days respectively. It demonstrates the daily rainfall at failure conditions is highly correlated with 3 days cumulative rainfall at failure and decreases as duration increases.

3.3 Suspended Sediment Rating Curve

The maximum discharge and maximum suspended sediment in the monsoon of 2022 was 6.99 m3/s and 4952.22 mg/L

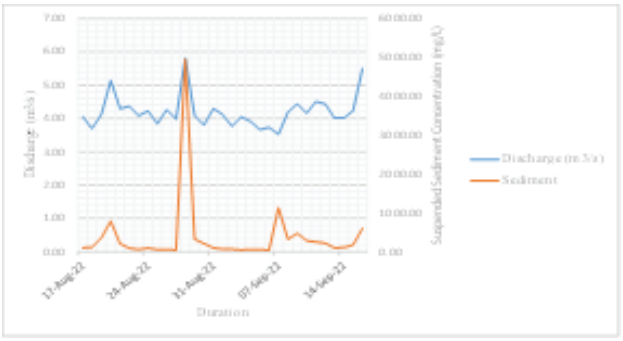

Figure 5: Discharge and sediment in the month of monsoon, 2022

The relationship between suspended sediment and discharge was developed with the coeffecient of determination R2 = 0.388. The equation of the suspended sediment rating curve is shown in equation 2.

$SSD = 0.019 * Q^{6.3105}$ (2)

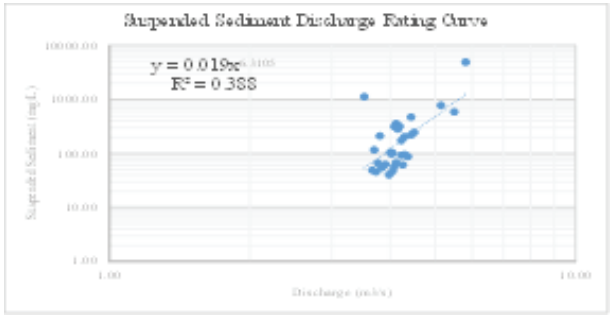

Figure 6: Suspended sediment rating curve

4. CONCLUDING REMARKS

The conclusion drawn from this research are

- The average intensity of rainfall above which the risk of landslide initiation is high in the Kavre district is 0.01mm/h.
- The rainfall intensity at 24 and 48 h at which the risk of occurrence of landslide is high are 0.61mm/h and 0.34mm/h.
- The analysis of landslide and rainfall data indicates that the antecedent rainfall plays a significant role in inducing landslides. It is more significant within 3 days and risk decreases as rainfall duration increases.
- The sediment rating curve was developed and also found that the maximum discharge and maximum suspended sediment in the monsoon of 2022 were 6.99 m3/s and 4952.22 mg/L respectively.

ACKNOWLEDGMENT

The author would like to thank the Department of Hydrology and Meteorology, Kathmandu, Nepal for providing the meteorological data and would also like to acknowledge RDI, Kathmandu University for providing partial financial support.

REFERENCES

[1] R. K. Dahal and S. Hasegawa, "Representative rainfall thresholds for landslides in the Nepal Himalaya," Geomorphology, vol. 100, no. 3–4, pp. 429–443, 2008, doi: 10.1016/j.geomorph.2008.01.014.

[2] H. K. Shrestha, R. Yatabe, and N. P. Bhandary, "Groundwater flow modeling for effective implementation of landslide stability enhancement measures: A case of landslide in Shikoku, Japan," Landslides, vol. 5, no. 3, pp. 281–290, 2008, doi: 10.1007/s10346-008-0121-8.

[3] A. Chhetri, R. B. Kayastha, and A. Shrestha, "Assessment of Sediment Load of Langtang River in Rasuwa District, Nepal," J. Water Resour. Prot., vol. 08, no. 01, pp. 84–92, 2016, doi: 10.4236/jwarp.2016.81007.

#Gen-13:

How most hydro-torrential hazard are being ended up inviting geo-disaster in Nepal ?

Narayan Gurung[1]*, Monique Fort[2], Gilles Arnaud Fassetta[2], Rainer Bell[3]
[1]Kadoorie Agricultural Aid Association, British Gurkhas Nepal, Pokhara
[2]Université de Paris, UMR 8586 PRODIG, 75205 Paris Cedex 13, France
[3]Department of Geography, University of Bonn, Germany
**Corresponding email: jyonus@hotmail.com*

1. EXTENDED ABSTRACT

On recent years, number of geo-disaster cases are increasing worldwide so do in Nepal Himalaya causing loss of lives, properties and environment. Though geo-disasters are still commonly perceived as natural events by most people in Nepal, geo-disasters as such are not natural and should not be seen as the inevitable outcome of a natural hazard's impact. Hydro-torrential hazard (landslide, flood, avalanche) are natural events on the earth, hence can not be stopped but through the proper planning and management, most geo-disasters can be avoided.

This study is mainly intended to present how hydro-torrential hazards are being resulted in geo-disasters in Nepal Himalaya through the analysis of specific case examples from Nepal Himalaya including two River valleys i.e. Seti River valley and Kali Gandaki River valley.

2. METHODOLOGY

Methodology includes hydro-geomorphological mapping, hydraulic analysis including HEC-RAS modelling, use of functional flooding space and land-use and land-cover change analyses, interpretation of satellite maps and interview with local people.

3. RESULTS AND DISCUSSION

Most geo-disasters have taken place due to the un-scientific human activities. People have lived or built infrastructures within the functional flooding space of river resulting in their death or structures washed away during high floods. Growing anthropogenic activities mainly haphazard construction activities, unplanned urbanization, riverside settlement, sand mining have increased significant risk of geo-disasters in Nepal.

A significant change on the land use and land cover of the Seti River valley, mainly the urban/built-up area, which saw its increase by 405 % between 1996 and 2020, and by 47 % in between 2013 and 2020. Further, effect of climate change cannot be ignored to aggravate natural hazards change into geo-disasters. Instead of relocating people from vulnerable places of river banks to safer places, the government and local authorities rather seemed to have encouraged people to live in the floodplain by providing basic amenities such as drinking water, electricity and access road. Many settlements and infrastructures along major rivers in Nepal, have been identified vulnerable to hydro-torrential hazards and may invite geo-disasters in our future. By simply respecting rivers' functional flooding space, fluvial hazards in most cases, can be avoided from becoming disasters. The occupation of flood prone areas and encroachment of river banks are on increasing trend over time. The findings suggest that occupants of natural hazard prone areas have a good understanding of possible geo-hazard and its associated risk. However, these risks are contextualized in relation to other social concerns, mainly economy seems to outweigh the risk.

Figure 1: Consequence of the construction of road in the floodplain. An example from Kali Gandaki corridor road at Bhurung, Tatopani, Myagdi. The road was heavily damaged by the flash flood of July 20, 2020 with complete destruction to the R.C.C. shear wall.

4. CONCLUDING REMARKS

All in all, anthropogenic activities are responsible to transform active, hydro-torrential hazard into geo-disasters. The best way to deal with the hydro-torrential hazard is not to build any infrastructure or dwellings on the floodplain but implement strict land-use policy, have an effective early warning system in place, monitor rivers regularly for blockages especially after earthquakes or landslides, relocate riverside settlements to safer places and discourage settlements directly beside rivers. Both Seti River valley and Kali Gandaki River valley are as dangerous as they are beautiful.

5. ACKNOWLEDGEMENT

The authors would like to thank University of Paris, UMR 8586 PRODIG, France, and Kadoorie Agricultural Aid Association, Nepal.

REFERENCES

Fort, M., Adhikari, B.R., and Rimal, B., 2018. A Dramatic, Yet Geomorphologically Active Environment Versus a Dynamic, Rapidly Developing City. In: Thornbush, M.J. and Allen C.D. (Eds) Urban Geomorphology: Landforms and Processes in Cities, Ch. 12. Elsevier S&T Books, 231-258.

Gurung, N., Fort, M., Arnaud-Fassetta, G., Bell, R., and Sherchan, B., 2020. Construction of road bridges without consideration of geo-hazards and river-flow dynamics. A case study from Ghatte Khola, Myagdi, Nepal. Géomorphologie: Relief, Processus, Environnement, 26 (3), p. 195 – 215. DOI: 10.4000/geomorphologie.14777

Gurung N., Fort M., Bell R., Arnaud-Fassetta G., Maharjan N, 2021. Hydro-torrential hazard vs. anthropogenic activities along the Seti valley, Kaski, Nepal: Assessment and recommendations from a risk perspective. Journal of Nepal Geological Society, 2021, Vol. 62, PP 58 – 87, https://doi.org/10.3126/jngs.v62i0.38695

#Gen-14:

Analysis the effect of non-persistent rock joint with various rock bridge intensity and configuration on shear behavior using direct shear test on PFC3D

Gaurab Singh Thapa
National Central University, Taiwan

1. INTRODUCTION

Structural defects such as joints or faults are inherent to almost any rock mass. Such defects can control the possible failure mechanisms. Extent of discontinuitywithin theplane and roughness of the structure (morphology of the joint surface) are the major contributor to influence the shear strengthof rock mass. Due to various geological process, intact rock bridges could occur on the joint surfaces by merging the pre-existing fractures.

2. METHODOLOGY

The objective of this study is to understand the effect of rock bridge intensity and it's configuration on shear behavior (shear strength, modulus and displacement) of joint. The direct shear test by using particle flow code PFC3D can be used to establish the coplanar non-persistent joint model. Planar joint geometry can be prepared using PFC3D and if joint roughness is considered, real morphology of the exposed joint can be accessed with 3D laser mapping. Discrete element method would create the synthetic rock joint. Failure in rock mass occur through sliding along persistent discontinuities, but also through combination of sliding along non-persistent discontinuities andbridging across unbroken rock.

3. RESULTS AND DISCUSSION

Effect of latitudinal rock bridge on jointedrock was numerically investigated through series of direct shear test. Shear behavior of rock specimens containing multiple rock bridges with different area was investigated through direct shear simulations. Failure patternandfailuremechanism is observed through numerical jointed rock specimen by performing series of direct shear test. Increase in the area of rock bridge and normal stress increase the shear resistance distinctly. Shear strength increase with decrease in joint persistency. Shear displacement increase with decrease in joint persistency. Normal displacement decreases with increasing normal stress. Cohesion is the major dominant factors controlling the shear

strength. For the fixed area of longitudinal rock bridge cohesion remains almost constant with the change in the number of rock bridges.

4. CONCLUDING REMARKS

This complex interaction between natural discontinuities and brittle fracture propagation through intact rock bridges can be predicted well using Jennings criterion.

ACKNOWLEDGEMENTS

This work was performed as a research project of third semester during graduate study. This research was financed by National Central University, Taiwan.

Keywords: Non-persistent discontinuities, rock bridges, shear properties, PFC3D

REFERENCES

1. Lambert, C., & Coll, C. (2014). Discrete modeling of rock joints with a smooth-joint contact model. Journal of Rock Mechanics and Geotechnical Engineering, 6(1), 1-12. doi:10.1016/j.jrmge.2013.12.003
2. Lin, H., Ding, X., Yong, R., Xu, W., & Du, S. (2019). Effect of non-persistent joints distribution on shear behavior. Comptes Rendus Mécanique, 347(6), 477-489. doi:10.1016/j.crme.2019.05.001
3. Sarfarazi, V., & Haeri, H. (2016). Effect of number and configuration of bridges on shear properties of sliding surface. Journal of Mining Science, 52(2), 245-257. doi:10.1134/s1062739116020370

#Gen-15:

Strength Behaviour and Fracture Propagation in Un-grouted and Grouted Porous Rock Mass Subjected to Uniaxial Loading

Gaurav Kumar Mathur[1], Arvind Kumar Jha[2], Gaurav Tiwari[3]

[1]Research Scholar, Rock Mechanics and Rock Engineering Laboratory, Department of Civil and Environmental Engineering, IIT Patna, Bihar, India;

[2]Assistant Professor, Rock Mechanics and Rock Engineering Laboratory, Department of Civil and Environmental Engineering, IIT Patna, Bihar, India;

[3]Assistant Professor, Department of Civil Engineering IIT Kanpur, U.P., India;

ABSTRACT

Various triggering factors such as thermal loads, excavation, and seismic wave velocity impose the dynamic loading along the rock joints. Further, these loading ranging from pseudo to very high rates affect the discontinuities (either persistence or, non-persistence) present in any rock mass, resulting in a significant effect on the strength behavior. Hence, the strength of such rock mass needs to be restored by using a suitable technique to overcome future distress and damage in the stability analysis of slopes and tunnels. Grouting is the most suitable method to improve the strength of pre-stressed rock mass. In this study, the effect of grouting has been observed in jointed specimens with different joint ordination by conducting the UCS loading test. During the UCS test, an increasing trend in peak strength is noted when the un-grouted jointed specimens infilled with the cement paste as compared to un-grouted specimens. Further, grouting enhances the stress concentration at filled crack tips which are responsible for the dominance of tensile fractures in all the joint orientation specimens and hence, improves the elastic modulus and peak strength of the specimens.

Keywords: *Jointed Rock Mass; Grouting; Cement; Static behaviour; Impersistence*

1. INTRODUCTION

An intact rock is considered to be homogeneous and continuous at the scale of consideration. The intact rocks are common in nature for a limited range, though the presence of different kinds of imperfections makes the rocks inconsistent. The imperfections include fractures and joints of various shapes, sets, and dimensions, weak bedding planes, voids, etc. The overall strength and nature of brittle deformation of both intact and impersistent rocks are crucial in many engineering and rock mechanics applications. Along with a number of other factors like; physical, mechanical, geological, lithological, and environmental parameters, the imperfections are greatly controlled by the elasticity, strength, and fracture pattern of the intact and imperfect rocks. Rock mass generally fails due to the presence of different imperfections like persist (Lee et al., 2012; Sagong et al., 2011) and non-persist discontinuities which highly influence the mechanical properties of hard rock mass (Feng et al., 2022) and soft porous rock mass (Hoek and Bray 1974; Lajtai 1971; Mathur et al., 2022; Miller and Deere 1966; and Yang et al., 2019).

Rock mass weakening develops the threat of several dynamic loading and structurally controlled failures and these threats are often reported on underground constructions, tunnels, foundations, and slopes (Wyllie and Mah, 2004). Chen et al., (2018) and Yang et al., (2021) conducted UCS test on artificial jointed rock mass by varying joint orientations from 0° to 90°. They concluded that the crack propagation patterns and mechanical behavior are affected significantly by the joint orientations of the jointed rock mass. Failure of rock mass due to discontinuities can be improved by various methods like rock bolting (Li et al., 2017; Sakhno and Sakhno, 2023; Yang et al., 2021; and Zhang et al., 2016) and several infill grouting material, etc. (Jahanian et al., 2015; Kumar et al., 2022; Le et al., 2018; Xue et al., 2023; and Yi et al., 2023). It has been noted that the un-bolted strength of the specimen increases by providing the full-length anchorage condition in jointed specimens. Grouting is a well-established engineering practice for stabilizing the jointed and/or fractured rock mass. This process generally leads to the enhancement of the

mechanical properties of fractured rocks. Infill material slurry injected with suitable methods into the jointed rock mass develops a bond to the solid mass and hence improves its overall strength. The selection of the grouting material is usually based on the rock mass properties such as cohesion, friction angle, joint roughness, joint aperture, etc. Due to ease of user-friendliness and economical prospect, cement is considered as the suitable grout material for sedimentary rock mass (Azadi et al., 2017; Erol and François 2014; Safaei et al., 2021; Lu et al., 2017; and Zhong et al., 2020). The soft sedimentary rock mass is considered as susceptible in behavior subjected to dynamic conditions. Sometimes, the sedimentary rock mass is subjected to weathering due to the action of wind, rain, heat, and pressure to a particular location. These weathering actions are responsible for the deterioration of the bond in the rock mass which leads to the overall strength variation.

The present study focuses on the improvement of soft porous rock with the use of infill grouting material in the pre-existing impersistent jointed artificial rock mass, and to study the mechanical behavior and fracture propagations subjected to uniaxial static loading. The impersist jointed specimens are prepared by using Plaster of Paris with varying joint orientations in the middle portion of specimens. Further, the outcome from the static uniaxial compression tests could be used to predict the consequences in natural situations with consideration of the boundary conditions. Finally, the mechanism of strength variation in the un-grouted and grouted specimen are elucidated using fracture propagation subjected to uniaxial load.

2. MATERIALS AND METHODOLOGY

2.1 Sample preparation

The Plaster of Paris (PoP) is used as modeling material to prepare the specimens for the present study, which complies as soft porous sedimentary rock. A specific cylindrical mould is fabricated with a suitable slit of 20 mm long and 1 mm thick that can be inserted in the mould for creating a jointed specimen (Barton 1973; Ishii 2016; Mathur et al., 2022). The mixture of POP and water at a particular water content is prepared which is, then, poured into the specific mould of size 50 mm diameter and 100 mm height. Before pouring the POP:Water mixture, the cylindrical mould is greased properly to avoid the generation of friction inside the mould as well as to take out the sample easily after the completion of the drying period. The slit is taken out from the mould after 15-20 minutes to create proper artificial jointed in samples (Fig. 1a). Infill grout paste is prepared to fill the joint in samples by using Ordinary Portland Cement (OPC): Water at the ratio of 1.25:1. The grout paste is injected carefully inside sample joint by using the syringe to maintain uniform distribution of infill material (Fig. 1b) and later, curing is carried out to the grouted specimens for around 25 days.

2.2 Uniaxial static loading test

The compression tests were carried out using a uniaxial testing machine operated under displacement-controlled mode (mm/min) with a maximum capacity of 5 tons (Fig. 2). The load frame performs under a range of desired displacement rates and is controlled by a motor drive system. The tests are carried out at the displacement rate of 1.25 mm/min and the loading direction is parallel to the cylindrical specimen axis.

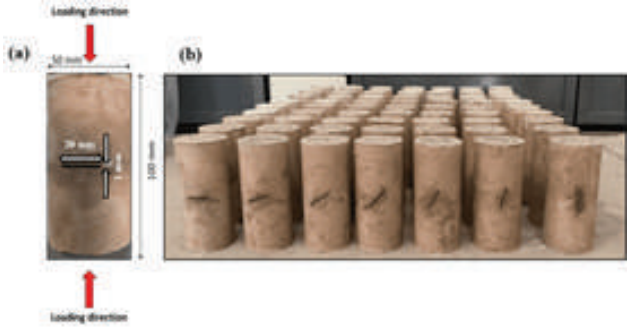

Figure 1: (a) Jointed specimen; (b) Cement grouted specimens

Figure 2: Uniaxial compression strength apparatus

3. RESULTS AND DISCUSSION

In this study, the strength of un-grouted and grouted specimens is investigated by performing the uniaxial static loading test. The strength behavior of specimens is presented in Fig. 3-4.

The peak strength of the intact specimen prepared at 80% water content is observed to be 2.46 MPa. Based on the strength criteria of Choudhary and Sonu (2013) and Hoek and Brown (1997), the specimen can be categorized as very low strength and of grade R1 (i.e., very weak), respectively.

The stress-strain behavior of un-grouted specimens shows that all specimens with different joint orientations follow Hook's law except joint orientations of 15°, 30°, and 45° because, at these specimens, the stress concentration at the pre-existing crack tips is very low which is responsible for the undulating path after peak strength with higher strain and due to which low elastic modulus observed (Fig. 3a), while when the pre-existing cracks filled with cement slurry, all the specimens follows Hook's law up to peak strength due to increase in stress concentration at the crack tips which responsible for the increase in peak strength and elastic modulus (Fig. 3b). After post-peak strength, the stress-strain curve starts to decrease linearly until complete failure of the specimen. The peak strength of un-grouted jointed specimen reduces with joint orientation up to 30°, and increases thereafter till 90° (Fig. 3a). Further, it has appeared that filling of joint with infill material (i.e. cement paste) enhances the peak strength of the specimen irrespective of joint orientation. It is interesting to note that the increase in the peak strength of the un-grouted jointed specimens is infilled with cement paste up to 30° joint orientations and marginal thereafter as compared to the same with un-grouted joint specimens. The behavior of this mechanism appears because up to 30° joint orientations, grouting diminishes the shear behavior along the pre-existing crack and hence the enhancement of peak strength appears (Fig. 4) and after joint orientation 30°, as soon as the maximum stress concentration reaches at the filled crack tip, the solid form of cement paste acts like a plate inside the specimens which provides the shear failure path from the cement paste boundary and hence marginal increase in peak strength appears.

Therefore, it can be concluded that the grouting is efficient only up to 30° joint orientations. After that, there are very slight changes in peak strength occur in the very soft porous rock after applying cement paste grouting.

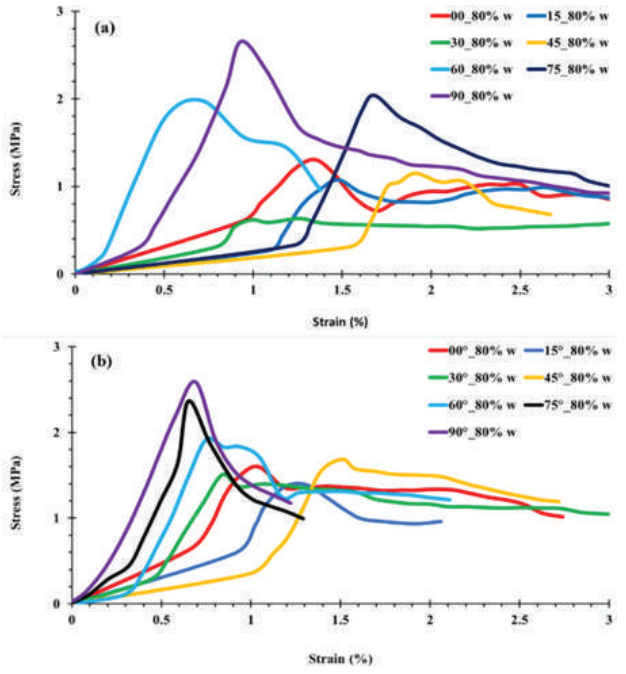

Figure 3: Specimens with different joint orientations subjected to uniaxial static loading; (a) Un-grouted; (b) Cement grouted

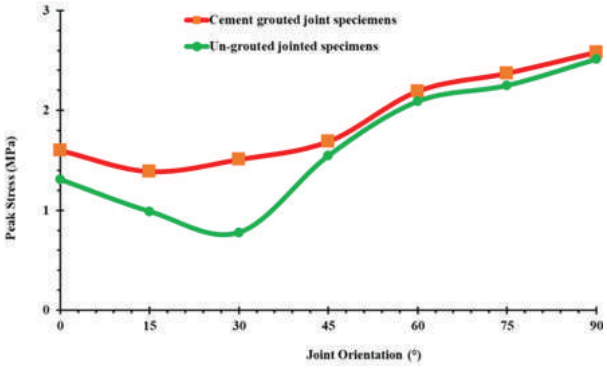

Figure 4: Variations of peak strength of un-grouted and cement-grouted jointed specimens subjected to UCS loading

Fracture Propagation in specimens:

The fracture propagations of tested UCS samples are examined to elucidate the experimental results. It is observed that the crack propagation starts from the pre-existing crack tips in both un-grouted and grouted specimens. The crack initiation position is directly related to the pre-existing joint orientations of the specimens. The tensile fracture is generally responsible for the wing cracks at the end of pre-existing cracks in the specimens. While shear fractures appear due to the possible slip along the pre-existing crack. In un-grouted specimens (Fig. 4a), tensile wing cracks are generated from the pre-existing

crack tip from 0° to 45° joint orientations specimens while shear cracks are experienced in 60° and 75° jointed orientations because of possible shear path although tensile splitting is observed in the upper crack tip and two shear paths appeared in the lower crack tip of 90° joint orientation specimens. When the cement grouting is introduced in the cleaned pre-existed cracks of specimens, the fracture behaviors of the specimens are also affected (Fig. 4b). Joint orientation with 0° fails in tensile mode and as the load continues, the trapezoidal failure shape effect is observed in the upper portion of the specimens. The tensile wing crack is observed at both tips of 15° joint orientation specimens. The dominance of tensile cracks with shear cracks due to failure path changes from crack tip to cement paste boundary is continuing till 75° joint orientation specimens. The upper crack tip remains unaffected on 90° joint orientation specimens, while, the lower crack tip is influenced by a tensile crack. It is also observed that as the loading continues after the initiation of primary tensile and shear cracks in all un-grouted and grouted specimens, the crack branching appears throughout the specimens which are responsible for the surface spalling and complete failure of the specimens.

Therefore, it can be elucidated from the above description that, the behavior of fracture propagation is mostly tensile mode up to 45° joint orientations in un-grouted jointed specimens, and after that shear failure is dominating in higher joint orientations. After applying the cement paste grouting to the un-grouted specimens, the stress concentration increases at the grout-filled crack tips which are accountable for the dominance of tensile fractures in all the joint orientation specimens.

4. CONCLUSION

This study investigated the grouting effect on the mechanical behaviour of impersistent jointed specimens made of gypsum, under uniaxial compressive load. The following key outcomes may be drawn from this investigation:

6. An increase in the peak strength is observed from un-grouted joined specimens to cement-grouted specimens prepared from 80% water content.

7. The stress-strain curves of all un-grouted and grouted specimens follow Hook's law except joint orientations of 15°, 30° and 45 for un-grouted specimens due to low-stress concentration at the pre-existing crack tips which are responsible for low elastic modulus and undulating path after peak strength. However, grouting improves the elastic modulus and peak strength.

8. It is experienced that the behavior of fracture propagation is mostly tensile mode up to 45° joint orientations in un-grouted jointed specimens and after that

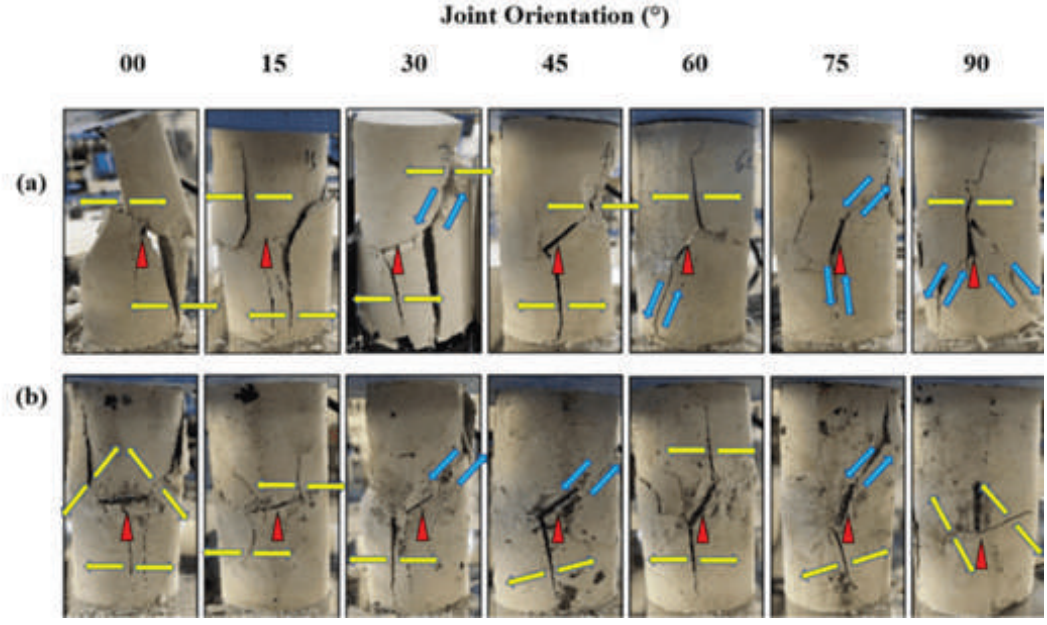

Figure 5: Fracture propagations in different joint orientation specimens; (a) Un-grouted; and (b) Cement grouted. The red arrowhead marks the locations of the induced joint segment; tensile wing cracks and shear cracks were represented by yellow and sky blue arrows respectively with the arrowhead specifying the directions of fracture movement.

shear failure is dominating in higher joint orientations. Grouting enhances the stress concentration at filled crack tips which are responsible for the dominance of tensile fractures in all the joint orientation specimens.

9. Prolongation of the loading after primary tensile and shear cracks initiation in all un-grouted and grouted specimens, the crack branching appears throughout the specimens which is responsible for the complete failure of the specimens.

REFERENCES

Barton, Nicholas. "Review of a new shear-strength criterion for rock joints." Engineering geology 7.4 (1973): 287-332.

Choudhary, Bhanwar S., and Kumar Sonu. "Assessment of powder factor in surface bench blasting using schmidt rebound number of rock mass." International Journal of Research in Engineering and Technology 2.12 (2013): 132-138.

Deere, Don Uel, and R. P. Miller. Engineering classification and index properties for intact rock. Illinois Univ At Urbana Dept Of Civil Engineering, 1966.

Feng, Peng, et al. "Mechanical behaviors of conjugate-flawed rocks subjected to coupled static–dynamic compression." Acta Geotechnica 17.5 (2022): 1765-1784.

Hoek, Evert, and J. W. Bray. "Rock slope engineering: institution of mining and metallurgy." London, England (1974).

Hoek, Evert, and Edwin T. Brown. "Practical estimates of rock mass strength." International journal of rock mechanics and mining sciences 34.8 (1997): 1165-1186.

Ishii, Eiichi. "Far-field stress dependency of the failure mode of damage-zone fractures in fault zones: Results from laboratory tests and field observations of siliceous mudstone." Journal of Geophysical Research: Solid Earth 121.1 (2016): 70-91.

Jahanian, Homayoun, and Mohammad Hosein Sadaghiani. "Experimental study on the shear strength of sandy clay infilled regular rough rock joints." Rock Mechanics and Rock Engineering 48 (2015): 907-922.

Kumar, Sachin, et al. "Rate-dependent mechanical behavior of jointed rock with an impersistent joint under different infill conditions." Journal of Rock Mechanics and Geotechnical Engineering 14.5 (2022): 1380-1393.

Lajtai, E. Z. "A theoretical and experimental evaluation of the Griffith theory of brittle fracture." Tectonophysics 11.2 (1971): 129-156.

Le, Huilin, et al. "Effect of grout on mechanical properties and cracking behavior of rock-like specimens containing a single flaw under uniaxial compression." International Journal of Geomechanics 18.10 (2018): 04018129.

Mathur, Gaurav Kumar, et al. "Effect of displacement rates on the mechanical integrity of soft-porous rock analogue containing non-persistent joints of variable lengths." Journal of Earth System Science 131.2 (2022): 118.

Mokhtarian, Hadi, Hassan Moomivand, and Hussamuddin Moomivand. "Effect of infill material of discontinuities on the failure criterion of rock under triaxial compressive stresses." Theoretical and Applied Fracture Mechanics 108 (2020): 102652.

Sakhno, Ivan, and Svitlana Sakhno. "Numerical Studies of Floor Heave Control in Deep Mining Roadways with Soft Rocks by the Rock Bolts Reinforcement Technology." Advances in Civil Engineering 2023 (2023).

Wyllie, Duncan C., and Chris Mah. Rock slope engineering. CRC Press, 2004.

Wong, L. N. Y., and H. H. Einstein. "Crack coalescence in molded gypsum and Carrara marble: part 1. Macroscopic observations and interpretation." Rock Mechanics and Rock Engineering 42 (2009): 475-511.

Yi, Wenhao, et al. "The effect of rock hardness and integrity on the failure mechanism of mortar bolt composite structure in a jointed rock mass." Engineering Failure Analysis 143 (2023): 106831.

Zhang, Jon Jincai. Applied petroleum geomechanics. Gulf Professional Publishing, 2019.

Zhang, Bo, et al. "Reinforcement of rock mass with cross-flaws using rock bolt." Tunnelling and Underground Space Technology 51 (2016): 346-353.

#Gen-16:

Comparative Study of Soil Constitutive Models for Deep Excavation in Kathmandu Clay

Sandip Regmi1, Bhim Kumar Dahal2
[1] *Department of Civil Engineering*
Pulchowk Campus, IOE, Tribhuvan University, Nepal

1. INTRODUCTION

Due to unplanned, rapid urbanization, limited and expensive land values of the major cities in Nepal like Kathmandu, the necessity of high-rise buildings, underground spaces, and underground infrastructures has been increasing. It needs more deep excavation and care while excavating so that excavation works have no adverse consequences in adjacent structures.

Kathmandu Valley is composed of fluvio- lacustrine deposits and mostly soft soil. Due to poor practices and an inadequate support system in deep excavation, cracks in nearby structures due to differential settlements are more common nowadays. To lessen problems and make excavations more efficient, identification of mechanical behaviors of soils (Dahal et al. 2019) and selection of appropriate constitutive soil models as per performance evaluations of models are more necessary.

Tukucha, a core area of Kathmandu Valley, is taken to identify the mechanical behaviors of soils from laboratory tests. Constitutive soil models: Mohr Coulomb (MC) Model, Hardening Soil (HS) Model, Hardening Soil Small Strain (HS Small) Model and Soft Soil (SS) Model are used in numerical simulation using Plaxis 2D V20 and compared with the laboratory results. The findings of the evaluation of constitutive models are further used in the performance of the support system for deep excavation.

2. METHODOLOGY

Undisturbed samples were collected from Tukucha, in between the Bagmati River and the Department of Immigration in Tripureshwor, Kathmandu, from different boreholes of 15 m depth. Undisturbed samples from molds are extruded in a sampler for the consolidated undrained (CU) triaxial test. The triaxial test apparatus of the Department of Civil Engineering, Pulchowk Campus, is used for testing. Three samples from each layer were tested using an effective consolidation pressure of 50, 100, 200, and 400 KN/m2. From the test result, Mohr's circle, stress- strain relationship, effective stress path, total stress path, normalized q vs axial strain, pore water pressure vs axial strain, etc. were plotted for the evolution of the mechanical properties of the soil.

Furthermore, samples are prepared for the one-dimensional consolidation test (oedometer test), which

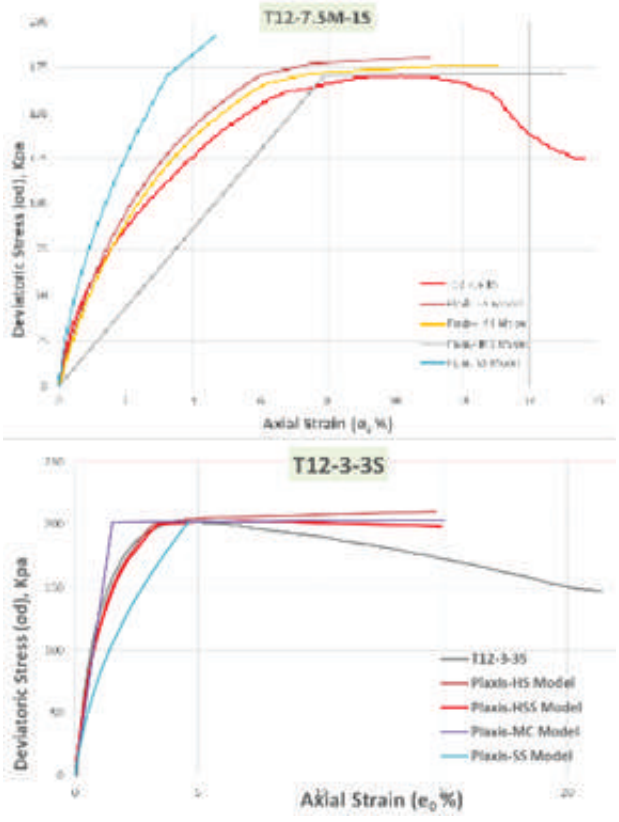

Figure 1: Comparison of stress-strain relations obtained from Plaxis and laboratory test

helps to determine the coefficient of consolidation (Cv), pre-consolidation pressure, initial void ratio (eo), compression index (Cc), recompression index (Cr), coefficient of compressibility (av), coefficient of volume change (mv), etc. Similarly, other index properties were evaluated using standard laboratory procedures to characterize the soil. Due to its lower

specific gravity, an organic content test was also performed.

Using the laboratory results and empirical relations, the parameters required for different models were determined, and Plaxis was used for finite element analysis to compare stress-strain relations with laboratory test results. The model that was close to its laboratory value was used to compare the model during deep excavation analysis.

3. RESULTS AND DISCUSSION

The soil profile of the site consists of a surface soil layer up to 2 m depth, which contains waste materials such as cotton clothes, plastic bags, sand with silty clay, etc. While the remaining layers are dark gray, medium- soft to stiff organic clay of medium-to-high plasticity, which lies under soil class 'OH' as per the USC Soil Classification.

Evaluation of Constitutive Model

In this study, Plaxis 2D, a FEM tool, is used to simulate each sample while maintaining laboratory triaxial conditions, and the output is compared with the laboratory results. As given below, the stress-strain graph obtained using the Hardening Small Strain (HSS) model seems closer to the relation obtained

from the triaxial laboratory test in all samples. Therefore, during deep excavation analysis, the wall deformation obtained from the HSS model, are taken as realistic ground conditions and compared with the outputs of the other models. The comparison between the outputs of different models is presented below.

Numerical Analysis of Deep Excavation

Different constitutive models were used to evaluate the deformation of the support structure for a deep excavation, and Figure 2 displays geometric model and the results. Comparing the results from the MC model, the wall deformation is similar to the HSS

model except for the third and final excavation stages, where the results are much smaller. Similarly, the results of the HS model analysis are very close to those of the HSS model, and at the final excavation stage, wall deformation is slightly less than the HSS model output, which is consistent with the findings of previous study (Lim, C, & Hsieh, 2010). This confirms that the HS model is also suitable for analyzing typical Kathmandu soil. Additionally, the SS model's prediction is overly optimistic, with the lowest value among the models, making it unsuitable for deep excavation modeling.

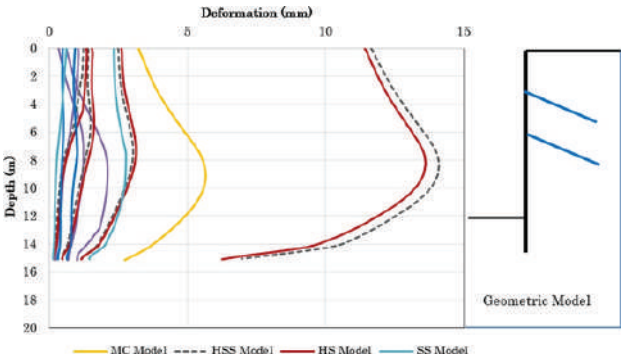

Figure 2: The comparison of measured wall displacement with predicted using HSS Model.

4. CONCLUDING REMARKS

The HSS model is the best constitutive model for typical Kathmandu soil because it produces mechanical behavior predictions that are more similar to laboratory test results and obtained outputs. In the final stage of excavation, the predicted wall displacement using the HS model is generally close to the HSS model, but slightly larger for other stages. Both the HS and HSS models provide better results than other models. However, the MC model and Soft Soil (SS) model produce displacement patterns that are significantly different from the HSS model, and therefore, these models cannot accurately predict the stress and deformation state for all loading conditions.

To make the model evaluation more realistic, it is recommended to compare the results with actual field measurements taken during excavation.

REFERENCES

Dahal, Bhim Kumar, Jun-Jie Jie Zheng, and Rong- Jun Jun Zhang. 2019. Evaluation and Modelling of the Reconstituted Clays Considering Pre-peak Stiffness Degradation. International Journal of Geosynthetics and Ground Engineering 5. Springer International Publishing: 9. https://doi.org/10.1007/s40891-019- 0159-9.

Koirala, A., Shrestha, O. M., & Karmacharya, R. (1993). Engineering geology of the southern part of Kathmandu Valley. Jour. Nepal Geol. Soc, 3, 151-159. Lim, A., C, O., & Hsieh, P. (2010). Evaluation of clay constitutive models for analysis of deep excavation under undrained conditions. Journal of GeoEngineering, 9–20 (https://doi.org/10.6310/jog.).

#Gen-17:

Sediment Quantification of the Andheri Khola Sub-Watershed of Fewa Lake in Nepal and the Socio-economic Impact of Climate Change

Naba Raj Sharma[1], Milan Bhattrai[2], Bikash Devkota[3], Arjun Baniya[4], Mahendra Baniya[5]

[1]*Senior Divisional Engineer, Government of Nepal*

[2]*Engineer, Watershed Management Centre, Government of Nepal*

[3]*Ph.D. Candidate, UniSA STEM, University of South Australia, Mawson Lakes Campus, Adelaide, Australia*

[4]*Research Director, United Technical College, Bharatpur, Chitwan, Nepal*

1. INTRODUCTION

The temperature and precipitation extreme events have been already experienced and are expected to continue in the future globally with the increasing risks related to heat waves, rainfall, and droughts [1]. The hilly zone of Nepal has experienced numerous natural disasters like debris flow, landslides, and flooding over the years. As Nepal is susceptible to climate change and has complex, rugged, and fragile topography, the vulnerability is expected to increase in the future. Sediment generated in various watersheds has significant negative impacts at the source and downstream. Pokhara is one of the economic centers of Nepal including tourism with a beautiful Fewa Lake. The watershed of this lake has steep and irregular topography with a deeply weathered and transportable nature of soils. The deposition of sediments has gradually decreased the lake's area, water-holding capacity, and beauty of the lake.

This study aims to quantify the sediment at Adheri Khola as it is very crucial to conserve Fewa Lake. Furthermore, it aims to understand climate change impacts on the socio-economic activities of the study area.

2. METHODOLOGY

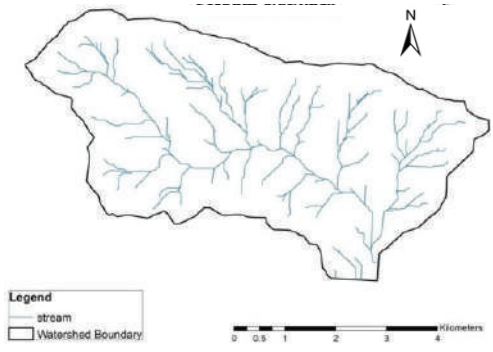

Figure 1: Stream network of the Andheri Khola Sub- watershed.

Soil erosion was quantified using the RUSLE (Revision of the Universal Soil Loss Equation) model
[2] in the Andheri Khola sub-watershed shown in Figure 1. The impact of climate change was studied using a questionnaire for the targeted stakeholders.

In the RUSLE model soil loss by erosion is estimated using precipitation, a digital elevation model

(DEM), and various maps (soil type, land cover, and satellite). The precipitation data were taken from three weather stations— Airport, Lumle, and Bhadurae operated through the Hydrological and Meteorological office. DEM data acquired from the National Land Survey office of Nepal was used in ArcGIS for the determination of flow length including slope steepness. The soils of the sites were characterized as loam, silty, and sandy loam.

3. RESULTS AND DISCUSSION

ASTER (Advanced Spaceborne Thermal Emission and Reflection Radiometer), a DEM with 30 m resolution and 20 m sampling, and satellite images were used to identify slope maps, relief features, river sites, landslides, landforms, and prone areas. The elevation of the Andheri Khola sub-watershed ranges from 799.866 to 2067.68 meters.

3.1 Annual average soil loss (A)

Annual average eroded soil mass (A) in t ha-1 was calculated using Equation (1) [3] and the factors used are described below:

$$A = R \times K \times L \times S \times C \times P \qquad (1)$$

R is a soil rainfall and runoff erosivity in MJ.mm ha-1 h-1 yr-1. It was estimated using Equation (2) as the rainfall intensity of the study area was higher than 850 mm [3].

$$R = 587.8 - 1.219 \times P + 0.004105 \times P2 \qquad (2)$$

where P = average annual precipitation in mm.

K represents the soil erodibility factor. It depends on the soil's properties such as texture, particle stability, hydraulic conductivity, and water absorption capacity that determine the easiness of soil particle dislodgment [4]. Here, suggested values of K- factor were from 1 to 0.01 for highly erodible to highly stable soil respectively. In this study, its value was taken as
0.8 t h / MJ mm.
Factors L and S are dimensionless and denote the slope length and steepness respectively. These two factors combinedly describe the relationship between topography and soil erosion. They were generated using ArcGIS in this study.

The dimensionless factor C is the cover management factor representing the easily manageable conditions that help to reduce soil erosion [2]. According to them, its values range from 0 to 1.5 for highly protected soil to a surface producing high

runoff leading to a high potential for erosion. The land covers in the study area were forest (9.44 km2), agriculture (16.39 km2), and wasteland (1.36 km2).

The next dimensionless parameter P is a supporting practices factor to account for control practices that reduce the erosion potential of the site representing the surface conditions that affect flow paths including hydraulics. [2,4]. P values were chosen based on land use or soil management in the study area.

As a result of the RUSLE model, the soil erosion risk map of the Andheri Khola watershed was generated based on the annual soil loss as shown in Figure 2. Four risk classes based on the soil loss ranges including corresponding area and their sediment losses are shown in Table 1.

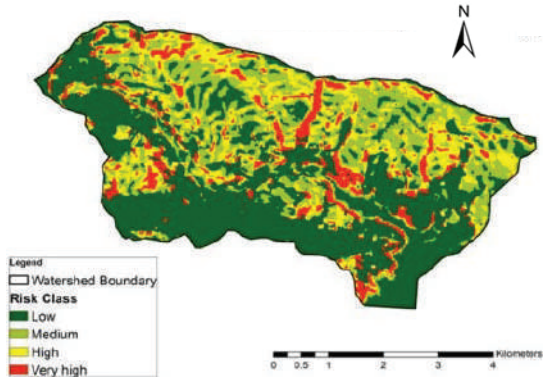

Figure 2: Soil erosion risk map of Andheri Khola sub-watershed

Table 1: Annual loss of soil from Andheri Khola sub- watershed and risk class.

Range of soil loss (t $ha^{-1}y^{-1}$)	Risk class	Area (km^2)	Soil loss (t $ha^{-1}y^{-1}$)
<15	Low	14.27	5915
15-25	Medium	5.009	10018
25-50	High	7.094	26602.5
>50	Very High	0.824	5479.6
Total		27.19	48015.1

The outcome of this research helps the stakeholders with the remedial measures of sediment control in the Andheri Khola watershed leading to the conservation of Fewa lake. As shown in Figure 2, most of the northern and central zones of the watershed are medium to highly vulnerable to sediment generation. Hence, the locations indicated by yellow and red marks (Figure 2) are needed with immediate watershed conservation intervention.

3.2 Impact of climate change on the study area

Climate change had an impact on the socio- economic activities of the study area. The causes and effects of climate change were evaluated using a questionnaire for the targeted stakeholders. Most respondents stated that the sedimentation process was caused by rainfall, while a few minor respondents stated that it was due to snowfall. Out of 123 respondents, 84 (68.3%) answered that the sedimentation process was triggered due to rainfall, 24 (19.5%) by drought, 13 (10.6 %) by an earthquake, and only 2 (1.6%) by snowfall.

Change in seasonal calendars of rainfall was mostly irregular and unpredictable, which induced

natural disasters. Most of the key informants reported that such changes affected the livestock and human health, water availability, and livelihoods of the people. Furthermore, according to the respondents, the seeding, planting, and harvesting times of cereal crops such as maize and wheat had been changed. The respondent's perception towards the effect of climate change is shown in Figure 3 where the majority of the people believed that the decline of crop yield and increase in landslide events were the major consequences. This shows that special attention is required to increase the production and prevention of mass movement

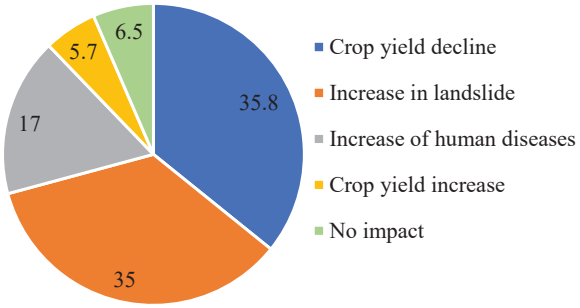

Figure 3: Percentage of respondents towards the effect of climate change

4. CONCLUDING REMARKS

According to the RUSLE model, 48015.1 t ha-1yr-1 sediment was produced from the Andheri Khola sub-watershed of Fewa Lake. Besides, the changing climate of this watershed affected not only the rainfall patterns and temperature increment but also the crop yield and geophysical processes like a landslide. The outcomes of this research help to know the intervention required for the conservation of the Andheri Khola watershed and strategies for the increase of agricultural production.

ACKNOWLEDGEMENT

The authors acknowledge Pokhara University for this research opportunity and support. Likewise, we would like to acknowledge Pokhara Metropolitan City and Annapurna Rural Municipality Office for the field coordination.

REFERENCES

1. Pfleiderer, P.; Schleussner, C.-F.; Kornhuber, K.; Coumou, D. Summer weather becomes more persistent in a 2 C world. Nature Climate Change 2019, 9, 666-671.
2. Renard, K.G.; Foster, G.R.; Weesies, G.A.; Porter, J.P. RUSLE-Revised universal soil loss equation. Journal of Soil and Water Conservation 1991, 46, 30-33.
3. Renard, K.G.; Freimund, J.R. Using monthly precipitation data to estimate the R-factor in the revised USLE. Journal of hydrology 1994, 157, 287-306.
4. Artiola, J.; Walworth, J.; Musil, S.; Crimmins, M. Soil and land pollution. In Environmental and pollution science; Elsevier: 2019; pp. 219-235.

#Gen-18:

Landslide Susceptibility Map of Uwajima (Japan) produced with machine learning technique and XRAIN radar acquired rainfall data

José Maria dos Santos Rodrigues Neto[1], Netra Prakash Bhandary[2]

[1]Grad. School of Sci. & Eng., Ehime University, Japan

[2]Faculty of CRI, Ehime University

1. INTRODUCTION

A recent example of rainfall-induced landslide disaster was the event of the heavy rains of July 2018 in Southwestern Japan, when along the course of 10 days, rainfall-induced disasters took a toll of 225 lives, 11 of those in the small town of Uwajima, in Ehime Prefecture. It is judged that new strategies and tools are necessary in urban planning and disaster prevention management to avoid such damage. One of these tools are landslide susceptibility maps (LSMs), which appoint slopes prone to failure in a rainfall event. In this study, the novel technologies of XRAIN (eXtended Radar Information Network) radar-acquired rainfall data and the machine learning technique random forest were used in order to create an LSM for the area of Uwajima City.

2. METHODOLOGY

An empirically based LSM requires a collection of landslide conditioning factors (LCFs) and a collection of registered slope failure points. In this study, 8 LCFs were used, including radar acquired XRAIN rainfall data, provided by DIAS (2020). The collection of landslides comprises of 494 points representing the crowns of landslides occurred during the July 2018 disasters. These points were separated into training and test sets in a proportion of 30% and 70%, respectively.

Recent studies show that machine learning, specifically the random forest (RF) algorithm finds outstanding results in LSM production (Youssef & Pourghasemi, 2021, Yilmaz, 2009). In this study, the algorithm utilized was the one provided in the scikit-learn ML library. The predictions provided by the RF ML technique are converted to GIS form in landslide susceptibility index (LSI) values, classified into 5 LSI zones resulting in the final LSM.

3. RESULTS AND DISCUSSION

The LSM produced in this study with RF ML technique is exhibited in Figure 1, where blue pixels represent areas with lowest LSI (less susceptible to landslide) and red pixels represent highest LSI (more susceptible to landslide), along with the collection of landslides used for the map production, relative to the disaster event of July 2018. It is noticeable that actual landslide occurrences are mostly concentrated in areas of high LSI, particularly in the hills of Yoshidacho, north of the Hokezu Bay. Performance assessment of the resultant LSM was done with the area under the receiver operating characteristic (AUROC), a method that compares true positive rates and false positive rates, plotting those in a graph and producing a curve which represents better results with a larger area under it. The AUROC results in a score of 0.94, considered excellent in the production of LSMs. Additionally, landslide density was calculated for each of the 5 susceptibility zones, as shown in Figure 2. It is noticed that landslide density rises steadily with each LSI zone step, characterizing a favorable susceptibility assessment.

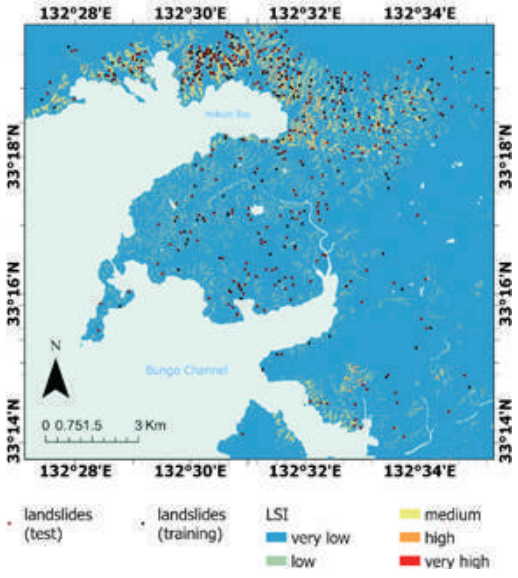

Figure 1: LSM produced with ML technique random forest, along with points representing the crowns of 494 landslides from the July 2018 disasters in Uwajima City, Ehime Prefecture, Japan.

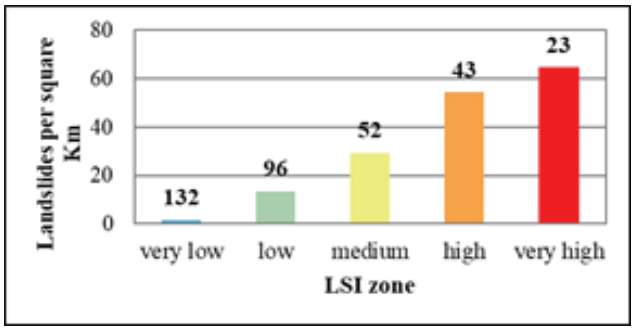

Figure 2: Distribution of landslide density per km2 in each of the 5 LSI zones. Numbers above bars indicate absolute number of landslides in zone. Steady rise of

landslide density accompanying the LSI zone increase indicates an accurate LSM.

4. CONCLUDING REMARKS

This study produced an LSM for Uwajima City, Japan, using the machine learning technique random forest. AUROC performance assessment resulted in a score of 0.94, which is considered excellent in landslide susceptibility assessments. It is judged that the use of machine learning techniques, as well as of XRAIN radar acquired rainfall data, is efficient for LSM production, resulting in efficient susceptibility assessments that may be used for landslide disaster prevention management. Recommended future studies include experiment similar assessment trials with machine learning techniques in other areas with different scales and distinct geological and topographical settings.

REFERENCES

Data Integration & Analysis System (2020). XRAIN Realtime Precipitation Data. The University of Tokyo, sponsored by the Ministry of Education, Culture, Sports, Science and Technology. Available at <https://diasjp.net/>. Access in June 2020.

Yilmaz, I. (2009). Landslide susceptibility mapping using frequency ratio, logistic regression, artificial neural networks and their comparison: A case study from Kat landslides (Tokat—Turkey). Computers & Geosciences, 35(6), 1125–1138.

Youssef A. H., Pourghasemi H.R. (2021) Landslide susceptibility mapping using machine learning algorithms and comparison of their performance at Abha Basin, Asir Region, Saudi Arabia, Geoscience Frontiers, V. 12, I. 2.

#Gen-19:

Physical modelling of debris flow – flexible barrier interaction: impact force reduction using novel brake elements

Sunil Poudyal[1], Charles W. W. Ng[1]

[1]Department of Civil & Environmental Engineering, The Hong Kong University of Science and Technology, HKSAR, China, spoudyal@connect.ust.hk

1. INTRODUCTION

Flexible barriers commonly installed on mountainous slopes to intercept rock falls have been impacted by debris flows in the past two decades, proving to be effective at arresting debris flows (Wendeler et al., 2006). For effective use of flexible barriers as structural countermeasures to arrest debris flows, there is clearly a need to understand flow barrier interaction in detail, especially the role of energy dissipating elements in reducing impact force.

Among different scientific approaches used by researchers in modelling debris flow impact on barriers, large-scale physical flume modelling provides well controlled initial and boundary conditions while alleviating scale effects that are prevalent in small-scale flume modelling.

In this study, using novel energy dissipating brake elements developed in-house at HKUST, reduction of peak impact force of debris flows on a flexible barrier is systematically investigated in a 2 m wide 28 m-long flume.

2. METHODOLOGY

Physical experiments are conducted in a 28-m long flume to elucidate the mechanisms of two-phase debris flow impacting a side anchored flexible barrier. A 2000 mm wide by 800 mm high ring net flexible barrier is installed in the flume which has a rectangular cross-section of 2 m width and 1 m depth (Figure 1) and an inclination of 20°. Debris material of 2.5 m3 is stored in the container at the top of the flume by using a mechanical double-leaf door system, which swings open in 0.5 s to mode a dam break flow.

The flume is equipped with basal instrumentation cells to measure basal normal stress, shear stress and pore pressure of debris flow. The flexible barrier equipped with novel brake elements is mounted on load cells along the flume side walls to measure impact force. Barrier deformation during impact is captured using high-speed cameras.

3. RESULTS AND DISCUSSION

The newly developed dual bilinear spring brake element exhibits a bilinear elastic load-displacement response (Figure 2). Each of the dual spring element comprises two compression springs—one stiff (k_1) and the other soft (k_2)—in series inside a cylinder. The springs are separated inside the cylinder by a coaxial separator. The flexible spring is preloaded to a user specifiable load (P_{pre}) by adding a spacer between the spring and separator inside the cylinder. Before the applied load reaches the inflection point (Ppre), only the stiff spring resists the load at a slope $K_1 = k_1$. After reaching the inflection point, the load is shared by both springs in series and the equivalent stiffness reduces to model the elongation of energy dissipating elements The peak deformation of dual spring elements is preserved by a pneumatic locking system.

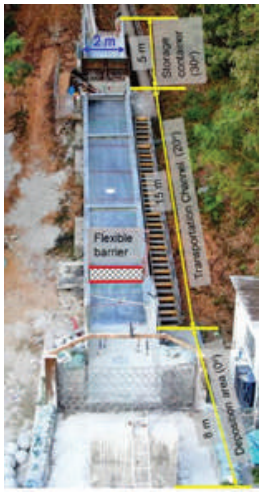

Figure 1. Twenty-eight-metre-long debris flow flume (Hong Kong).

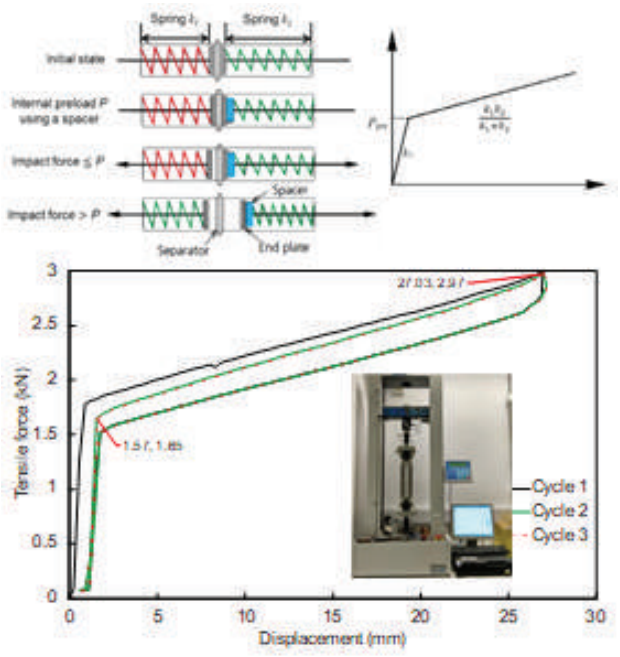

Figure 2. Novel dual bilinear spring brake element working principle (top) and repeatable uniaxial tension response.

Figure 3 shows the deflection of the load bearing cables and the barrier mesh resulting from different normal impact forces. The measured peak deflection of the cables and the barrier mesh are normalized by the barrier span (L) while the peak normal impact force is normalized by the hydrodynamic impact force (Kwan & Cheung 2012). The hydrodynamic impact force is defined as:

$$F_{dyn} = \alpha \rho v^2 h w \quad (1)$$

where α is the hydrodynamic pressure coefficient, ρ =2000 kg/m^3 is the bulk density of debris flow, v=6 m/s is the velocity of debris flow front impacting the barrier, h=0.06 m is the average flow depth of the debris flow and w=2.0 m is the flume width. Kwan & Cheung, (2012) proposes a hydrodynamic impact pressure coefficient of 2 for the design of flexible barriers subjected to debris flow impact, which is shown for comparison. The results of current study show that the measured normalized peak impact force (F/Fdyn) is 0.57, 0.64 and 1.10 for flexible barrier with two brakes per cable (square), one brake per cable (circle) and no brake elements (triangle) respectively. This discrepancy of more than 80% in the normalized peak impact force indicates there is large room for optimizing the design impact coefficient value for debris flow impact on flexible barriers without sizeable boulders.barriers without

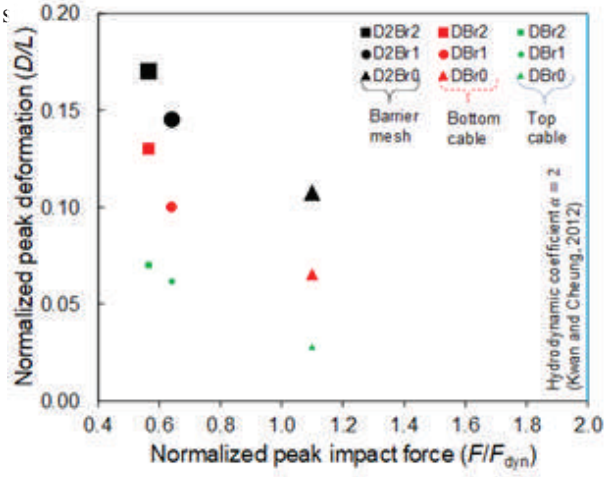

Figure 3. Normalized peak impact force and normalized peak deformation for different brake element configurations.

The size of the markers corresponds to the magnitude of the normalized deflection and impact force. The peak deflection of the bottom cable with two brake elements is 30% larger than that measured in test with only one brake element and 80% larger than in test without any brakes. The influence of larger barrier deflections is reflected in the decreasing trend of the normalized peak impact force. Use of two brake elements per cable reduces the peak normal impact force by 50% compared to the test with no brake elements in the cables. The deflection of the barrier increases the impact duration and allows increased internal shearing of the flow by promoting frictional dissipation (Ng et al., 2020).

4. CONCLUDING REMARKS

A series of physical experiments were conducted in modelling the impact of debris flow on a single flexible barrier anchored to the sides in a state-of-the-art 28 m-long flume. Novel dual bilinear energy dissipating brake elements developed in-house at HKUST are used to reduce the stiffness of supporting cables. A large deflection of the load bearing cables equipped with brake elemtns (D/L> 5%), results in the reduction of the peak impact force on the barrier by up to 50 %. The measured impact forces compared to design forces shows large room for improving the impact coefficient for more economical design.

ACKNOWLEDGEMENTS

The work described in this paper is supported by the grant AoE/E-603/18 provided by the Research Grants Council of HKSAR, China. S. Poudyal gratefully acknowledges the support of Hong Kong PhD Fellowship Scheme (HKPFS).

REFERENCES

Kwan J.S.H. and Cheung R.W.M. 2012. Suggestion on design approaches for flexible debris-resisting barriers. Discussion Note DN1/2012. The Government of Hong Kong Standards and Testing Division, Hong Kong, China.

Ng C.W.W., Wang C., Choi C.E., De Silva W.A.R.K. and Poudyal S. 2020. Effects of barrier deformability on load reduction and energy dissipation of granular flow impact. Comput. Geotech, 121, 103445.

Wendeler C., McArdell B.W., Rickenmann D., Volkwein A., Roth A. and Denk M. 2006. Field testing and numerical modeling of flexible debris flow barriers. In Proc of the 6th Intl. Conf. on Phys. Mod. in Geo., Hong Kong, 1573–1578.

#Gen-20:

Correlation of California Bearing Ratio with Dynamic Cone Penetration Index and Index Properties of Sub-Grade Soil Basantapur – Padam Road

[1]Bharat Bahadur Dhakal, [2]Bhim Kumar Dahal
[1]Affiliation (I.O.E., Pulchowk Campus, Lalitpur, Nepal)
[2]Affiliation (I.O.E., Pulchowk Campus, Lalitpur, Nepal)

1. INTRODUCTION

TPavement is the most important component of road infrastructure. A relatively stable layer constructed over the natural soil for the purpose of supporting and distributing the wheel load and providing an adequate surface for the movement of the vehicles may be defined as road pavement. Pavements have been divided into three broad categories: flexible, rigid, and composite pavements. In order to provide a stable and even surface for the traffic, the roadway is provided with a suitably designed and constructed pavement structure over a prepared subgrade soil (Kadiyali, 1997).

The subgrade is the native material or foundation beneath the pavement structure that eventually disperses the pavement load to the earth mass. It is also called the formation level. The Indian Road Congress (IRC:37, 2001) provides the exact procedures for the pavement layer design based upon the subgrade strength. It is a fact that weaker subgrade needs thicker layers whereas stronger sub-grade needs thinner pavement layers for the sub-grade without getting over stressed. In this context, research into subgrade materials for pavement design works is required to optimize the structural safety and economic aspects of road infrastructure. One of the activities during the site investigation is the determination of the subgrade material strength with different in-situ and laboratory tests, such as the Dynamic Cone Penetrometer Test (DCPT) and the California Bearing Ratio (CBR) test. CBR is a common and comprehensive test currently practiced in the design of pavement to assess the stiffness modulus and shear strength of subgrade material. This test involves sampling, transporting, preparing, compacting, soaking, and penetrating with a plunger of the CBR machine to measure the soil resistance. The type of soil is not the only parameter that affects the CBR value, but it also varies with different soil properties, such as related fines percent, liquid limit, and specific gravity, to determine the compaction characteristics possessed by the soil. There lies a linear correlation between the CBR soaked and un-soaked values also influenced by the nature of index properties. In road construction civil engineers always encounter difficulties in obtaining representative CBR as the laboratory CBR test requires a relatively large effort and is time-consuming.

In Nepal, most of the highway consists of flexible pavements, and there are numerous different techniques to design the flexible pavements (DoR, 2013). It recommends the appropriate design of flexible pavement based on design traffic in terms of the cumulative number of standard axles and CBR values of subgrade soil strength.

2. METHODOLOGY

This study attempted to analyze the correlation of CBR with DCPI and the index properties of subgrade soil.

Primarily in order to have satisfactory data for utilizing the correlations, laboratory tests were conducted. Samples were collected from different geographical locations in Nepal so as to get records of test results for CBR values along with the associated soil indices, particularly the grain size analysis, Atterberg limits, and moisture-density relationships. Then, discussions on sample collection and a summary of laboratory test results were presented. Statistical regression analyses of test results were carried out using SPSS software, and correlations were developed and also analyzed to fit the test results.

In this study, the targeted population was the different types of road segments in various regions of Nepal. The DCPT data from selected sections, Basatpur-Padam road section (length: 25 km), was collected for every 500 m. The DCPT data at the Basatpur – Padam road section was taken at an interval of 500 m since the soil was seen with the same property. The sample is collected according to the Standard Specification for Road and Bridge Works (DoR, 2013).

Basatpur - Padam Road section) during the excavation stage. The representative samples were chosen based on

the visual identification of a suitable subgrade soil, and thus diverse samples were obtained from various areas. For the study, 51 samples at an interval of 500 m were collected at the Basatpur- Padam road section (25 km). Samples of soil were collected from the same spot where DCPT was done.

3. RESULTS AND DISCUSSION

The use of DCP test and soil properties to predict the field CBR is preferred because it is simple and inexpensive and it enables rapid measurements of the in-situ strength of pavement layers and subgrades. Several correlations developed between the DCP penetration rates and CBR values are available in the literature.

Scatter plot for Sandy Clay with Gravel Mixed soil of Basatpur - Padam Road by Using Field CBR

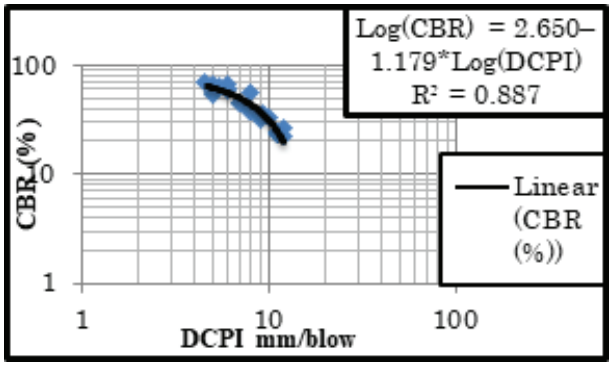

Scatter plot for Sandy Clay soil of Basatpur - Padam Road by Using Field CBR

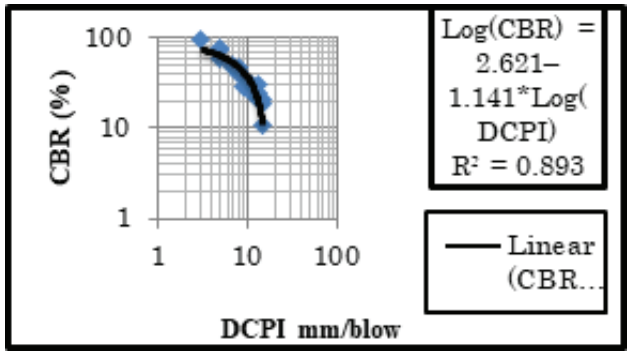

Multiple Linear Regression Analysis (for Sandy Clay and Gravel Mixed Soil of Basantapur-Padam Road, Bara District Road)

The resulting regression analysis after correlating CBR with, LL, MDD, DCPI, PL, OMC, and PI is expressed by the following multiple linear equations with its corresponding correlation coefficients:

a) CBR = 4.279 + 0.033*LL + 0.003*PL, with R2 = 0.117, Adj. R2 = -0.036, n = 25, α = 0.256

b) CBR = 4.303 – 0.034*LL – 0.009*PL + 0.032*PI, with R2 = 0.118, Adj. R2 = -0.008, n = 25, α = 0.405

c) CBR = 1.713 – 0.039*LL – 0.020*PL + 0.111*PI + 1.417*MDD, with R2 = 0.208, Adj. R2 = 0.050, n = 25, α = 0.299

d) CBR = 0.868 – 0.036*LL - 0.015*PL + 0.082*PI + 1.674*MDD + 0.025*OMC, with R2 = 0.217, Adj. R2 = 0.011, n = 25, α = 0.415

The details of the statistical out-put of this indicates that the relationship developed between CBR with LL, DCPI, OMC, PI, PL and MDD is significant (α<0.05). Besides, the R2 value of this is better than all the above stated models.

CONCLUDING REMARKS

The research was conducted to find a localized correlation between CBR value and soil index properties within the scope of the study. Accordingly, required laboratory tests were conducted on samples retrieved from different geographical area of Nepal. Using the obtained Fifty-one test results, a single and multiple linear regressions were analyzed and a relationship was developed that predict CBR value in terms of DCPI, LL, PL, PI, MDD and OMC. For the study 51 samples at an interval of 500 m were collected at Basatpur- Padam road section (25 km). Therefore, the total 51 number of samples were tested and analyzed. Sample soils were collected from same spot where DCPT was done.

The suitability of the developed correlation is validated by utilizing a separate control test results. From the results of this study the following single linear and multiple linear regressions relationship conclusions are drawn:

REFERENCES

AASHTO T217, 2007. Determination of Moisture in Soil by Means of Calcium, Neyyork: American Association Of State Highway And Transportation Officials.

AASTHO, 2001. Aashto standard specifications for transport materials, Neyyork: American Association Of State Highway And Transportation Officials.

Agarwal, K. &. G. K., 1970. Prediction of CBR from Plasticity Characteristics of Soil., Singapure: American Journal of Engineering Research (AJER).

ASTM D 698, 2012. Standard Test Methods for Laboratory Compaction Characteristics of Soil., Washington: West Conshohocken.

ASTM D2216, 2010. Laboratory Determination of Moisture Content of Soil. West Conshohocken: ASTM International(ASTM).

ASTM D4318-10e1, 2010. Standard Test Methods for Liquid Limit, Plastic Limit, and Plasticity Index of Soils, West Conshohocken, PA: ASTM International.

ASTM. D 1883 – 99, 2003. Laboratory CBR Testing, Annual Book of American Standards Testing Machine Standards, Volume 04. 08,. America: West Conshohocken, Pennsylvania.

#Gen-21:

Study of Behaviour of Composite Caisson-Pile Foundation (CCPF) based on experimental and numerical analysis

Rajan KC[1], Indra Prasad Acharya[1], Prishati Raychowdhury[2], Keshab Sharma[3]

[1]*Department of Civil Engineering, Pulchowk Campus, IoE, TU, Nepal*

[2]*Indian Institute of Technology Kanpur, Kanpur, India*

[3]*BGC Engineering Inc., Canada*

1. INTRODUCTION

Caisson foundations are commonly used in South Asian countries for constructing bridge piers and abutments. However, sinking challenges have led designers to abandon this foundation type (Abdrabbo and Gaaver, 2012). To address this issue, a composite caisson-pile foundation (CCPF) has been developed, which combines the benefits of both foundation types to enhance their strengths without introducing any weaknesses (Zhang et al., 2019). The CCPF has been used to build bridge foundations in Nepal and has proven effective in difficult site conditions, reducing construction time and costs. The CCPF has not been widely used due to a lack of research on its geotechnical and structural behavior (Zhong and Huang, 2014; Tu et al., 2020).

This study reviews pioneering research on CCPF systems, categorizing them by loading type (static, cyclic, and dynamic) and research methodology (experimental, analytical, and numerical) to provide a summary of prior research and the current state of the art. Physical model tests were conducted on instrumented sand-embedded CCPF under static vertical, monotonic lateral, and combined loading to examine load settlement, load improvement ratio (LIR), settlement reduction ratio (SRR), and load-sharing characteristics. A three-dimensional finite element model of CCPF was developed in PLAXIS 3D using experimental data to analyze the impact of significant factors influencing the performance of this foundation during loading.

The study investigates the impact of pile configuration, pile diameter, pile length, pile size, and caisson depth on the performance of CCPF embedded in sand and subjected to various loads. The findings of this study may be used as a guide for achieving cost-effective construction of composite caisson-pile foundations and will likely inspire additional research in this area. It will pave the way for more effective and general design and construction strategies to maximize the CCPF's potential.

2. METHODOLOGY

The framework of the study is shown in Fig. 1. The loading tests of reduced scale CCPF model was conducted in structural laboratory of the Indian Institute of Technology (IIT), Kanpur, India. The setup and arrangement is as shown in Fig. 2. Instrumentation was done as shown in the figure. After analysing the experimental data, a three dimensional modelling was done in PLAXIS 3D. The model was validated with the experimental results and parametric analysis done with the validated model.

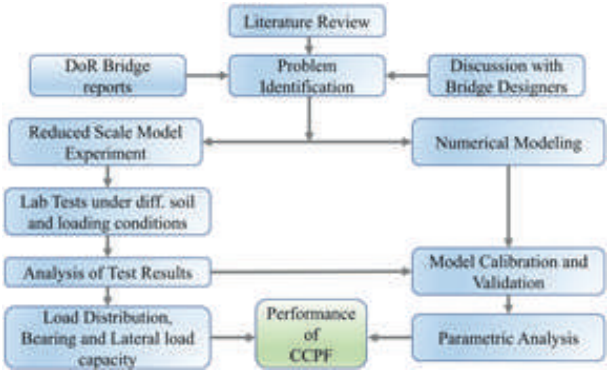

Figure 1: Methodological flowchart of the study

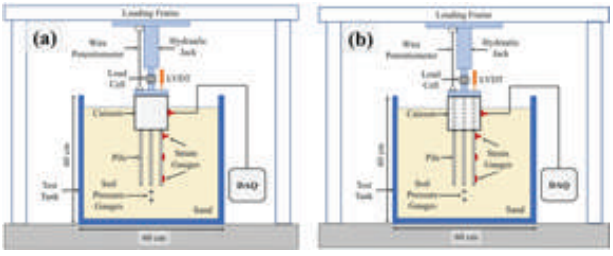

Figure 2: Schematic diagram showing the experimental setup for Vertical Load Testing of (a) CCPF with piles upto bottom (b) CCPF with piles upto top of caisson

3. RESULTS AND DISCUSSION

3.1 Effect of Caisson Length

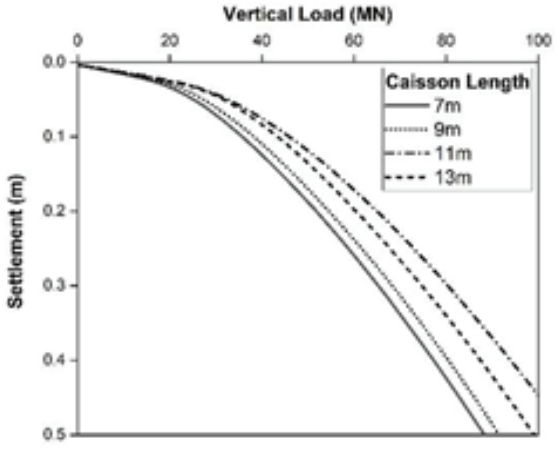

Figure 3: Load-settlement response of CCPF for various pile lengths

The series of analyses involved studying a 2 x 2 piled caisson (CCPF) with varying caisson depths of 7m, 9m, 11m, and 13m. The load-settlement curves for each case are shown in Fig. 3.

3.2 Effect of Friction Angle

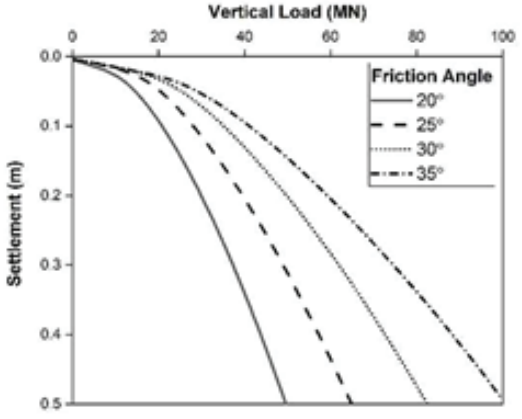

Figure 4: Load-settlement response of CCPF for various pile lengths

A series of experiments were carried out on CCPF foundations using soil samples with internal friction angles (ϕ) ranging from 20° to 35°, while keeping the remaining parameters and geometry unchanged from the previous section. The results of this series are presented in Fig. 4 in the form of load-settlement curves for varying internal friction angles. It was observed that as the internal friction angle increased from 20° to 35°, there was a significant reduction in settlement.

3.1 Effect of Pile Length

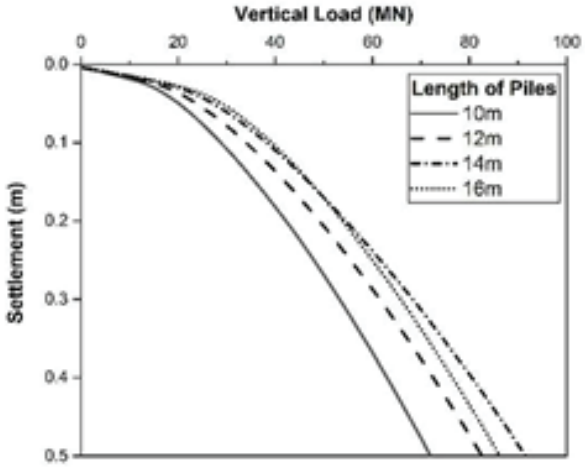

Figure 5: Load-settlement response of CCPF for various pile lengths

To evaluate the impact of pile length on the performance of CCPF, the study investigated four different pile lengths (10m, 12m, 14m, and 16m). The load-settlement response of CCPF for each pile length is shown in Fig. 5. It was observed that the settlement decreased considerably as the pile length increased from 10m to 14m. However, after reaching 14m, the settlement for the 16m long piles increased again.

4. CONCLUSIONS

The experimental and numerical study on CCPF yielded the following conclusions: Increasing the pile length from 10m to 16m for a 30 MN load led to a significant reduction in settlement of approximately 48%. However, the settlement for 16m long piles was higher than for shorter piles (>60 MN) after reaching an optimal length of 14m. The load-carrying capacity of CCPF increases with the length of the pile or caisson at any settlement level, but extending beyond the optimal length does not affect its capacity. Increasing the angle of shearing resistance from 20 to 35° for an ultimate load of 30 MN resulted in a rapid decrease in settlement by approximately 70%. Moreover, lower settlement levels (0.1 m) exhibited a greater improvement in CCPF capacity than higher settlement levels (0.5 m) in all analyses.

Despite the clear evidence of satisfactory CCPF performance under different loading and soil conditions, there is currently no standard or code available for designing CCPF for bridges. Therefore, it is necessary to establish a comprehensive set of design methods to promote the use of CCPF as an innovative foundation for deep water bridges built on dense alluvial deposits.

REFERENCES

Abdrabbo, F., & Gaaver, K. (2012). Challenges and Uncertainties Relating to Open Caissons. DFI Journal - The Journal of the Deep Foundations Institute, 6(1), 21–32. https://doi.org/10.1179/dfi.2012.002

Tu, W., Huang, M., Gu, X., & Chen, H. P. (2020). Nonlinear dynamic behavior of laterally loaded composite caisson-piles foundation under scour conditions. Marine Georesources and Geotechnology, 38(10), 1265–1280. https://doi.org/10.1080/1064119X.2020.1724217

Zhang, C., Zhang, X., Huang, M., & Tang, H. (2019). Responses of caisson-piles foundations to long-term cyclic lateral load and scouring. Soil Dynamics and Earthquake Engineering, 119(January), 62–74. https://doi.org/10.1016/j.soildyn.2018.12.026

Zhong, R., & Huang, M. (2014a). Winkler model for dynamic response of composite caisson-piles foundations: Seismic response. Soil Dynamics and Earthquake Engineering, 66, 241–251. https://doi.org/10.1016/j.soildyn.2014.07.005

#Gen-22:

Why can't we use dry granular flow model to design spacing between barriers in mitigating debris flows?

Aastha Bhatta[1], Charles Wang Wai Ng[1]

[1]The Hong Kong University of Science and Technology, Hong Kong SAR, China

1. INTRODUCTION

Debris flow is a natural disaster which is either landslide induced, or rainfall induced and is a frequently occurring geohazard in Nepal. Multiple barriers, compared to a single rigid barrier at the end of a catchment, are one of the viable options that prevents debris flow at the early stage of development. These multiple barriers are often designed based on the kinematics observed from the dry granular flows. This study aims to highlight need of considering two-phase, i.e., fluid and granular mass, behaviour of the debris flows during multiple barrier design.

2. METHODOLOGY

Existing design method of dual rigid barrier which are based on dry granular flows (Koo et al., 2017, Kwan et al., 2015) and two-phase flows (Ng et al., 2022) are reviewed. A flume with 2.7 m flow length is used for the study (Figure 1). Results from four tests of two-phase flows are used to compare the prediction of barrier spacing from dry granular flow model and two-phase flow model. Water, Kaolin Clay and Toyoura Sand are used as debris material, with varying concentration of water and clay, keeping sand concentration constant. The water content ranges between 50 to 60% by volume of the debris for all the tested flows. Dam break flow is modelled by opening the gate while the overflow dynamics at the first barrier is studied.

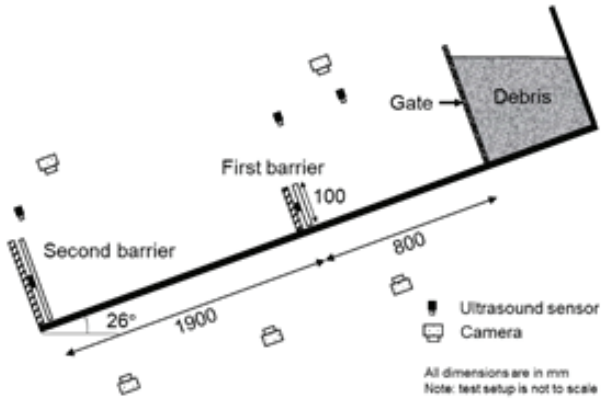

Figure 1: Schematic of model setup with instrumentation.

3. RESULTS AND DISCUSSION

Figure 2 shows the comparison of calculated overflow distance with the measured overflow distance. The overflow distance for all data points is normalised by first barrier height. Two methods are used to calculate overflow distance, details of which are provided in Ng et al (2022). A line of equality is plotted to represent the condition where calculated overflow distance exactly matches the measured overflow distance. Data points plotted below this line (light red shading) represent underprediction of overflow distance by the calculation method used in current design guidelines. Similarly, data points plotted above this line (light green shading) shows overflow distance is conservatively predicted by the calculation method.

Figure 2 shows that the overflow distance increases with increase in water content of the two-phase debris. It can be observed that all the data points calculated using the dry

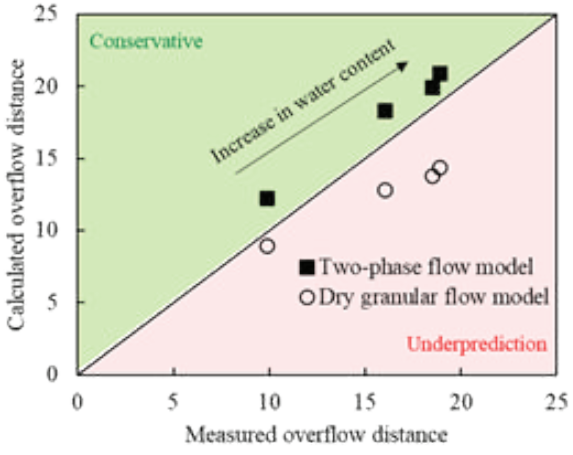

Figure 2: Comparison of calculated overflow distance with measured overflow distance.

granular flow model (circle) fall below the line of equality and always underpredicts the overflow distance. Furthermore, this underprediction increases with increase in water content of debris. On the contrary, all the data points calculated using two-phase flow model (square) lie above the line of equality. This is because dry granular flow model is unable to capture increase in overflow distance due to launch angle and reduced energy loss during shearing of two-phase flow (Ng et al., 2022).

4. CONCLUDING REMARKS

This study shows that the spacing between debris resisting barriers based on overflow distance using the dry granular flow model is not suitable for two-phase flows. For cases where flow impacts the barrier piles up behind the barrier into a static deposit, dry granular flow model can be used to estimate the minimum spacing between barriers. However, for two-phase flows, where flow runs up after impact, barrier spacing should be designed using the two-phase flow model.

ACKNOWLEDGEMENT

The work described in this paper was supported by a grant from the Research Grants Council of the Hong Kong Special Administrative Region, China (AoE/E-603/18). A. Bhatta acknowledges support from the Hong Kong PhD Fellowship scheme provided by the RGC of HKSAR, China.

REFERENCES

Koo, R. C. H., Kwan, J. S. H., Ng, C. W. W., Lam, C., Choi, C. E., Song, D., & Pun, W. K. (2017). Velocity attenuation of debris flows and a new momentum-based load model for rigid barriers. Landslides, 14, 617-629.

Kwan, J. S. H., Koo, R. C. H., & Ng, C. W. W. (2015). Landslide mobility analysis for design of multiple debris-resisting barriers. Canadian Geotechnical Journal, 52(9), 1345-1359.

Ng, C. W. W., Bhatta, A., Choi, C. E., Poudyal, S., Liu, H., Cheung, R. W. M., & Kwan, J. S. H. (2022). Effects of debris flow rheology on overflow and impact dynamics against dual-rigid barriers. Géotechnique, 1-14.

#Gen-23:

Geo-Hazard; its causes and recommendation Case study of Karnali Province

Bal Deep Sharma[1], Sushil Shrestha[2], Pawan Babu Bastola[3] Harish Paneru[4]
[1,2,3,4] *Affiliation (National Disaster Risk Reduction and Management Authority)*

1. INTRODUCTION

Monsoon precipitation is dominant in the Asia and Pacific region which is a major cause of the flood. The precipitation pattern over time and space is not uniform and it has been changing. Natural disasters kill on average forty-five thousand people per year, globally [1]. where nearly half of the top events occurred on the Asian continent and many of them were caused by significant inundation and landslides in India, China, Nepal, Sri Lanka, and Bangladesh.

Due to continuous rainfall in the upper part of Karnali Province in the month of October 2022, extensive damage has occurred to the infrastructures and buildings. After the disaster, detailed damage and loss assessment has been done in the government- declared disaster-hit four districts Humla, Jumla, Kalikot, and Mugu. The landslide and flood due to the rainfall have claimed the life of around 50 people leaving thousand to search for shelter as their permanent residence has become inhabitable.

2. METHODOLOGY

Initially, a desk study has been done to determine the essential parameters to be collected from the field. District Disaster Management Committee meeting has been conducted in every district and the required data has been collected from the local governments. It is followed by the walk-over survey to the disaster-hit site for the verification of the data and for the site assessment.

Based on the collected data and assessment, data analysis has been done to determine detailed sectoral damage, the extent of damage, and economic loss due to the disaster. Finally, the main causes of widespread damage have been evaluated and possible disaster mitigation methodologies have been recommended.

3. RESULTS AND DISCUSSION

The field visit was conducted within different places in four districts. The type of disaster and its causes are similar for the most area of the district. The main reason for the wide range of damage in infrastructure and houses is due to the unexpected continuous rainfall as shown in Figure 3. These rainfall events have caused runoff, and increased flow in the local rivers and stream which in turn affected settlements and infrastructures near those streams.

In addition to that, the toe cutting by the river of already saturated hill slope and erosion caused by the unmanaged runoff water flowing along the slope has worsened their odds of landslide susceptibility let alone in some cases have already failed to take all the structures such as water supply lines, local road,

transmission pole, farmlands and houses with it thereby, impairing the services within the vast region of these districts.

Table 1 Total sectoral damage by district

Description	Humla	Jumla	Kalikot	Mugu	Total
Death	8	11	8	8	**35**
Injury	6	4	25	5	**40**
Missing	0	1	15	0	**16**
Private house complete damage	687	1117	1595	885	**4284**
Private house partial damage	316	2277	523	799	**3915**
School	27	90	140	34	**291**
Health Post/Hospital	5	6	10	0	**21**
Public/Government Building	7	34	35	9	**85**
Road/Walking trail (km)	54	202	101	119	**476**
Bridges, Suspension bridges and Crossings	13	211	42	12	**278**
Micro Hydropower & supply line	8	34	11	12	**65**
Water supply system	21	153	274	121	**569**
Irrigation	0	101	252	99	**351**
Religious structure	1	54	49	30	**134**

Table 2 Total estimated loss (in lakh)

Particulars	Districts				Loss NPR.lakh
	Humla	Kalikot	Jumla	Mugu	
Housing and Settlement	4226	4830	9410	4090	**2,25,55**
School	614	1697	1118	1000	**44,29**
Hospital / Health-post	185	206	25	0	**4,16**
Road and walking trail	1175	2818	2195	1499	**76,87**
Bridge	383	883	1241	957	**34,63**
Temple	10	232	89	108	**4,39**
Water supply/ Sewerage	421	1923	958	633	**39,36**
Irrigation	0	3610	1092	3177	**78,79**
Hydropower	310	531	1094	727	**26,62**
Water Mill	0	0	208	365	**57,3**
Public / Government Building	250	355	532	289	**14,26**
Agricultural / Farm Land	49	0	4076	0	**41,26**
River Training works & Slope protection	0	3979	523	93	**45,95**
Grand Total (NPR.)	**76,23**	**2,10,64**	**2,25,60**	**1,29,37**	**6,41,84**

The extent of damage to human life may be minimal owing to the fact that the extent of the disaster is relatively high but these slopes are going to fail in future if the agricultural practices along these lands are continued and surface and sub-surface water management are taken lightly.

Figure 1: Infrastructure damaged due to disaster

Figure 2: Settlement vulnerable to disaster

One of the most lacking things that has been found is the poor management of water in steep residual slopes which has led to erosion and debris flow at multiple locations. These kinds of situations can be dealt through the provision of catch drains to divert water from problematic slopes and disposal of the collected water at a site with proper provision for energy dissipation of flowing water and check dams to reduce debris flow.

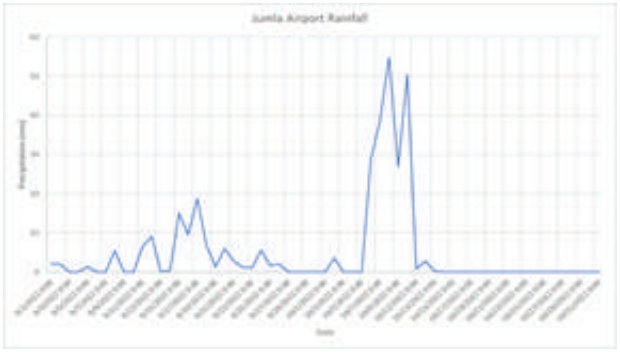

Figure 3: Precipitation in the month of September and October Jumla Airport (Source: DHM 2022)

It has been found that the number of bridges have been constructed within the flood plain without adequate hydrological study. Our building construction technology is also being serious threat during these

disasters. Residential buildings are constructed along the steep slope without proper channelization of runoff which results in the entire village being shifted to a temporary settlement as seen in Figure 4.

Figure 5: Temporary Settlement after disaster hit Moreover, massive deforestation and improper cultivation is triggering disasters. Infrastructure damage as per different sectors is presented in Figure 5.

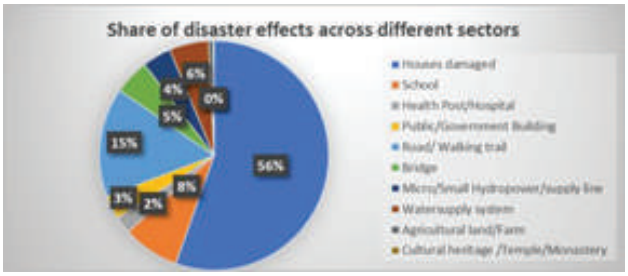

Figure 5: Infrastructure damaged due to disaster

4. CONCLUDING REMARKS

After the assessment, it has been concluded that our infrastructures are not resilient to disaster primarily to floods and landslides in this case.

The main causes for widespread damages are concluded as below:

1. Prolonged rainfall
2. Poor management of drainage for surface and sub-surface water along the hill slope
3. Poor agricultural practices
4. Encroachment of the bank of the river
5. Un-engineered road cutting

ACKNOWLEDGEMENT

The authors extend sincere thanks and appreciation to the National Disaster Risk Reduction and Management Authority for their support.

REFERENCES

Hannah R, Pablo R and Max R, 2022, Natural Disaster, Our World in Data

#Gen-24:

Numerical Study on the Performance of Shallow Foundation on Liquefiable Soil During an Earthquake

Abinash Aryal[1], Santosh Kumar Yadav[2], Pawan Babu Bastola[3]

[1]Department of Roads, Government of Nepal

[2]Department of Civil Engineering, Pulchowk Campus, IOE, TU, Nepal

[3]National Disaster Risk Reduction and Management Authority

1. INTRODUCTION

The phenomenon of saturated and cohesion-less soil losing all or part of its shear strength due to increased pore water pressure and a resulting reduction in effective stress is known as liquefaction. Mogami and Kubo created the phrase in 1953, and it has since been applied to a number of phenomena involving soil deformation produced by monotonic, temporary, or recurrent disturbance of cohesion-less soil in an undrained state. When granular material is subjected to cyclic shear deformation, the tendency for it to compact causes increased pore water pressure. The change of state is most common in loose to moderately dense granular soils with poor drainages, such as silty sands or sands and gravel covered by or containing impermeable sediment seams. Our repeated experience with earthquake-induced liquefaction has demonstrated the danger liquefaction presents to structures. During a sequence of 1964 earthquakes in Niigata, Japan (Ms=7.5) and Prince William Sound, Alaska (Mw=9.2), it piqued the curiosity of geotechnical engineers and researchers all over the world for the first time. It caused massive structural damage, including dramatic bearing failure beneath buildings, floating of buried buoyant structures, and bridge collapses, including the Showa Bridge in Niigata. This research is focused on studying the settlement induced in the shallow foundation due to liquefaction using the FEM approach. Different parameters of building structure (storey height, foundation width, bearing pressure) are varied to study their effect on liquefaction-induced settlement.

2. METHODOLOGY

Two dimensional (2D) plain strain geometrical assumption is used because of limitations of time, resources, and computation, capabilities. The finite element model consists of a structure of height H and width B, resting on the ground surface with soil domain of width and depth of 20m. The structure is modelled as block of concrete resting on soil at the ground surface level for the simplification of model and ease of analysis. The ground consisted of three layer, viz. upper non-liquefiable layer (HC), liquefiable layer (HL), and non-liquefiable base (HB).

The soil elements were modelled using SSPquadUP elements which enables faster computation by reducing the number of Gaussian points from 4 to 1. This is a four nodded 2-D element and has three DOF in each node, i.e., 2 for displacements and 1 for pore water pressure. The boundary condition consisted of compliant base, reciprocal side boundaries and dry surface.

The analysis was performed in three consecutive stages: gravity loading, dynamic excitation, and dissipation phase. Gravity analysis of the model was performed with large time steps and high permeability for faster convergence of analysis. During dynamic excitation phase, new analysis parameters were defined by removing the analysis object used for gravity analysis and dynamic analysis was executed. Ground motion signal was applied at the base in form of shear stress time history by transforming velocity time history. During this stage, excess pore water pressure is generated at soil elements along with liquefaction-induced shear and volumetric deformation of soil elements during the strong ground motion. The water and thickness of liquefiable layer was varied during the parametric study. Calibrated model constants for Ottawa Sand were used as per the recommendation of Najma et.al. The numerical parametric study in this thesis used the material parameters listed in the table.

3. RESULTS AND DISCUSSION

It can be observed from figure 1 that liquefaction induced settlement in free field occurs primarily during post liquefaction consolidation phase whereas settlement of structure occurs during the strong motion. Furthermore,

the rate of settlement decreases substantially after strong ground motion peaks have passed. Similar observations have been reported by Hausler during centrifuge experiments.

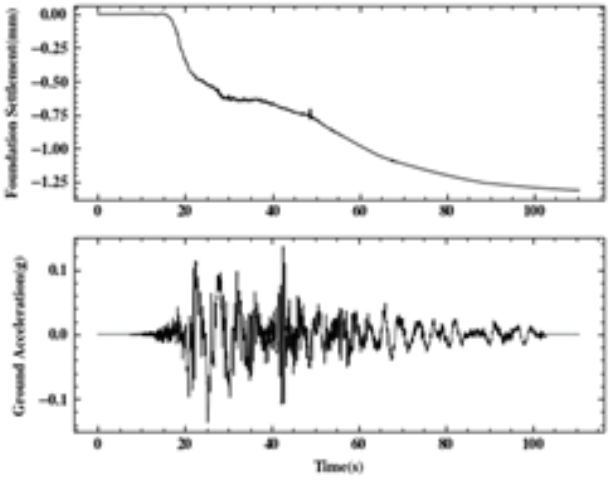

Figure 1 Numerical prediction of settlement of typical foundation due to liquefaction plotted with reference to acceleration time history.

The PGA was reached between 20 and 40 second, which coincides with the time at which peak excess pore water pressure (EPWP) was achieved, as seen in Figure 2. Due to higher confinement pressure beneath a structure, stress reversal under given earthquake loading is reduced and this suppresses generation of excess pore water pressure. This was also reported by (Dashti et al., 2009) during numerical simulation.

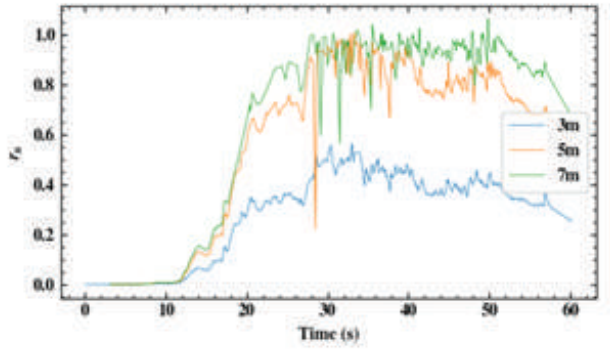

Figure 2 Comparison of excess pore water pressure with depth for free field condition.

Magnitude of settlement of structure was found to decrease with increase in foundation width at given intensity of ground shaking.

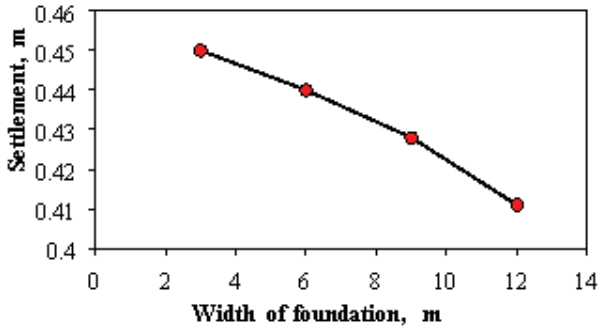

Figure 3 Effect of width of foundation on settlement of structure due to liquefaction.

Simulation was run on a baseline model with bearing pressure varying from 50 to 200 kPa. As seen in the figure 4, settlement of structure increases with increase in contact pressure. However, rate of increase in settlement decreases with increase in bearing pressure and asymptotic relation can be inferred for higher bearing pressure values.

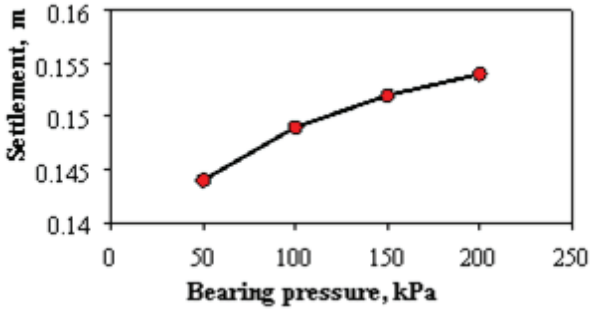

Figure 4 Effect of bearing pressure on settlement of structure due to liquefaction.

With change in height, structure's dynamic response to ground motion alters and therefore the inertial soil-structure interaction differs. This causes change in shear induced ratcheting effects which will ultimately change its settlement during liquefaction. Numerical simulations of structures were run with structure height varying from 3 to 9m. Figure 10. shows the variation of liquefaction induced settlement of structure with change in its height.

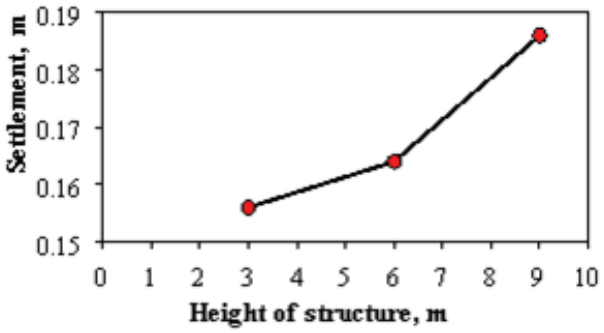

Figure 10. Effect of height of structure on settlement of structure due to liquefaction. (Constant Q=50Kpa)

4. CONCLUDING REMARKS

The initiation, rate, and amount of liquefaction induced building settlement depends greatly on the shaking intensity rate of the ground motion. Numerical simulations with the Manzari-Dafalias model implemented in OpenSees were used to estimate building settlements.

Rate of settlement is found to be governed by the acceleration time history of ground motion with maximum settlement occurring during the peak acceleration period. Shear induced displacement governs the final settlement which implies that the empirical methods developed for evaluation of settlement in the free field cases cannot be relied upon.

EPWP fluctuates around its maximum value as the ground acceleration reaches to its peak and rapidly reduces after the end of ground motion.

Although it was found that the magnitude of settlement decreases with the increase in foundation width, the maximum reduction in settlement was only about 19 percent, indicating that the change in foundation width does not significantly affect the liquefaction-induced settlement. Therefore, in case of liquefaction-induced settlement, the general notion that an increase in the foundation width lowers the settlement cannot be accepted.

REFERENCES

M. Srbulov, "Geotechnical earthquake engineering: Simplified analyses with case studies and examples. (Vol. 9).," In Springer Science & Business Media, vol. Vol 9. Springer Science & Business Media., 2008.

K. &. S. H. Tokimatsu, "Evaluation of settlements in sands due to earthquake shaking.," Journal of Geotechnical Engineering, vol. 113(8), p. 861–878., 1987.

Y. D. M.T.Manzari, "A critical state two-surface plasticity model for sands," Geotechnique, vol. 47, no. 2, pp. 255-272, 1997.

#Gen-25:

Unified Framework for Slope Stability Prediction using Machine Learning Algorithm and Multiple Linear Regression

Milan Aryal[12], Indra Prasad Acharya[2], Rajan KC[23]
1DUDBC, GoN, Nepal
[2]Pulchowk Campus, IoE, TU, Nepal
[3]Geo-Infra Research Institute, Nepal

1. INTRODUCTION

The safety of various engineering projects such as roads, railways, dams, and retaining walls greatly depends on the stability of the slope, which is influenced by multiple factors. With increased development activities, predicting slope stability has become a major task for geotechnical engineers to ensure cost-effective and reliable slope design. Accurately estimating slope stability is challenging and requires the assessment of various geotechnical, hydrological, and physical parameters in a short time to prevent disastrous effects. While experimental and numerical methods have been used to assess slope stability, they have limitations such as difficulties in assessing physical properties and high costs. Machine learning algorithms, such as artificial neural networks, have been effectively used to predict slope stability in recent years.

Utilizing machine learning techniques and improving dataset collection can effectively address slope stability issues. However, despite past studies using various machine learning algorithms to predict slope stability on smaller datasets, there is still a lack of comprehensive investigation using the most cutting-edge ML methods. While some research has been conducted in this field, there are still issues to be considered, such as the limited number of data sets used in developing ML models and the absence of a detailed comparison of advanced algorithms on larger training and testing datasets to identify the best model for slope problems.

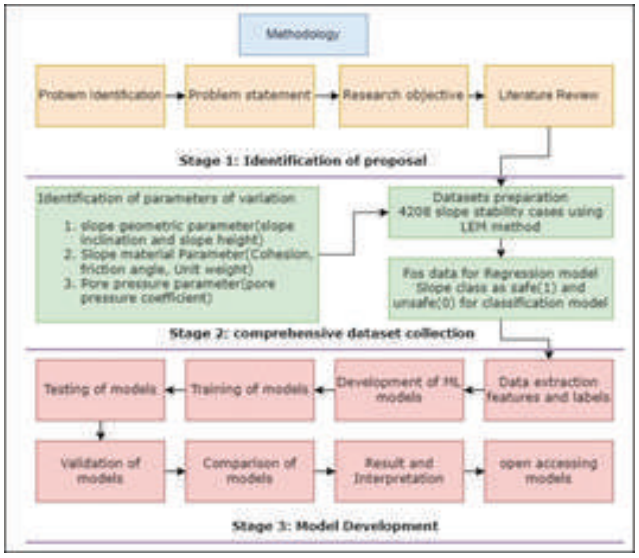

Figure 1: Methodological flowchart of the study.

2. METHODOLOGY

In this study, nine machine learning-based approaches are employed, including regression and classification algorithms. The supervised classification techniques utilized are multiple linear regression and artificial neural networks, while the seven classification algorithms include support vector machine, decision tree, random forest, Naïve Bayes, logistic regression, and two types of artificial neural network classifiers. All these models are constructed, and their predictability is compared and assessed to determine their appropriateness for predicting slope stability.

3. RESULTS AND DISCUSSION

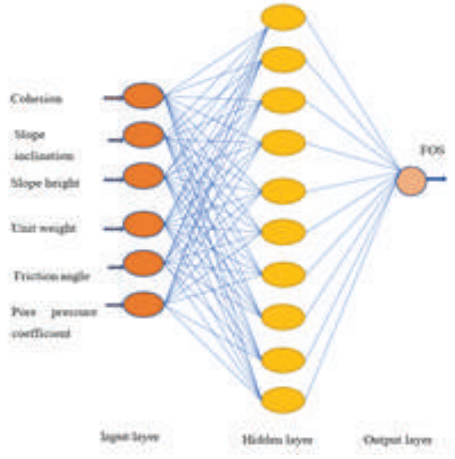

Figure 2: Neural Network Architecture for prediction of FOS in slope stability analysis

The analysis using multiple linear regression revealed that the regression line for each method fits well, with coefficient of determination values of 0.942, 0.948, 0.946, 0.925, and 0.924 for Morgenstern-Price, Bishop, Janbu, Fellenius, and Spencer methods, respectively.

The accuracy of all seven machine learning classification models for both testing and training datasets is over 90%, indicating their effectiveness in predicting slope stability.

4. CONCLUDING REMARKS

In conclusion, the study found that both ANN and MLR can be effective tools for predicting the stability of slopes. The FOS values generated by these models were in close agreement with those obtained from limit equilibrium methods. The best performing ANN model had two hidden layers with 20 and 1 neuron in each, and the ANN regression model developed for the Spencer method had the highest accuracy for both training and testing datasets. Overall, the ANN models outperformed the MLR models in all cases, indicating that machine learning techniques can provide a reliable alternative for slope stability prediction.

The model accurately classifies slope stability based on FOS and provides a quick assessment of slope class. Machine learning offers a reliable alternative for slope stability prediction, even with incomplete input data. The study's results are publicly available as a free and timely tool for slope analysis decision-making.

REFERENCES

Bui, D. T., Moayedi, H., Gör, M., Jaafari, A., & Foong, L. K. (2019). Predicting slope stability failure through machine learning paradigms. ISPRS International Journal of Geo-Information, 8(9). https://doi.org/10.3390/ijgi8090395

Choobbasti, A. J., Farrokhzad, F., & Barari, A. (2009). Prediction of slope stability using artificial neural network (Case study: Noabad, mazandaran, iran). Arabian Journal of Geosciences, 2(4), 311–319. https://doi.org/10.1007/s12517-009-0035-3

Gelisli, K., Kaya, T., & Babacan, A. E. (2015). Assessing the factor of safety using an artificial neural network: case studies on landslides in Giresun, Turkey. Environmental Earth Sciences, 73(12), 8639–8646. https://doi.org/10.1007/s12665-015-4027-1

#Gen-26:

Effect of Curing Period on Unconfined Compressive Strength of Cement Treated Soil.

Ujjwal Niraula1, Bhim Kumar Dahal[2]
[1]Everest Engineering College, Lalitpur, Nepal)
[2]Institute of Engineering- Pulchowk Campus, Lalitpur, Nepal

1. INTRODUCTION

This paper reports on a behavioral study that examines the strength improvement in weak soil over a prolonged curing-period resulting from cement application. Moisture in the subgrade for a long time has affected strength in cement stabilized roads, making this study promising for geotechnical and highway engineering. The pozzolanic reactions due to cement hydration significantly enhance soil properties over time, taking from days up to five years for completion. The cementation of weak soil after the pozzolanic reaction has significant enhancements in the peak and residual strengths (Zhang et al., 2014; Dahal et al., 2019). So, it is important to study the strength behavior of the cement-treated soil with respect to the curing time.

2. METHODOLOGY

Disturbed soil sample from Kopundol, Kathmandu was collected, dried, powdered, and mixed with cement in variations of 2%, 4%, 6%, 8% and 10%. Using the optimum moisture content and maximum dry density from the compaction test (following IS2720-Part 8), the UCS sample was prepared by the Harvard Miniature Apparatus. Then it was stored and tested (following IS2720-Part10) after 28, 60 and 90 days of curing. All the tests were performed at the Central Material Testing Laboratory, Institute of Engineering, which had well calibrated machines and apparatus. The calculations and correlations for the test results were obtained by using Microsoft Excel. All the results are justified either with the published research outcome or scientific theories.

3. RESULTS AND DISCUSSION

The trend (in Figure 2) for the results obtained from the UCS test for different cemented soils shows gains in strength values with the increase in the amount of cement. As cement in its raw state contains calcium, silica, alumina, and iron, the hydration of cement while mixing with weak soil consisting of silica and alumina produces gels of calcium silicate hydrate (CSH) and calcium aluminate hydrate (CAH). The gel coats weak soil particles, resulting in an interlocking structure upon crystallization and significantly enhancing the strength of soil (Sargent, 2015).

Data from Figure 2 shows that the UCS values increase with the curing period. The results in Figure 2.a depict that the increase in curing period from 28 days to 90 days leads

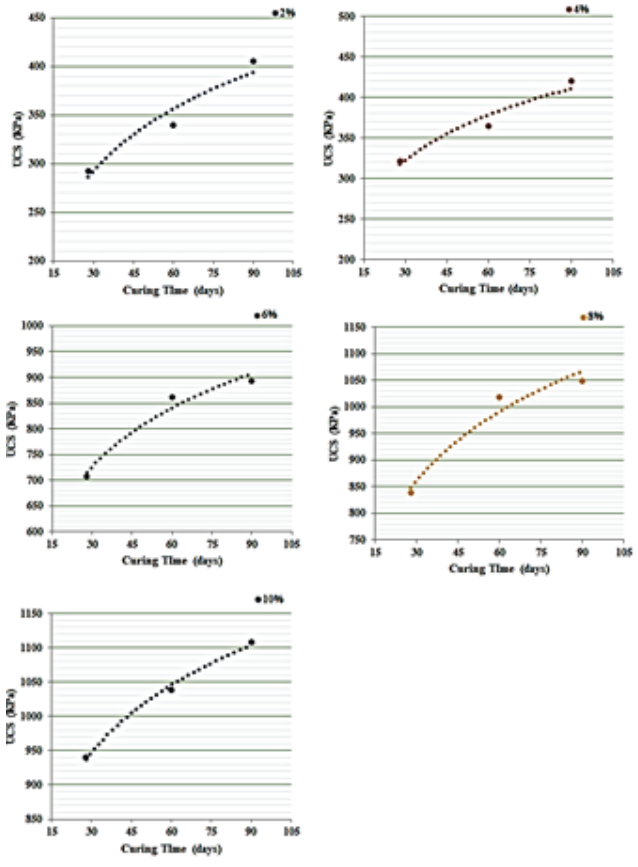

Figure 2: Curve of UCS vs. Curing Time for varying cement percentages.

to a strength gain from 290 kPa to 410 kPa, while increasing the cement by 4% (Figure 2.b) leads to a strength gain from 320 kPa to 430 kPa. Likewise, increasing the cement content by 6%, 8% and 10% (Figure 2.c, 2.d and 2.e) resulted in strength improvement from 700 kPa to 890 kPa, 840 kPa to 1050 kPa, and 940 kPa to 1110 kPa, respectively, for the same increase in curing period. It is suggested that both cement and the curing period have a significant impact on the unconfined compressive strength of the cement-stabilized soil.

4. CONCLUDING REMARKS

In conclusion, the study finds a decisive role of curing period and cement content in the unconfined compressive strength behavior of cement treated soil. The results show that a prolonged curing period from 28 days to 90 days leads to a significant gain in the strength of the soil. These findings can be used to determine the optimum strength of cement treated soil for construction applications by adjusting the curing period. However, as an improvement to the study, it is important to study more test data for better validation before selecting the optimum combination of cement and curing period for a specific application. Overall, the findings of this study provide a clear picture of the behavior of soil-cement mixes, which is essential to effective construction practices.

REFERENCES

Zhang, R. J., Lu, Y. T., Tan, T. S., Phoon, K. K., & Santoso, A. M. (2014). Long-term effect of curing temperature on the strength behavior of cement-stabilized clay. Journal of Geotechnical and Geoenvironmental Engineering, 140(8). https://doi.org/10.1061/(ASCE)GT.1943-5606.0001144

Dahal, B. K., Zheng, J. J., Zhang, R. J., & Song, D. B. (2019). Enhancing the mechanical properties of marine clay using cement solidification. Marine Georesources and Geotechnology, 37(6), 755–764. https://doi.org/10.1080/1064119X.2018.1484532

Sargent, P. (2015). The development of alkali-activated mixtures for soil stabilisation. In Handbook of Alkali-Activated Cements, Mortars and Concretes. Woodhead Publishing Limited. https://doi.org/10.1533/9781782422884.4.555

#Gen-28:

Evaluating the Performance of a Composite Well-Pile Foundation for a Bridge in Nepal: A Case Study

Jibendra Misra[1], Netra Prakash Bhandary[1]
[1]Ehime University, Matsuyama, 790-8577, Japan

1. INTRODUCTION

The Department of Roads in Nepal is currently constructing approximately 1600 bridges in both the strategic and local road networks under different budget heads. Additionally, they design around 400 new bridges every year. Nepal's dynamic geology is a result of ongoing lithospheric plate tectonics that began around 55 million years ago when the Indian plate collided with the Eurasian plate, forming the high Himalayas (Dhakal, 2014). The unique geology of Nepal leads to frequent variations in geotechnical parameters over short distances. The government is investing a significant portion of the infrastructure sector's capital budget in the transportation sector, particularly in road transport. However, due to insufficient geotechnical investigation, some bridge projects may encounter foundation construction difficulties and prolong the project period.

2. METHODOLOGY

It is crucial to calculate the allowable bearing pressure and perform lateral stability analysis under static load combinations for the stability assessment of wells. The well should be sunk to a depth below the scour level, known as the grip length, such that the lateral forces can be resisted by the resistance from the side, and the base pressures under the worst loading conditions should be within the permissible limit. The Indian Road Congress (IRC:45-1972) provides recommendations for estimating the resistance of soil below the respective scour level of abutment and pier in the analysis of well foundation in cohesionless soil. The various models used in this study are presented in Figure 1.Alkali-Activated Cements, Mortars and Concretes. Woodhead Publishing Limited. https://doi.org/10.1533/9781782422884.4.555

This estimation is based on elastic theory to determine the pressure at the side and base under design load. Teng (1962) suggested that settlement can be a guiding factor of the bearing pressure of well foundations embedded in sand

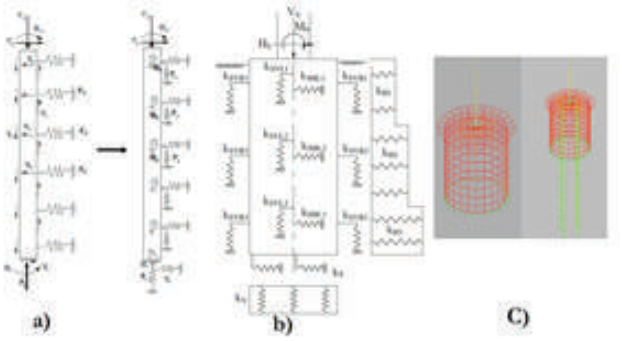

Figure 1 (a) Spring model for the soil reaction on pile, (b) spring model for soil reaction on well, (c) numerical model of well foundation without pile and with pile

and proposed an equation of bearing pressure for a permissible settlement. However, to determine the actual factor of safety against shear failure, the ultimate soil resistance needs to be calculated.

3. RESULTS AND DISCUSSION

3.1 Well Cap moment distribution

Max Induced bending moment for critical load along radial unit strip in case of no pile is observed as 1402.22 KNm/m and that of case with pile is observed as 845.5 KN-m/m. Similarly circumferential direction unit strip moment is 1311.74 KN-m/m and 655.72 KN-m/m for the condition well without pile and with pile respectively under critical load condition.

The deflection of well cap center is reduced from 15 mm to 5.3 mm indicating significant influence of composite behavior for deflection control. 3.2 Well stem moment distribution

Bending moment in with influence of pile is reduced by factor 0.25 for circumferential strip and 0.34 for vertical indicating significant improvement with the composite behavior of pile and well for the reduction of well stem

bending moment. Well end vertical settlement due to induced case loading is decreased from 20 to 7 mm with the introduction of pile.

3.3 End bearing pressure

End bearing pressure is observed critical at link id 682, the maximum bearing pressure in model without pile is 1025 kN/m2. While bearing pressure with pile model is reduced to 460 kN/m2. It indicates significant end bearing pressure reduction due to composite behavior of well and pile.

4. CONCLUDING REMARKS

During the sinking process, bridges that were initially designed with well foundations may encounter unexpected boulder strata at certain depths, resulting in obstacles for further sinking.

A capacity-based design method was proposed for designing a Composite Well Pile Foundation (CWPF) bridge with a post-tensioned cast in-situ superstructure spanning five spans and 175 meters long. The study found that a large proportion of the axial load is carried by the well foundation, but the amount of load carried by the well is dependent on the depth of the well foundation below the scoured depth. The results indicate that the hybrid foundation behaved satisfactorily. Generally, the caisson could bear the top load and be used as a construction platform during the bridge's construction. The piles under the caisson could control the settlement after the bridge was built.

REFERENCES

Aswathy, M.G. and Jacob, B. (2015). Seismic Analysis of Caisson Foundation International Journal of Engineering Research & Technology (IJERT), 4 (10), 460-463.

Basudhar, P. and Dey, A. (2007). Computer aided analysis and design of well foundation National Conference on foundation and Retaining Structures (NCFRS-2007), Indian Institute of Technology, Roorkee

Dhakal, S. (2014) Geological Divisions and Associated Hazards in Nepal. In: Khadka, U.R., Ed., Contemporary Environmental Issues and Methods in Nepal, Central Department of Environmental Science, Tribhuvan University Nepal, Kirtipur, 100-109.

F.Y. Liang, L.Z. Chen, X.G. Shi (2003). Numerical analysis of composite piled raft with cushion subjected to vertical load. Comput Geotech, 30 (6), 443-453.

IRC (Indian Road Congress). 1972. Recommendations for estimating the resistance of soil below the maximum scour level in the design of well foundations of bridges. IRC 45. New Delhi, India: IRC

J.S. Chiou, Y.Y. Ko, S.Y. Hsu, Y.C. Tsai (2012): Testing and analysis of a laterally loaded bridge caisson foundation in gravel, Soils and Foundations, 52 (3) (2012), pp. 562-573.

#Gen-29:

Effects of river bed degradation and sediment flow in sustainability of headworks of irrigation projects in Jhapa, its effects, causes and Issues.

[1]Er. Krishna Prasad Rajbanshi, [2]Mohan Prasad Acharya
[1]Division Chief at Water Resources and Irrigation Development Division Jhapa (Oct. 2018 –Oct.2022)
Now Division Chief at Water Resources and Irrigation Development Division, Khotang
[2]Mohan Prasad Acharya, Senior Geotechnical Specialist, NEA Engineering Company

1. INTRODUCTION

covers 160600 hector of land out of which 98217 hector is agricultural and 90000 hector is irrigable. There are more than 100 small to medium size irrigation schemes some of which have side intakes and some of which have permanent diversion structures like weirs or core wall. Government of Nepal has invested huge sum of money since establishment of Department of Irrigation for providing irrigation to agricultural land of Jhapa. Most of the irrigation schemes performed well in the first few years of construction. After few years of operation some of irrigation projects became defunct due to foundation failure of head works, outflanking of side banks etc. Government has reinvested for reconstruction of these defunct projects. This situation is repeating in the recent schemes as well. Similar situation might exists in the irrigation schemes located in similar geological and topographical condition throughout the country.

This paper aims to presents the case examples observed and studied by authors during the last five years while working in Jhapa district. This paper tried to show how the sediment & floating debris, bed erosion, downstream bank and bed erosion causes outflanking and foundation failure of headworks of irrigation projects. In addition, the performance of adopted remedial measures are discussed and recommendations for sustainability of irrigation projects are made.

2. METHODOLOGY

Seven irrigation schemes located at the different part of Jhapa district have been selected for this case study; two of them which were outflanked have been reconstructed. Three irrigation schemes with foundation failure are under reconstruction. One recently constructed project is suffered by river bed degradation. The seventh one is damaged by outflanking of banks & still defunct.

These projects are studied to analyze how these projects failed due to bed erosion, sediment & floating debris flow. The changes in the river channel, changes before & after the construction and failure of headworks, and condition after reconstruction are presented in the google earth images, of respective time.

Each cases are than analyzed and discussed based on project documents, field data, before and after construction images. Finally the conclusions based on findings in historical google images, field data and achievements after reconstruction are derived and presented.

3. RESULTS AND DISCUSSION

Table 1 presents the list of projects selected for this study.

Table 1: List of projects selected for case study

S.N.	Name of Project	Command Area (ha)	Remarks
1	Tallo Kisne IP, Gauriganj,Jhapa	1500	Outflanked
2	Aduwa Khola IP, Chakchaki, Jhapa	500	Outflanked
3	Lafadi IP, Gauradaha-9, Jhapa	180	Outflanked
4	Harchana Kishak Kulo IP, Haldibari, Jhapa	180	Foundation Failure
5	Deuniya Khola IP, Birtamode	270	Foundation Failure
6	Hadiya Regulator IP, Duwgadhi, Jhapa	300	Foundation Failure
7	Integrated Biring IP, Buddhashanti	1144	River Bed degradation

Case 1: Outflank of side bank

This is the case concerned to projects listed in S, No. 1. 2

&3 of table no 1 above. From the field data and observations, it was found that outflank of side banks in all three cases occurred not only due to excess high flood but due to the following;

a. The water way, i.e., the width of weir was not enough to pass the sediment loaded peak flood.

b. There was foot trail bridge over weirs supported by piers above weir. These piers chocked by floating debris carried by flood which blocked the passes of flood over weir and resulted into outflank of upstream side bank.

c. Seepage control was done by simple cutoff wall only. This resulted into damage of the foundation as well.

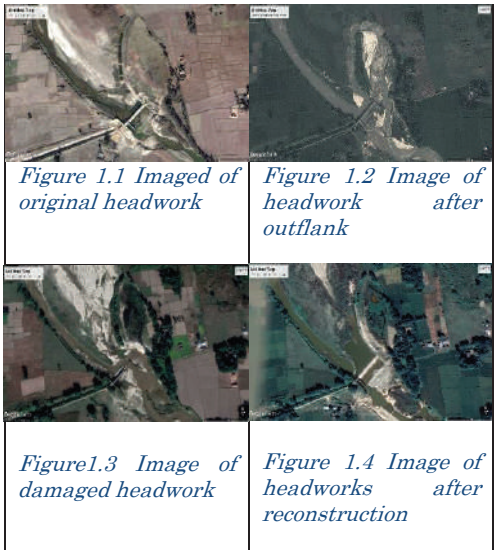

Figure 1.1 Imaged of original headwork | *Figure 1.2 Image of headwork after outflank*

Figure1.3 Image of damaged headwork | *Figure 1.4 Image of headworks after reconstruction*

Figure No: 1, Google Images of Tallo Kisne IP, Gauriganj, Jhapa

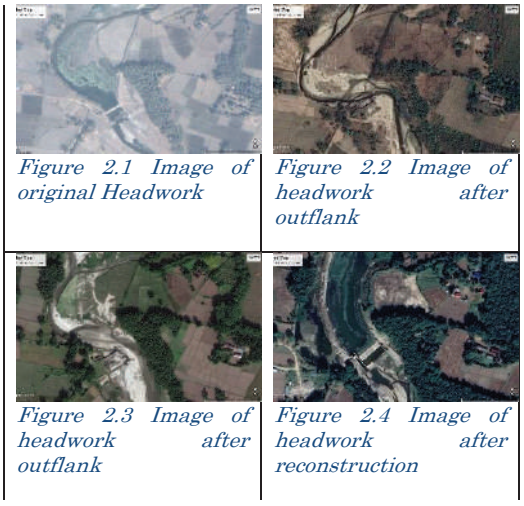

Figure 2.1 Image of original Headwork | *Figure 2.2 Image of headwork after outflank*

Figure 2.3 Image of headwork after outflank | *Figure 2.4 Image of headwork after reconstruction*

Figure No: 2 Google Image of Aduwa Khola IP, Chakchaki

Figure 3.1 Image of original Headwork | *Figure 3.2 Image of headwork with upstream bank erosion*

Figure No: 3 Google Image of Lafadi IP, Gauradaha 9, Baigundhura

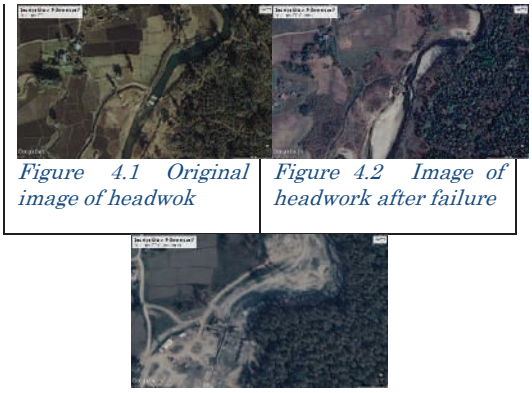

Figure 4.1 Original image of headwok | *Figure 4.2 Image of headwork after failure*

Figure 4.3 Image of headwork under reconstruction

Figure No: 4 Google Image of Deuniya IP, Birtamode

Figure 5.1 Image of headwork with outflank and damage foundation | *Figure 5.2 Image of Reconstructed headwork*

Figure No:5 Google Image of Harchana Krishak Kulo IP, Haldibari

Figure 6.1 Image of Temporary diversion headwork | *Figure 6.2 Image of permanent diversion (Core wall) headwork*

Figure 6.3 Image after upstream core wall failure

Figure No:6 Google Image of Hadiya Regulator IP, Duwagadhi

The figures 4 to 6 illustrate the Case 2, the foundation failure of irrigation schemes; Deuniya IP Birtamode, Harchana Krishak Kulo IP Haldibari and Hadiya Regulator IP Duwagadhi IP respectively. The images have clearly illustrated the before and after foundation failure situations and after reconstruction situation. The remarkable measures adopted for reconstruction are;

a. RCC weir was constructed with sheet pile provided as upstream & downstream cutoff.

b. Adequate upstream and downstream protection measures provided to reduce chance of outflank as well as bed erosion.

c. In case of Hadiya Regulator IP, it is in operation by temporary diversion measures using gabion crates and jure bags.

Case 3: Lowering of Full Supply Water Level due to River Bed Degradation.

This is the case concerned to project listed in S, No. 7 of table no 1 above. From the field data and observations, it was found that the river bed was intensively degrading year by year and the newly rehabilitated system is at the verge of defunct because;

a. The headwork is side intake type, there is no permanent diversion structure like core wall or weir.

b. The riverbed has degraded by more than 1 meter in the course of its rehabilitation of 3 years' duration and it has become difficult to maintain full supply level at intake to feed the canal.

c. The rapid river bed degradation of the Biring river is due to excessive and uncontrolled river bed material extraction, and it is because Biring river is considered as major source of construction material in Jhapa district.

The river bed degradation of Biring river is still active. Many discussions among local bodies and stakeholders have been made for controlling excess riverbed material extraction but still not controlled effectively.

4. EFFECTS OF RIVERBED DEGRADATION AND OUT FLANK OF HEADWORKS

The cases of riverbed degradation and outflank of headworks of selected irrigation projects in Jhapa were illustrated and discussed above. The effects of these disasters in irrigation projects can be summarized as follows;

a. The damaged irrigation projects remain defunct for many years and wait fundings for reconstruction which causes less crop production and decreases the income of poor farmers.

b. Government has to reinvest in the same project for reconstruction.

5. CONCLUDING REMARKS

From the analysis of the above cases, it is concluded that sediment and floating debris should be taken into consideration for hydraulic design of irrigation headworks. Excessive riverbed material extraction should be controlled to reduce riverbed degradation and to reduce the chance of foundation failure. Precise field data like river section & profile, river bed silt size should be taken and appropriate peak flood discharge calculation should be adopted for design of headworks. Also adequate upstream and downstream protection measures should be provided to avoid outflank and foundation failure.

This case study of selected projects is just discussion of various problems found due to bed erosion and outflank of upstream bank of irrigation beadworks based on field data, observations and google images. However, each case may be researched to verify causes based on historical real time data of precipitation, disasters occurred and analyzing adopted different design parameters. This detailed study of these cases may be research paper for Masters students and for PhD students of concerned topics.

ACKNOWLEDGEMENT

First of all, I would like to acknowledge Dr. Mohan Acharya for encouraging me to write a paper for this 1st NGS International Conference 2023. I also would like to acknowledge organizing committee of this conference for accepting my paper and providing opportunity to share my experience in such a great international forum.

REFERENCES

District Profile of Jhapa district. District Coordination Committee of Jhapa

Project documents and field data from 2018 to 2022, Water Resources and Irrigation Development Division, Jhapa

Historical Satellite Images, Google Earth

#Gen-30:

Case Study: Landslide Mitigation Measures at Narendranagar Landslide Uttarakhand, India

Gourango Singha1, Saurabh Chaurasia2, Harish Madupuri3
[1]*Director (P&G Geohazard Solutions Pvt. Ltd, India)*
[2]*Senior Manager Designs – Rockfall Mitigation (TechFab India Industries Limited, India)*
[3]*Manager Designs (TechFab India Industries Limited, India)*

1. INTRODUCTION

In June 2013, Uttarakhand, a state in north India, was hit by severe natural disasters including landslides and flash floods due to excessive rainfall. The region received heavy rainfall between June 15 and 18, which was 375% above normal levels and resulted in the loss of 580 human lives. Additionally, more than 5,400 people were reported missing.

The landslide that occurred on the Narendra Nagar Bypass Road was also a result of the excessive rainfall. Slope analysis conducted using the latest software revealed that the slope was unstable and required stabilization measures to prevent further landslides.

Consequently, stabilization measures were designed to stabilize the slope and prevent future landslides while constructing the road. The proposed measures included soil nailing, slope protection using wire meshes, erosion control using hydroseeding and erosion control mats, and the installation of a drainage system.

2. METHODOLOGY

To ensure an authentic design that meets the necessary requirements, slope analysis was conducted using the latest software. The analysis was based on field values directly taken from the site. The aim was to determine the failure pattern and identify the stability measures that were needed.

The causative factors of the slide were determined through a site reconnaissance survey, geological mapping, and geotechnical investigation. To determine the nature of the failure, kinematic analysis using Stereo nets was performed. Post-analysis stability analysis was carried out using Slide 2D software, and Mesh Stability checks were conducted to identify the remedial measures required.

3. RESULTS AND DISCUSSION

The proposed stability measures were developed based on the results of geotechnical investigation and geological mapping. The investigation was conducted in two locations on the slope. The region is prone to frequent earthquakes, flash floods, and heavy rainfall, which can cause repeated slides. During monsoons, the moisture in the landslide mass exacerbates the situation or triggers the landslide.

As a solution, high tensile wire mesh with a 300mm aperture size was proposed and additionally, a secondary mesh with an aperture size of 120mm hexagonal mesh was proposed to arrest small boulders to anchor both the wire meshes and for global stability of the slope self-drilling anchors were installed up to the required extent. Synthetic erosion control mats were suggested to promote vegetation growth and prevent facial erosion on the slope. These measures would improve the stability of the slope and prevent further landslides.

The factor of safety (FoS) obtained in the design of the mitigation measures are listed in Table 1 below.

Table 1: Factor of Safety Static and Seismic Case based on Slide analysis.

Load Case	Target FoS	Obtained FoS
Static Case	1.3	1.447
Seismic Case	1.05	1.137

Figure 1: Narendranagar Landslide on completion

4. CONCLUDING REMARKS

The proposed system was chosen for its versatility, seismic performance, cost-effectiveness, speedy construction, and compatibility with local materials. Apart from these significant advantages, this system also offers various general and technical benefits compared to conventional solutions.

As of July 2020, the mitigation measures have been successfully implemented, and they continue to function as intended, stabilizing the landslide and preventing any further movement of the slope.

REFERENCES

IS 1893 part1 (2002) "Criteria for earthquake resistant design of structures".

IRC-HRB-Special Report-23. State of the Art: Design and Construction of Rockfall Mitigation Systems. New Delhi., 2014.

M46-03.11, Geotechnical Design Manual, Washington State Department of Transportation.

#Gen-31:

Slope Stability Analysis Of A Vertical Cut: A Case Study Of Sarangkot Housing Sarangkot, Pokhara"

Aayush Adhikari[1], Bigyan Bhandari[2], Anup Lamichhane[3]
[1,2] *Paschimanchal Campus, IOE, Tribhuvan University*
[3]*Advanced College of Engineering and Management*

1. INTRODUCTION

The research is a case study on determination of slope stability of two vertical cuts, design of slope stabilizing structures for them if necessary, and their cost comparison. The goal of the research was to determine the most cost-effective slope stabilization structure.

2. METHODOLOGY

We analyzed the stability of the slope using limit equilibrium method through GeoStudio software by applying Bishop's method of slices. Guided by relevant codes and guidelines, we designed and evaluated cost effectiveness of different slope stabilizing structures using analytical approach complemented by Geo5 software.

Figure 1 Flowchart for determination of stability of slope

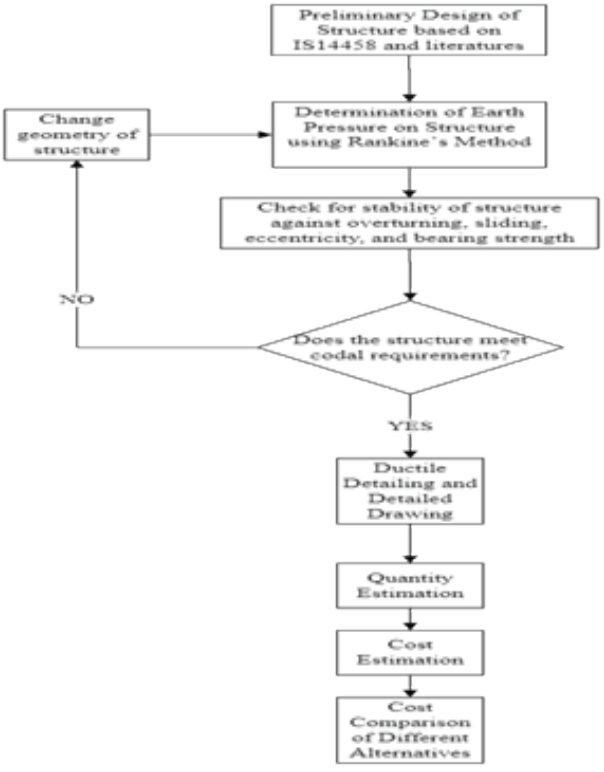

Figure 2 Flowchart for design of slope stabilizing structures

3. RESULTS AND DISCUSSION

Both vertical cuts at the site were unstable, with factor of safety values of 0.523 and 0.365. In both cases, gabion walls were the most economic options for slope stabilization. Furthermore, counterfort walls were found to be more economic than cantilever walls for slopes deeper than 6 meters.

Table 1: Cost comparison of structures at slope A

SN	Type of Wall	Cost	Cost compared to Cheapest Alternative
1	Gabion Wall	1,083,602.67	**Cheapest (1)**
2	Gravity Wall	2,698,761.87	1.49
3	Cantilever Wall	4,432,136.02	3.09
4	Counterfort Wall	3,655,264.56	2.37

Table 2: Cost comparison of structures at slope B

SN	Type of Wall	Cost	Cost compared to Cheapest Alternative
1	Gabion Wall	1,553,328.52	**Cheapest (1)**
2	Gravity Wall	3,739,989.89	1.41
3	Cantilever Wall	4,382,161.46	1.82
4	Counterfort Wall	4,049,069.20	1.61

4. CONCLUDING REMARKS

In summary, this research emphasizes that economic considerations should be taken into account when selecting slope protection measures. Overall, this study highlights the significance of a multidisciplinary approach to managing geological hazards and ensuring the safety and sustainability of infrastructure projects in slope-prone areas.

REFERENCES

Hashimoto, S., Y. Ohta, and C. Akiba. 1973. Geology of Nepal Himalayas. Sappdra: Himalayan Committee of Hokkaido University.

Das, B. 2007 Principles of Geotechnical Engineering: Taylor and Francis

IS 14458:1998 'Indian Standard Retaining Wall for Hill Area Guidelines'

#Gen-32:

Study of the Slope Failures in Kanti Highway along Lesser Himalayan Range

Er.Suresh Neupane
Kanti Lokpath Road Project, Department of Roads, Lalitpur

1. INTRODUCTION

Study of the slope behavior of highway along Himalayan range is crucial because of geodynamically youngest mountain region in the world with immature geotechnical, geological and topographical phenomenon. Kanti Highway, falling in Sub-Himalaya (Churia/Siwalik) and lesser Himalayan range of Nepal is the oldest planned highway connecting Kathmandu to Terai is not still in full flagged operation due to frequent blockage triggered by the slope failures at various locations. The road alignment belongs to the rocks of Siwalik Group and Lesser Himalaya crosses the regional thrust the Main Boundary Thrust (MBT). Most of the landslides are seen in Lesser Himalaya rocks including some of in the Siwalik range. To study the behavior of slope and investigate the subsurface condition around the slide area between chainage of 15+000 to 79+000 2D-Electrical Resistivity Tomogram (ERT) is used.

2. METHODOLOGY

Field study is carried out and focusing on size, effect to the road and settlements, land-use pattern, hydrological condition and surface geology of the landslides is investigated for the categorization of the slopes. To identify the depth of the bedrocks and thickness of overburden materials on hill slope, ERT is carried out at five different location of combined total length of one thousand meter.

Table 1: Details of 2D ERT Coverage

Profile No.	Location	Length (m)	Coordinate of ERT profile			
			Start point of Profile		End point of profile	
			Northing	Easting	Northing	Easting
ERT-1	Makawanpur Gadhi (Ch 15+320)	245	27° 24' 32.05"	85° 08' 48.47"	27° 24' 35.41"	85° 08' 40.33"
ERT-2	Makawanpur Gadhi (Ch15+560)	220	27° 24' 33.03"	85° 08' 50.09"	27° 24' 36.69"	85° 08' 41.85"
ERT-3	Makawanpur Gadhi (Ch 15+827)	180	27° 24' 36.93"	85° 08' 59.74"	27° 24' 34.51"	85° 08' 51.90"
ERT-4	At Chainage (Ch 43+700)	215	27° 27' 02.64"	85° 14' 29.10"	27° 26' 56.34"	85° 14' 24.37"
ERT-5	Sitalelh (Ch 46+760)	240	27° 26' 07.53"	85° 15' 08.14"	27° 26' 07.53"	85° 15' 01.24"

Mapping of vertical as well as horizontal variation of electrical resistivity is carried out for the detection of subsurface lithology and possible countermeasures is proposed from the analysis of tomogram and lithological Interpretation

3. RESULT AND DISCUSSION

The model sections obtained from data inversion of ERT are described in respective resistivity tomogram sections. These tomogram sections show the variation of modeled electrical resistivity in depth and along the line of investigation. These variations in modeled physical properties have relation with the subsurface geological and hydro-geological set up. Representative resistivity tomograms for first ERT profile are presented in Figure 1 and the interpretations of each are presented in Figures 1B to 5.

3.1. Resistivity Tomogram and Lithological Interpretation of ERT-1

This profile runs along the road section on the left side, near around the Makwanpur Gadhi and lies on the landslide mass. The starting of the profile is towards the Makwanpur Gadhi road. The total length of the profile is 245 m. Representative resistivity tomogram is presented in Figure 1 while the lithological interpretation of resistivity tomogram is presented in Figure 2.

The lithological section can be interpreted as three layered model. Top layer with high resistivity value greater than 200 Ω m from the starting of the profile to the end of the profile represents dry overburden of landslide mass deposit/colluvial deposit containing boulders of fractured rock fragments. The thickness of the top layer varies from 6-11 m.

Second layer with low resistivity value of below 100 Ω m from 25 to 190 m indicates overburden of fine sediments or partly saturated sediments with varying thickness 3-27 m. The thickness of this layer is greatest at the center of the profile.

Very thin layer of hard and competent bedrock is expected to be found at depth of 20 m from the 190 to 205 m. highly weathered/fractured rock is found from the 60 to 190 m at depth of 16-32 m and from 195 to 225 m at depth of 4-11 m.

Similarly the lithological interpretation of resistivity tomogram is presented in Figure 3-5 and details of lithological interpretation of was carried out.

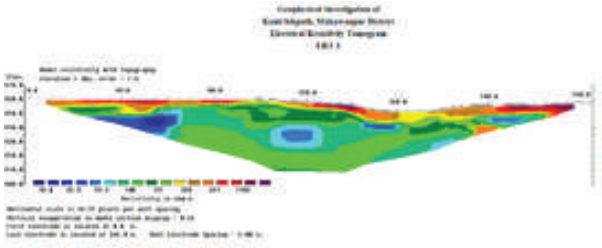

Figure 1: Electrical Resistivity Tomogram of ERT-1

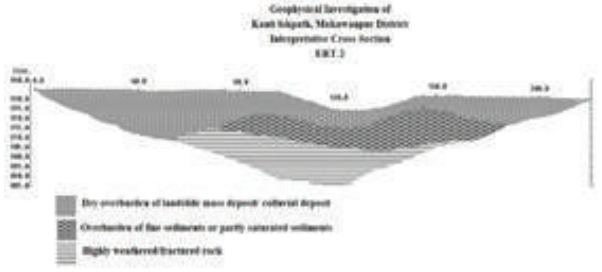

Figure 2: Interpretative Cross section of of ERT–2

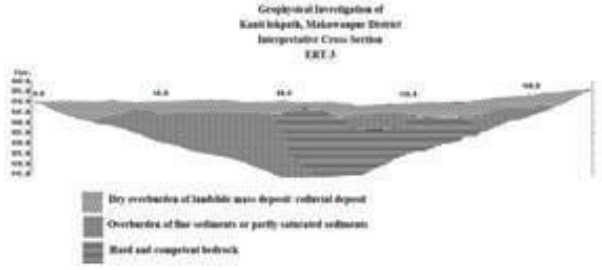

Figure 3: Interpretative Cross section of of ERT –3

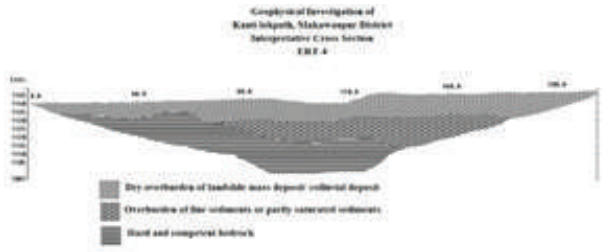

Figure 4: Interpretative Cross section of of ERT

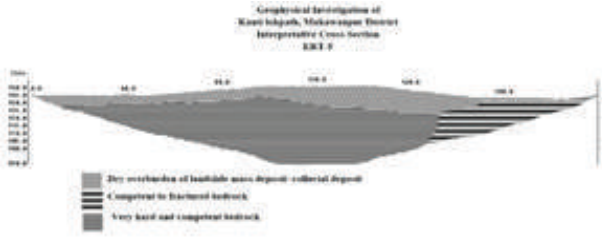

Figure 5: Interpretative Cross section of of ERT –5

Description of Major Slide

Slope stability condition along the road alignment in the rocks is analyzed based on the natural hill slope and wedges formed by intersection of the joints and foliation plane. The wedges are identified based on plotting in stereographic projection. One major slides presented herewith.

Pratapdanda slide Ch: 46+600-46+950: This slide is comparatively severe than other slides along the road. The slide is developed in rocks of marble and phyllite as well as quartzite. Rocks are hilly fractured and thin bedded on both hill and valley slope. The main causes for occurrence of slide are dipping of the hill slope and foliation in same direction, presence of fractured and thin bedded rocks. The slope stability is seem to be very critical in bedrocks due to chances of occurring plane failure along foliation plane (Figure-6).

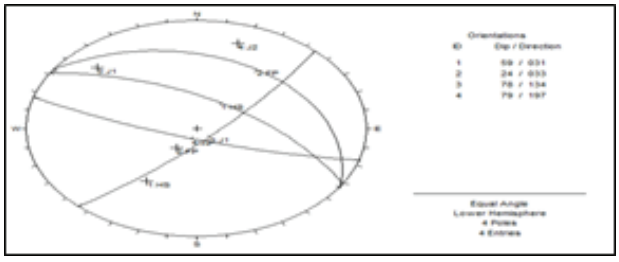

Figure 6: Stereographic Projection of rock mass between chainage 46+600 and 46+950

4. CONCLUSIONS

The slopes of the study area is highly distorted due to roadway excavation, weathering effect and seismically activeness of the region. Most of the landslides are seen in Lesser Himalaya rocks and some are seen in the rocks of the Siwalik Group. The orientation of discontinuities, ferruginous material between open discontinuities, steepness of slope, intensely fractured rock, poorly managed construction methodology are the key factors for the instability of slopes. The slides near to MBT zone (43+000-44+000), Pratapdanda (46+600-950); Nayagaon (68+600) are still active and proper countermeasures

should be provided. But the slides of Jhakridanda (68+000), Kalche (55+950), Baguwa (51+250), Chapeli (62+300) are slowly getting stabilized.

REFERENCES

Acharya G, De Smedt F, Long NT (2006) Assessing landslide hazard in GIS: a case study from Rasuwa, Nepal. Bull EngGeol Environ 65(1):99–107

Dahal RK (2004) Rainfall triggered landslides along roadside slopes of Nepal and their mitigation. Proceedings of 2nd one day international seminar on disaster mitigation in Nepal, Nepal Engineering College and Ehime University, Japan, pp 31–41 Bieniawski, Z.T. (1973) Engineering classification of jointed rock masses. Trans. S. Afr. Inst. Civil Engg., v.15, pp.335–344. Coggan,

J.S., Stead, D., Eyre, J.M. (1998). Evaluation of techniques for quarry slope stability assessment. Transactions of the Institutions of Mining and Metallurgy, Section B: Applied Earth Science, v.107, pp.139–147.

#Gen-33:

Design of Tunnel Support System, Shotcrete versus Rock Bolts in Middle Modi Hydroelectric Project (MMoHP)

Er. Milan Paudel[1], Prof. Dr. Akal Bahadur Singh[2], Er. Mohan Raj Panta[3]

[1]Senior Divisional Engineer, Water Resources and Irrigation Development Division, Nawalparasi (Bardaghat Susta East)

[1]Member, Nepal Geotechnical Society, Kathmandu, Nepal

[2]Formor Professor, Institute of Engineering, Pulchowk Campus, TU

[3]Peoples Energy Limited, Kathmandu

1. INTRODUCTION

This research aimed to assess the benefits of the shotcrete tunnel lining method over the other conventional methods in terms of time and economy by conducting the numerical modelling of the headrace tunnel of the Middle Modi Hydroelectric Project in Parbat, Nepal. The Himalayan Geology of Nepal is not only the young formations but is also highly weathered, fractured, and weak in strength and is thus challenging for the construction of underground structures like a tunnel, and caverns for hydropower development in Nepal (Panta 2011). The economic design, on the other hand, is also of the utmost importance for developing countries like Nepal for the underground development project. The most efficient tunnel lining is one that mobilizes the strength of the ground permitting controlled ground deformations (Singh & Goel 2006). The design of tunnel lining must account for large uncertainties and variations in the ground conditions, construction procedures, and ground behaviors during construction. Although tunnel support system designs are explained in literature and previous studies (Singh & Goel 2006; Hoek & Brown 1980), the limitations are mostly attributable to the specific geological conditions and conventional methods of shotcrete and rock bolts, which created the necessity of this research for the efficient tunnel support system design.

2. METHODOLOGY

The research aim of this project is fulfilled by applying the quantitative research methodology with main three study phases which are data preparation, support system design, and result and discussion as shown in Figure 1. The specific procedure followed in these phases was study area selection which was Middle Modi Hydroelectric Project in Parbat, Nepal, and data collection from different sources specially geological and lab test data, rock mass classification, and support design by empirical, analytical, and numerical modelling methods, cost and time estimate followed by result analysis and interpretation.

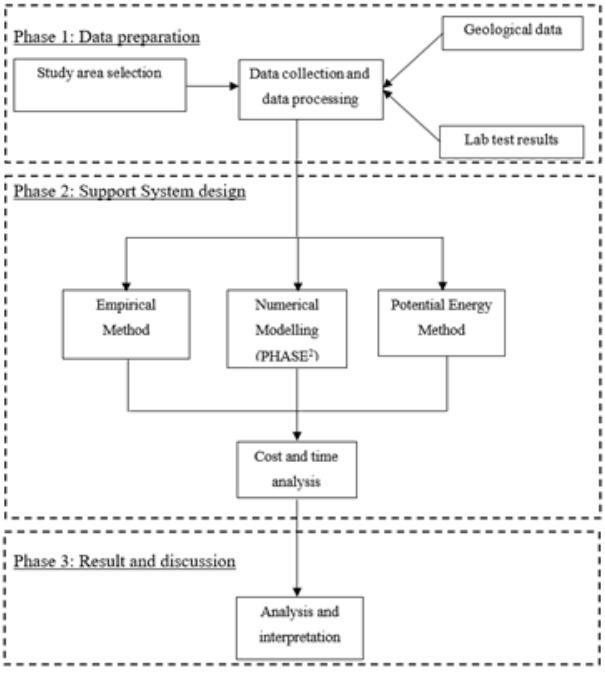

Figure 1: Flow chart for research methodology

3. RESULTS AND DISCUSSION

To fulfill the research objectives, support system design from the empirical method for a typical section is shown in the Table 1.

Table 1 Assigned rock support with respect to rock mass and rock support class (MMoHP geology report, 2010)

Chainage (m)	Rock mass class	Rock support class	Assigned rock support measures
2+300-2+700	*Class IV*	*RS II*	25mm diameter 3 meters long systematic grouted rock bolts at a spacing of 1.3m x 1.5m and 15cm thick steel fiber shotcrete. Pre-injection grouting with 500 kg per tunnel meter.

Similarly, support system design by numerical analysis with shotcrete and rock bolts is shown in Figure 2, and shotcrete only is shown in Figure 3 respectively. The maximum total displacement is decreased from 50mm to 40mm in the first case and 38mm in the second case before and after the support installation which shows not any considerable change in maximum displacement.

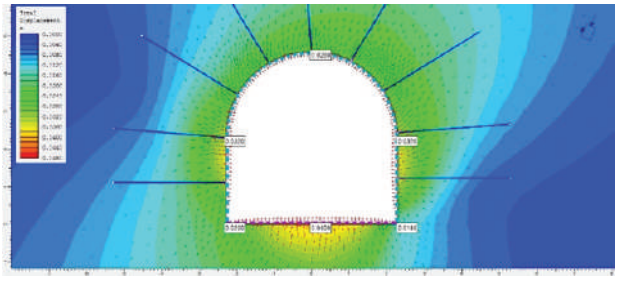

Figure 2 Total displacement diagram after support analysis at chainage 2+400 using rock bolts and shotcrete.

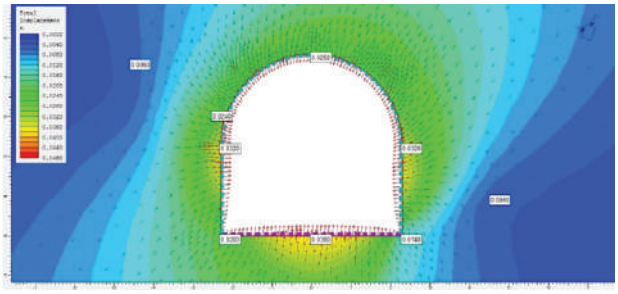

Figure 3 Total displacement diagram after support analysis at chainage 2+400 using shotcrete only.

The results from the numerical analysis was also verified using the potential energy method in which the rock load was calculated using Protodyakonov theory. Using that value of rock load, bending moment around the cross section of the tunnel has been calculated. The lining thickness is then determined from calculated value of bending moment using the limit state method of design which is 370 mm at 2+400.

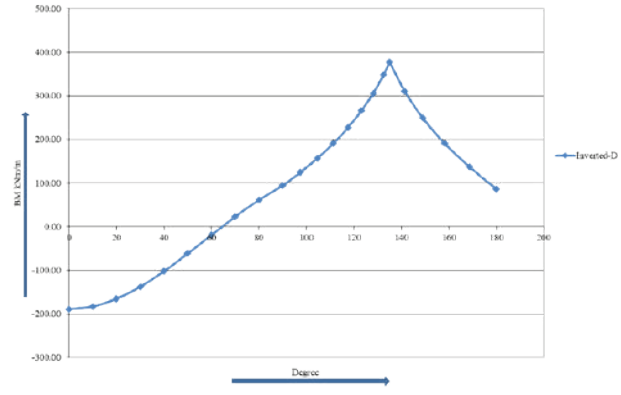

Figure 4 Bending moment diagram at tunnel lining at chainage 2+400 m

Table 2 Analysis of Result for Inverted D-shape Tunnel Section by Potential Energy Method at Chainage 2+400

Degree	M				σ_{ck} (Mpa) 30	Fy (Mpa) 415	Adopted Depth (mm)
	Ground Reaction (KN)	Vertical Rock Load (KN)	Lateral Rock Load (KN)	M (KN)	d (mm)	D (mm)	
0	13.56	184.54	-8.96	189.14	261.78	270	
10	13.47	181.06	-11.40	183.14	257.59	260	
20	13.21	171.05	-18.63	165.63	244.97	250	
30	12.78	155.69	-30.44	138.03	223.63	230	
40	12.19	136.81	-46.46	102.54	192.75	200	
50	11.47	116.67	-66.22	61.92	149.78	150	
60	10.64	97.65	-89.11	19.18	83.35	90	
70	9.72	82.00	-114.44	-22.72	90.72	100	
80	8.73	71.57	-141.43	-61.12	148.82	150	
90	7.72	67.56	-169.26	-93.99	184.53	190	
90	7.72	67.56	-169.26	-93.99	184.53	190	
97	6.96	67.12	-198.55	-124.47	212.37	220	
105	6.19	66.68	-229.76	-156.89	238.42	240	370
111	5.43	66.24	-262.91	-191.25	263.23	270	
118	4.67	65.79	-298.00	-227.53	287.12	290	
123	3.91	65.35	-335.01	-265.75	310.30	320	
128	3.15	64.91	-373.96	-305.90	332.92	340	
132	2.38	64.47	-414.84	-347.98	355.08	360	
135	1.88	64.18	-443.17	-377.11	369.64	370	
135	1.88	64.18	-443.17	-377.11	369.64	370	
141	1.07	110.30	-422.47	-311.10	335.74	340	
149	4.21	156.41	-401.77	-241.14	295.58	300	
158	-12.40	202.53	-381.07	-190.94	263.02	270	
169	-25.06	248.65	-360.37	-136.78	222.62	230	
180	-41.67	294.77	-339.67	-86.58	177.11	180	

Finally, the cost analysis has been performed considering the factors such as rock type, tunneling methods, labour rate and project importance. The cost of steel fiber reinforced shotcrete (SFRS) seem slightly costlier than conventional shotcrete initially but considering the final in place cost and unevenness in rock mass, SFRS seem to be only the best economical solution.

4. CONCLUDING REMARKS

The main aim of this research is to design the thickness of shotcrete lining and to compare the suitability of conventional rock bolts and shotcrete lining methods with steel fiber reinforced shotcrete in terms of time and economy. Three different design methods have been used based on the data from rock mass classification and rock mass strength, field investigation reports, lab test reports, and secondary published data. The research concluded with the remarks that SFRS can be used as a sole lining element and the rate of tunneling progress can be increased considerably in tunneling by limiting the use of rock bolts only in localized failure and the additional support system is required in case of wedge failure, swelling and squeezing rock mass condition.

ACKNOWLEDGEMENT

I would like to acknowledge Himal Hydro and General Construction Ltd. for all the geological data, lab test reports, drawings, and other relevant materials. I am also thankful to Er. Rabi Lal Sharma, Er. Kiran Kumar shrestha, NEA, Er. Narayan Nyaupane and Er. Sagun Shrestha for their kind support and guidance during this research work.

REFERENCES

Singh, B & Goel, RK 2006, Tunneling in Weak Rocks, Elsevier Ltd.

Hoek, E & Brown, ET 1980, Underground Excavations in Rock, The Institution of Mining and Metallurgy, London.

Panta, MR 2011, 'Stability Assessment of Headrace Tunnel, Middle Modi Hydropower Project, Nepal', M.Sc. Thesis, Department of Hydraulic and Environmental Engineering, Norwegian University of Science and Technology (NTNU), Trondheim, Norway.

#Gen-34:

Pile Tests in Nepal – Current Practice and Enhancements

Arun Kumar Pandit[1],* and Anand Gupta[1,2]
[1]*N.S. Engineering and Geotechnical Services Pvt. Ltd, Lalitpur, Nepal*
[2]*Universal Engineering and Science College, Chakupat, Lalitpur, Nepal*

ABSTRACT

According to the information collected by various researchers and available database, 90% of the major bridges and high rise buildings have pile foundation. In past few years, few cases of bridge failures due to failure of pile foundation have been noted. Hence quality assurance of piles is essential. Pile Integrity tests and Pile Load tests are the quality assurance plan for the piles. Static Pile load Test is in practice in Nepal for quite a long time. PIT test was introduced here just around 5 years ago. Some of the latest developments in these areas of pile tests, available in Nepal, are Cross Hole Sonic Test, High Strain Pile Dynamic Test. Proper practice of these tests are essential for Quality Assurance of the built-up structures and also for the reliable and economical design of those structures.

1. INTRODUCTION

Kavre district experiences a huge number of shallow landslides in the monsoon season. The hydrologic characteristics of a watershed like discharge and sediment play an important role in river morphology and sedimentation. Dahal et al. 2008 conducted research 2008 on rainfall threshold affirming exceeding 144mm of daily rainfall increase the risk of landslides high in the Himalayan mountain [1]. Shrestha, H.K. et al., 2008 researched creeping landslide for effective use in the planning and execution of slope stability enhancement measures in Otoyo town, Shikoku, western Japan utilizing a three-dimensional model [2]. Chhetri A. et al. 2016 researched the sediment of River Langtang of Rasuwa, Nepal calculating the concentration of suspended sediment and then generating the sediment rating curve [3]. This study aims to determine the rainfall threshold for the initiation of shallow landslides in the Kavre district, Nepal. It also includes the hydrological study of discharge and sediment dynamics of Roshi River with the development of a suspended sediment rating curve.

2. METHODOLOGY

Khando Bridge at Kanchanpur-Kamala Road Project was taken as a site for the study.

2.1 High Strain Dynamic Test (HSDT)

This test is also popularly known as Pile Dynamic Test (PDA). High Strain Dynamic testing like a static load test can be used to evaluate pile capacity. The test procedure is standardized as per ASTM D4945-2000 and also forms part of various specifications and code provisions worldwide. The method is convenient, reliable and helps evaluate pile capacity and integrity in quick time and one or more piles can be tested per day. The testing is conducted using Pile Driving Analyzer TM (PDA) by obtaining and analyzing records of force and velocity under drop weight impacts. The field results are further analyzed with a signal matching technique (Case Pile

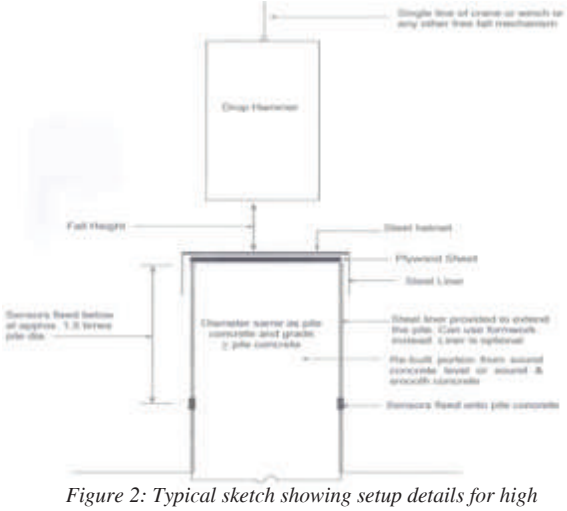

Figure 2: Typical sketch showing setup details for high strain dynamic pile testing

Wave Analysis Program – CAPWAP) to refine the soil parameter assumptions. The output from the test result can be summarized as below.

1. Static capacity of the pile at the time of testing.
2. Simulated static load test curve
3. Total skin friction and end bearing of the pile
4. Skin friction distribution along the length of the pile
5. Compressive stress developed in the pile during testing
6. Net and total displacement of the pile.
7. Pile integrity

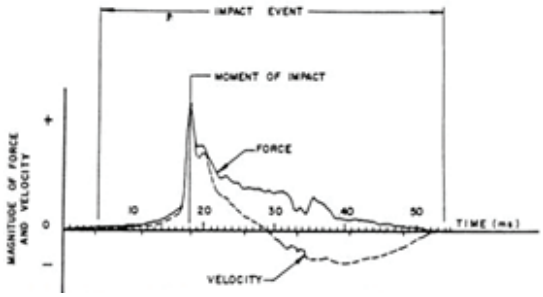

Figure 3: Typical Force and Velocity Traces Generated by the Apparatus for Obtaining Dynamic Measurements

2.2 Pile Integrity Test (PIT)

Integrity refers to the change in physical dimension, continuity of a pile, consistency of pile material. Pile integrity test is non-destructive test for evaluation of integrity in concrete piles. This test is standardized by ASTM D5882 Standard Test Method for Low Strain Impact Integrity Testing of Deep Foundations.

Pile Integrity Test can be applied to any concrete pile. The test is performed with a hand held hammer, an accelerometer or geophone and data acquisition and interpretation electronic instrument. Hammer is used to induce impact of low strain. An accelerometer of geophone measures the response of hammer impact.

The test is based on wave propagation theory. The name "low-strain dynamic test" stems from the fact that when a light impact is applied to a pile it produces a low strain. The impact produces a compression wave that travels down the pile at a constant wave speed. Changes in cross sectional area - such as a reduction in diameter - or material - such as a void in concrete - produce wave reflections.

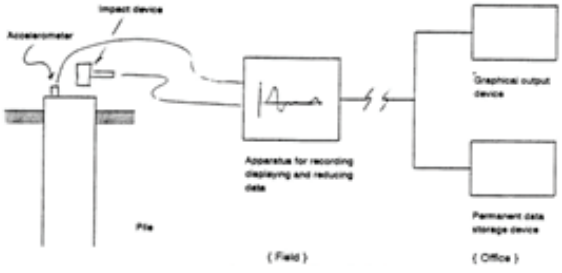

Figure 5: Schematic Diagram of Apparatus for Integrity Testing

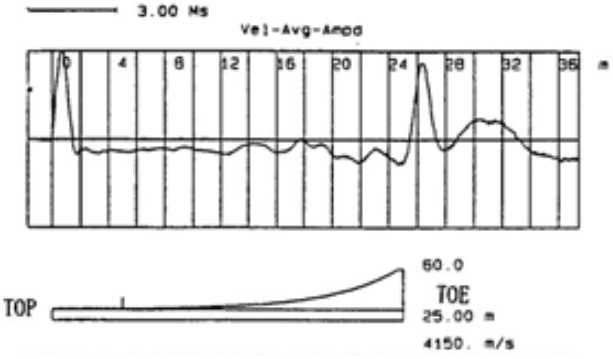

Figure 6: Typical Velocity Record Indicating Pile of Generally Uniform Nature (Gradual Impedance Changes or Soil Friction) (note the orientation of the input pulse is shown as positive in this standard; orientation could also be shown negative)

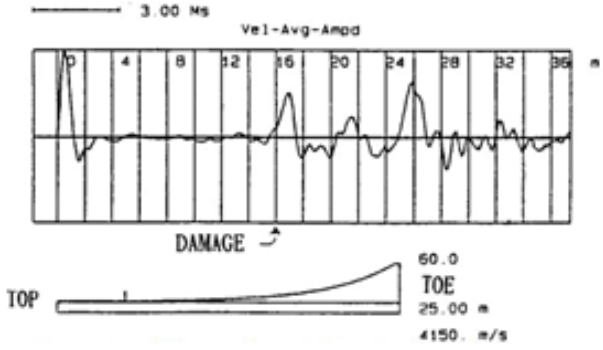

Figure 7: Typical Velocity Record Indicating Major Changes in Impedance (Severe Damage or a Cracked Pile (note the orientation of the input pulse is shown as positive in this standard; orientation could also be shown negative))

Figure 8: Pile Integrity Test (PIT)

2.3 Cross Hole Analyzer (CHAMP-Q)

Cross Hole sonic test is a type of test which covers procedures for checking the homogeneity and integrity of concrete in deep foundation such as bored piles, drilled shafts, concrete piles or auger cast piles.

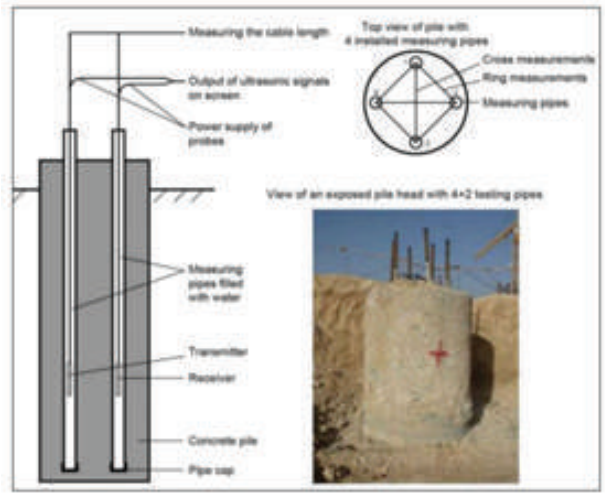

Figure 4: Access Tube Installation

Mostly used for drilled shafts and slurry walls, cross hole test is reliable when addressing drilling below groundwater level. Necking and caving in of drilled shafts, reinforcing cage buckling, pile damage, tremie 'burping' and excess water intrusion can all have serious effects on structural integrity. Cross Hole detects location, presence of multiple defects such as voids, soil intrusion and honeycombing. The shape, size and nature of such defects can also be accurately identified. This is a non-destructive test (NDT) method for the integrity testing of the concrete pile foundations.

Figure 9: Cross hole Analyzer (KTFT Road Project)

2.4 Static Pile load Test

2.4.1 Anchorage Method

Most test loads are applied with hydraulic jacks reacting against a test frame anchored to reaction piles. A number of reaction (anchor) piles can be placed surrounding the test pile and will provide the required tensile capacity and act as reaction against the compression test pile. Transfer of the forces involved is carried out by a series of beams, bars and the beams are placed over the piles and securely connected by the couplers/wielding to high strength threaded bars cast into the anchor piles and specifically designed for the purposes of the test. The size of the testing apparatus is 2 generally a function of the pile size and loading to be applied. Anchor piles or the supports for a reaction load must be placed a sufficient distance from the test pile to avoid influencing its performance. This minimum distance

Figure 10: Static Pile Load Test (Anchorage Method)

will depend on such things as the magnitude of load to be applied and the subsoil conditions. In this type of test, the loading and unloading process conducted by hydraulic jacks under the reaction of surrounding anchor pile. Where hydraulic jacks are used this can be accomplished by activating the jack pump with a compressed gas control system. Precautions should

be taken to avoid eccentric loading by carefully centering test beams or jacks and maintaining a balanced load. And these actions are done at every interval of time specified in the loading cycle of the test as mentation in loading procedure. The settlement is recorded by suitably positioned dial gauges at every loading and unloading made.

2.4.2 Kent ledge Method

The test will be done by application of an axial static load to a single pile by compression method .In this type of test, compression load is applied to the pile top by means of a hydraulic jack acting directly opposite in reaction to the series of statically placed Kent ledges loads. The loading and unloading process of these weights will be in increments for increasing the loads and decrements for decreasing the loads. And these actions will be done at

every interval of time specified in the loading cycle of the test. Settlement will be recorded by suitably positioned dial gauges at every loading and unloading made.

Figure 11: Static Load Test (Kent ledge Method)

Abandonment of load test The test is continued till one of the following takes place:

A) In case of initial load test:

- Applied load reaches 2.5 times the safe estimated load; or 5
- Maximum settlement of pile exceeds a value of 10 percent of pile diameter in case of uniform diameter piles and 7.5 percent of bulb diameter in case of under-reamed piles.

B) In case of routine load test:

- Applied load reaches 1.5 times the working load; or
- Maximum settlement of pile exceeds a value of 12 mm for piles diameter up to and including 600 mm and 18 mm or maximum of 2 percent of pile diameter whichever is less for piles of diameter more than 600 mm.

C) Other case of abandonment of test

- Pre-loading before the commencement of the test.
- Improper setting of datum.
- Faulty of pile cap or instability of the anchorage system.
- Faulty jack or gauge.
- Pile head crack or broken.
- Initial readings are incorrect.

3. RESULTS AND DISCUSSION

For each pile tested, the averaged, amplified velocity versus time record shall be included in the report, with a table summarizing results and conclusions. Additional plots and analyses can be included as required or suggested by the testing engineer.

4. LIMITATIONS

- No information on load bearing capacity of pile
- Cannot be used for existing foundation
- The low strain impact integrity test evaluation should not be used as the sole factor in establishing pile acceptance or rejection.

5. CONCLUDING REMARKS

The conclusions drawn from this research are

- The average intensity of rainfall above which the risk of landslide initiation is high in the Kavre district is 0.01mm/h.
- The rainfall intensity at 24 and 48 h at which the risk of occurrence of landslide is high are 0.61mm/h and 0.34mm/h.
- The analysis of landslide and rainfall data indicates that the antecedent rainfall plays a significant role in inducing landslides. It is more significant within 3 days and risk decreases as rainfall duration increases.
- The sediment rating curve was developed and also found that the maximum discharge and maximum suspended sediment in the monsoon of 2022 were 6.99 m3/s and 4952.22 mg/L respectively.

ACKNOWLEDGMENT

The author would like to thank the Department of Hydrology and Meteorology, Kathmandu, Nepal for providing the meteorological data and would also like to acknowledge RDI, Kathmandu University for providing partial financial support.

REFERENCES

[1] R. K. Dahal and S. Hasegawa, "Representative rainfall thresholds for landslides in the Nepal Himalaya," Geomorphology, vol. 100, no. 3–4, pp. 429–443, 2008, doi: 10.1016/j.geomorph.2008.01.014.

[2] H. K. Shrestha, R. Yatabe, and N. P. Bhandary, "Groundwater flow modeling for effective implementation of landslide stability enhancement measures: A case of landslide in Shikoku, Japan," Landslides, vol. 5, no. 3, pp. 281–290, 2008, doi: 10.1007/s10346-008-0121-8.

[3] A. Chhetri, R. B. Kayastha, and A. Shrestha, "Assessment of Sediment Load of Langtang River in Rasuwa District, Nepal," J. Water Resour. Prot., vol. 08, no. 01, pp. 84–92, 2016, doi: 10.4236/jwarp.2016.81007.

TITLE SPONSOR

1st GeoMandu Geohazards and Geo-Infra Disasters

Organizer

Title Sponsor:

TERRE ARMEE

Organizing Partners:

Educational Partners:

Sponsors:

Nepal Geotechnical Society
Kathmandu, Nepal
Email: ngeotechs@gmail.com
Web: www.ngeotechs.org